Evaluating the transport of surface seawater from 1956 to 2021 using ^{137}Cs deposited in the global ocean as a chemical tracer

Yayoi Inomata[1], Michio Aoyama[2]

5   1 Institute of Nature and Environmental Technology, Kanazawa University, Kanazawa, 920-1192, Japan

2 Center for Research in Isotopes and Environmental Dynamics, University of Tsukuba, Tsukuba, 305-8572, Japan

Correspondence to:Yayoi Inomata (yinomata@se.kanazawa-u.ac.jp)

Abstract. We analysed the spatiotemporal variations in the ^{137}Cs activity concentrations in global ocean surface seawater from
10   1956 to 2021 using the HAMGlobal2021: Historical Artificial radioactivity database in Marine environment, Global integrated version 2021 and other published data. The global ocean was divided into 37 boxes. The 0.5-yr median value of ^{137}Cs in each box in the Pacific Ocean, the values were gradually increased or almost constant levels in the 1950s and1960s, and then decreased exponentially in 1970–2010, immediately before the Fukushima Nuclear Power Plant (F1NPS) accident. In the northern North Atlantic Ocean and its marginal sea, the 0.5-yr median value of ^{137}Cs were large variation by the direct
15   discharged ^{137}Cs from the reprocessing plants. The ^{137}Cs inventory in the surface mixed layer in 1970, when ^{137}Cs released into the surface seawater, was estimated to be 184 ± 26 PBq. In 1975 and 1980, the ^{137}Cs inventory increased to 201 ± 27 and 214 ± 11 PBq, respectively, due to direct discharge from the Sellafield and La Hague nuclear fuel reprocessing plants. In 2011, the ^{137}Cs inventory in the global ocean mixed layer increased to 50.7 ± 7.3 PBq compared to that before the F1NPS accident, in which the contribution from the accident was estimated to be approximately 15.5 ± 3.9 PBq. Mass balance analysis indicates
20   that ^{137}Cs deposited by the global fallout in the western North Pacific Ocean moved to the eastern North Pacific Ocean. Subsequently, ^{137}Cs was transported southwards, followed by westwards transport in the subtropical and equatorial Pacific Ocean and inflowed into the Indian Ocean via the Indonesian Archipelago. The longer apparent half residence times in the Indonesian Archipelago (36.7 years from 1973 to 1997) and Central Atlantic Ocean (38.0 years from 1992 to 2016) also support the interpretation of the global-scale transport of ^{137}Cs from the western North Pacific Ocean to the Indian (20-30 years) and Atlantic Oceans (30-40 years). In the northern North Atlantic Ocean and its marginal sea, ^{137}Cs discharged from
25   nuclear reprocessing plants is transported to the North Sea, Barents Sea and coast of Norway, and Arctic Ocean on a decadal scale. The dataset is available at doi: 10.34355/CRiED.U.Tsukuba.00085 (Aoyama, 2021), doi: 10.34355/Ki-net.KANAZAWA-U.00149 (Inomata and Aoyama, 2022a), doi: 10.34355/Ki-net.KANAZAWA-U.00150 (Inomata and Aoyama, 2022b), doi: 10.34355/Ki-net.KANAZAWA-U.00151 (Inomata and Aoyama, 2022c).

30   ## 1 Introduction

^{137}Cs is regarded as one of the most abundant artificial radionuclides in the ocean because of its long half-life (30.17 yr) and large fission yield that originates from large-scale atmospheric weapons tests. Atmospheric nuclear weapons tests occurred from 1945 to 1980. During 1945 to 1963, the large scale atmospheric nuclear weapons tests were conducted by the United States. In 1963, the Partial Nuclear Test Ban Treaty was signed and these tests in the atmosphere by the United States and
35   Soviet Union, and Great Britain conducted the underground. However, France continued the atmospheric test until 1974 and China until 1980. In addition, ^{137}Cs has been released into the Pacific Ocean by local fallout from ground tests on Bikini Atoll in the Marshall Islands between 1946 and 1958 by the United States (e.g., UNSCEAR 2000; Aoyama et al., 2006; Aoyama, 2010; Inomata, 2010). Because large amount of ^{137}Cs released into the atmosphere fallout onto the ocean surface, the ocean is recognized as the largest receptor of ^{137}Cs on Earth. Furthermore, other sources, such as the accidental release from nuclear
40   facilities (the Three Mile Island nuclear power plant in 1979), sea dumping of nuclear wastes from nuclear facilities carried

out in 1986 in the north–central East Sea/Japan Sea by the former Soviet Union and Russian Federation, lost nuclear weapons, and the use of radioisotopes in human activities, such as industry, medicine, and science, are recognized. These contributions in the environment are minor compared to those from the dominant sources listed above (UNSCEAR, 2000; IAEA, 2005).

The ^{137}Cs released by the large-scale nuclear weapons tests was largely deposited in the western part of the North Pacific Ocean at approximately 30–45°N latitude and the western part of the North Atlantic Ocean at approximately 30–50°N latitude from the late 1950s to the early 1960s (UNSCEAR, 2000; Aoyama et al., 2006). By using a dataset of ^{137}Cs measurements in rainwater, seawater, and soil, ^{137}Cs deposition estimated by global fallout in the Northern Hemisphere with a 10°×10° grid was 765±79 PBq (Aoyama et al., 2006). The deposition of ^{137}Cs in the Southern Hemisphere was significantly lower than that in the Northern Hemisphere. The maximum deposition of ^{137}Cs in the Southern Hemisphere occurred approximately one year after that in the Northern Hemisphere, owing to the stratosphere air mass exchange between the northern and southern stratosphere (Hirose et al., 2003a, b).

The dissolved ^{137}Cs discharged from nuclear reprocessing plants, namely, the Sellafield plant (Irish Sea, the United Kingdom) and the La Hague facility (English Channel coast, France), are also large sources. Since 1952, the discharge of several radionuclides from the Sellafield plant has occurred in the Irish Sea. The released ^{137}Cs amount reached a maximum in the mid- to late 1970s (Gray et al., 1995; Guegueniat et al., 1997; UNSCEAR, 2000). The discharged ^{137}Cs from the Sellafield plant from 1951 to 2020 was estimated to be 41.4 PBq (OSPAR, 2021). The maximum discharged ^{137}Cs from the La Hague plant occurred in 1971, and the amount of discharged ^{137}Cs decreased over time. The total amount of ^{137}Cs released from the La Hague plant was estimated to be 1.04 PBq (OSPAR, 2021). These discharged ^{137}Cs were then transported to the northern North Atlantic Ocean, its marginal seas, and the Arctic Ocean (Smith et al., 1998; Maderich et al., 2021).

The Chernobyl accident on the 26th of April 1986, also released ^{137}Cs into the environment (e.g., Molero et al., 1999; Steinhauser et al., 2014; Miyao et al., 1998), which was estimated to be 85±26 PBq (NEA, 2002). Although most of the ^{137}Cs derived from the Chernobyl accident was deposited on land, a significant amount of ^{137}Cs was released into the ocean, which was estimated to be 15-20 PBq (Aarkkrog et al., 2003). In particular, Chernobyl fallout increased the ^{137}Cs activity concentrations in the Baltic Sea (Zaborska et al., 2014), resulting in the most radioactive contaminated area, with 4.5 PBq of the total inventory (CEC, 1990). The Black Sea also received the Chernobyl ^{137}Cs fallout in 1986 (Bezhenar et al., 2019; Egorov et al. 1999), and the inventory was estimated to be 2-3 PBq (Egorov et al., 1999). The ^{137}Cs released into the Black Sea flowed into the Mediterranean Sea (Bezhenar et al., 2019). In the Mediterranean Sea, the total deposition of ^{137}Cs from the Chernobyl accident was estimated to be 2.5 PBq in 1986 (Delfanti and Papucci, 2010). Furthermore, the fallout of ^{137}Cs from the Chernobyl accident also occurred as a single small pulse in the western North Pacific Ocean and Japan Sea (Miyao et al., 1998: Inomata et al., 2009), and the Chernobyl release contributed only a few percent compared to the previous ^{137}Cs water column inventory in these regions (Aoyama et al., 1986).

The F1NPS accident is also recognized as a large source of ^{137}Cs. On the 11th of March 2011, large amounts of ^{137}Cs were released into the western North Pacific Ocean by atmospheric deposition and direct discharge of liquid-contaminated stagnant water from the F1NPS because of the extraordinary earthquake and the subsequent giant tsunami (IAEA, 2015; UNSCEAR, 2013). The released ^{137}Cs amount by the F1NPS accident and these distributions were investigated by numerous researches and summarized in Busseler et al. (2017). In this study, we used our estimation because these were considering the mass balances among atmosphere, land, and ocean. The atmospheric deposited amount of ^{137}Cs into the ocean from the atmosphere was estimated to be 11.7-14.8 PBq (Aoyama et al., 2016b). Directly discharged liquid ^{137}Cs from the F1NPS was estimated to be 3.6 ± 0.7 PBq by using the observation data around the F1NPS and model simulation (Tsumune et al., 2012, 2013). The ^{137}Cs inventory into the North Pacific Ocean in the surface mixed layer was estimated to be 15.2-18.3 PBq (Aoyama et al., 2016b), which are consistent with the estimated values by optical statistical analysis (Inomata et al., 2016) and model simulation (Tsubono et al., 2016). It is noted that the region that contains F1NPS deposition in the western North Pacific Ocean is almost the same region as those with global fallout of ^{137}Cs in the 1950s and 1960s.

Other sources, such as nuclear waste dumping, discharges from nuclear power plant operation, the release of radionuclides from satellite failures, local underwater nuclear tests, nuclear weapons accidents, and the use in industry and medicine, are considered minor contributors to ^{137}Cs concentrations in the global ocean (Livingston and Povinec, 2000; IAEA, 2005).

^{137}Cs exists mainly in the dissolved form, which allows it to move with seawater. After its release into the ocean, ^{137}Cs undergoes radioactive decay, with a half-life of 30.17 years, during transport into the ocean by undergoing oceanic physical processes, such as advection, diffusion, and downward transport. Therefore, ^{137}Cs has been used as a marine tracer for decades to study physical processes, such as the long-range transport of water masses (e.g., IAEA, 2005; Hirose et al., 2003a,b; Inomata et al., 2009, 2012; Nakano et al., 2010; Povinec et al., 2003; Tsumune et al., 2003, 2011). Furthermore, ^{137}Cs is used to assess the radioactive doses (or radiological effects) to the human body due to the uptake of marine foods containing anthropogenic radionuclides (e.g., IAEA, 2005; UNSCEAR, 2013).

The spatiotemporal variations in ^{137}Cs activity concentrations in the surface seawater in the global ocean from 1956 to 2021 were investigated in this study. This study is an extension of our previous research, in which we analysed the measured data up to 2005 (Inomata et al., 2009). The data used in this study were adopted from the HAMGlobal2021: Historical Artificial radioactivity database in the Marine environment, Global integrated version 2021 (Aoyama, 2021), which contains data from the F1NPS accident. The HAMGlobal2021 database contains information on several radionuclides (^{134}Cs, ^{137}Cs, ^{90}Sr, ^{3}H, ^{239,240}Pu, ^{241}Am, and ^{14}C) in the global ocean. The data were measured from 1956 to 2021. The dataset in International Atomic Energy Agency Marine Radioactivity Information System (IAEA MARIS) were also compiled in the HAMGlobal2021. In addition to this, the data measured in the North Atlantic Ocean and its marginal seas by IRSN (Bois et al., 2020) were also contained in this study.

In this paper, we present the following new insights:

1. The distribution of ^{137}Cs in the mixed layer in the global ocean:

1) spatiotemporal variations in ^{137}Cs activity concentrations in the surface seawater in the global ocean from 1956 to 2021;

2) spatiotemporal variations in the ^{137}Cs inventory in the surface mixed layer in the global ocean based on the reconstructed two-minute longitude/latitude ^{137}Cs deposition data and surface mixed layer depths in each box; and

3) an estimate of the apparent half residence time (Tap) in each box in the global ocean.

2. Behaviour of ^{137}Cs in the surface mixed layer in the global ocean:

4) a comparison between the amount of ^{137}Cs deposited from the atmosphere due to global fallout and that directly released from nuclear reprocessing plants; the behaviour of ^{137}Cs released from nuclear reprocessing plants in the Atlantic to the Arctic; and

5) an estimate of the amount of ^{137}Cs released from the F1NPS in 2011 by using the inventory in each box.

3. Mass balance:

6) an estimate of the ^{137}Cs amount in net outflow to the downstream box and downwards transport below the surface mixed layer; and

7) finally, a summary of the ^{137}Cs transport time in the global ocean.

2 Data and methods

2.1 Data availability; HAM Global 2021 database

The ^{137}Cs concentration data were obtained from the HAMGlobal2021: Historical Artificial radioactivity database in Marine environment, Global integrated version 2021; this database includes data measured from 1956 to 2021. These data are

available at doi: 10.34355/CRiED.U.Tsukuba.00085 (Aoyama, 2021). The data were measured by many organizations and institutes, including the Baltic Marine Environment Protection (MORS, Germany); the Bundesamt fur Seeschiffapparent und Hydrographie (BSH, Germany); the Korean Institute of Nuclear Safety (KINS, Korea); the Marine Ecology Research Institute (MERI, Japan); the Ministry of Agriculture, Fisheries and Food (MAFF, the United Kingdom); the Japan Coast Guard (JCG, Maritime Safety Agency until 2000, Japan); the Norwegian Radiation Protection Authority (NRPA, Norway); the Riso National Laboratory (RISO, Denmark); and the RPA V. G. Khlopin Radium Institute (VGKRI, Russia). Data were also obtained from various research projects, such as the Arctic Monitoring Assessment Program (AMAP), the Geochemical Ocean Sections program (GEOSECS), the South Atlantic Ventilation Experiment (SAVE), Transit Tracers in the Ocean (TTO), the World Ocean Circulation Experiment (WOCE), and the Worldwide Marine Radioactivity Studies (WOMARS). Furthermore, we included the data reported in various research papers (Aarkrog et al., 1994; Aoyama and Hirose, 1995, 2004; Aoyama et al., 2001a,b; Aoyama et al., 2008, 2011, 2013, 2016a–c, 2018a,b; Ballestra et al., 1984; Bourlat et al., 1996; Bowen et al., 1982; Broecker et al., 1966, 1968; Busseler, 2012; Busseler et al., 2017; Cochran et al., 1987; Dahlgaard et al., 1995; Delfanti et al., 2000; Folsom et al., 1960a,b, 1968, 1970, 1975, 1979; Fowler et al., 1991; Gulin and Stokozov, 2005; Hirose et al., 1987, 1991, 1999; Hirose and Aoyama, 2003a,b; Ikeuchi et al., 1999; Ito et al., 2003, 2005; Kaeriyama et al., 2013, 2014, 2015; Kamenik et al., 2013; Katsuragi, unpublished data; Kautsky et al., 1987; Kim et al., 2012; Kumamoto et al., 2014, 2015, 2016, 2017, 2018, 2019; Livingston et al., 1985, 2000; Matishov et al., 2002; Miroshnichenko and Parasiv, 2020; Miyake et al., 1960, 1961, 1962, 1963, 1968, 1978, 1988; Miyao et al., 1998; Nagaya et al., 1964a,b, 1965, 1970, 1976, 1981, 1984, 1987, 1993; Nakanishi et al., 1990, 1995; Nies et al., 1989; Noshkin et al., 1976,1978,1979,1981,1999; Pillay et al., 1964; Povinec et al., 2003, 2011; Sanchez-Cabeza et al., 2011; Shirasawa et al., 1968; Smith et al., 1998, 2017; Wong et al., 1992; Yamada et al., 2006, 2007). In HAMGlobal2021, the dataset produced by the IAEA Marine Radioactivity Information System (MARIS) were combined. Furthermore, we used the ^{137}Cs data reported in the IRSN database (Baily du Bois, P. et al., 2020). Finally, all these data were compiled into a single comprehensive database for this study.

This new database contains a total of 56,447 datapoints corresponding to ^{137}Cs measured in surface waters (0–20 m) in the global ocean between 1956 and 2021. The ^{137}Cs concentration data points used in this study were significantly larger than those employed in our previous research, which included 22,368 data points obtained until 2005 (Inomata et al., 2009). Measured ^{137}Cs data, however, was very limited and it is impossible to cover the distribution of ^{137}Cs in the global ocean. In this study, the global ocean was divided into 37 boxes to investigate the temporal variations in ^{137}Cs activity concentrations in surface seawaters by using the available almost all data (Inomata and Aoyama, 2022a) (Figure 1). These boxes were divided by showing the latitudinal and longitudinal distributions based on the known ocean currents (IAEA, 2005; Open University, 2004), the latitudinal distributions of global fallout, location of reprocessing plants and F1NPS under the assumptions that ^{137}Cs activity concentrations in the box is almost same (Hirose et al., 2003; Inomata et al., 2009; IAEA, 2005). Marginal Seas such as Japan Sea are based on the definition of IHO (1953). Subarctic North pacific Ocean (Box1, north 40°N) is the highest atmospheric deposition of ^{137}Cs occurred in the 1960s in the Pacific Ocean, western North Pacific Ocean and eastern North Pacific Ocean (Box2, Box 3),which locate in 25-40°N, are upstream and downstream of Kuroshio extension. These three regions are influenced the ^{137}Cs contamination derived from the F1NPS accident. Subtropical western and eastern North Pacific Ocean (Box 4, Box 5) are downstream and upstream of the north Equatorial Current associated with the subtropical Gyre. Subtropical western and eastern North Pacific Ocean includes the California Gyre (5-25°N). These boxes include the contamination of local fallout such as the Bikini Atoll. Western and eastern equatorial Pacific Ocean (Box 6, 7) are downstream and upstream of the South Equatorial Current. And upwelling od seawater occurs in the eastern Southern Pacific Ocean. Western and eastern subtropical North Pacific Ocean (Box 8, 9) are down stream and upstream of the weak South Equatorial Current. Eastern subtropical South Pacific Ocean includes the French nuclear weapons test sites. The western Southern Pacific Ocean (25-40°S) is Tasmania Sea (Box 10). Eastern South Pacific Ocean (25-40°S) is mid-latitude region of the South Pacific Ocean and includes South Pacific Current (Box 11). Eastern Southern Ocean (40-60°S) is affected by the Antarctic

Circumpolar Current (Box 12). Antarctic Ocean (below 60°S) are divided into three; Antarctic sector for Pacific (Box13),

170   Indian (Box 36), and Atlantic (Box 37) and locate the polar front and continental water boundary. In the Middle Southern Ocean (Box 19), the Leeuwin Current, which flow to southward along the continental shelf off the western Australia (22°S to 35°S) in the Southern Ocean (Box 17), transport eastward. The Southern Ocean is characterised as subtropical gyre, and connected with the Antarctic Circumpolar Current from the Atlantic Ocean side in the upstream and the Pacific Ocean side in the downstream. The Antarctic Circumpolar Current is banded structure with several current and formed as narrow jet with

175   sharp front. Indian Ocean (Box 16) is connected to Indonesian Archipelago (Box 35) by Indonesian through flow from the Pacific Ocean. The Arabian Ocean (Box 15, 10°S-30°N) is affected by the equatorial current system and the circulation in the Northern Indian Ocean associated with monsoon system. In the marginal seas of the North Pacific Ocean, South China Sea (Box 33), Eastern China Sea (Box 32), Japan Sea (Box 14), and Okhotsk Sea (Box 31) are classified. The Eastern China Sea influence of the bifurcation of Kuroshio Current and downstream of western North Pacific Ocean and connected to the Japan

180   Sea via Tsushima Warm Current. The northward transported seawater in the Japan Sea is connected to the Sea of Okhotsk. The Bering Sea (Box 34) is downstream of the subarctic North Pacific Ocean and upstream of the Arctic Ocean. The Atlantic Ocean was divided into three, South Atlantic Ocean (Box 28, 60°S-30°S), Central Atlantic Ocean (Box 29, 30°S-15°N), and North Atlantic Ocean (Box 30, 15°N-45°N). The South Atlantic Ocean is connected with the Southern Ocean via the Agulhas Current. The Irish Sea (Box 23) and English Chanel (Box 24) are considered as the ^{137}Cs direct discharged region. The North

185   Sea (Box 22) , Barents Sea and Coast of Norway (Box 20), Baltic Sea (Box 21), Arctic Ocean (Box 18) are downstream of the northern North Atlantic Ocean and affected the inflow the ^{137}Cs derived from the Irish Sea and English Chanel. The northern North Atlantic Ocean (Box 25) received ^{137}Cs global fallout by the large scale weapons tests in the 1950s and 1960s. The Baltic Sea (Box 21), the Mediterranean Sea (Box 27), the Black Sea (Box 26) received the fallout of ^{137}Cs from the Chernobyl accident.

190   The 37 boxes set in this study are almost identical to those in our previous study (Inomata et al., 2009). However, the box areas are slightly modified by taking into account the ocean current. The region in the South China Sea, which was in Box 33 in Inomata et al. (2009), is divided into two boxes: South China Sea (Box 33) and Indonesian Archipelago (Box 35) because the sea water in the Pacific Ocean transported into the Indian Ocean via the Indonesian Archipelago. The region in Antarctica, which was in Box 13 in Inomata et al. (2009), is divided into three boxes: the Pacific sector of the Antarctic Ocean (Box 13),

195   the Atlantic sector of the Antarctic Ocean (Box 36) and the Indian sector of the Antarctic Ocean (Box 37). The region in the Southern Ocean (Box 17) is divided into two boxes: the Southern Ocean (Box 17) and the middle Southern Ocean (Box 19). The boxes corresponding to the source region, such as the Irish Sea (Box 23; Boxes 23.1-23.5) for the Sellafield plant and the northern North Atlantic Ocean (Box 25; Boxes 25.1 and 25.2) and western North Pacific Ocean (Box 2; Boxes 2.0-2.6) for the F1NPS accident, were divided into several sub regions, because significantly large values around the discharged region cause

200   to larger values to estimate the ^{137}Cs inventory.

      The box numbers, their corresponding longitudes and latitudes, the box name abbreviations, and the data number are listed in Table 1. The sampling points in each box are displayed in the data set (doi:10.34355/Ki-net.KANAZAWA-U.00149, Inomata and Aoyama, 2022a). Temporal variations of ^{137}Cs activity concentrations and 0.5-yr median values in each box are displayed in the Figures in the data set (doi:10.34355/Ki-net.KANAZAWA-U.00150) in Inomata and Aoyama (2022b).

205

210

(a)
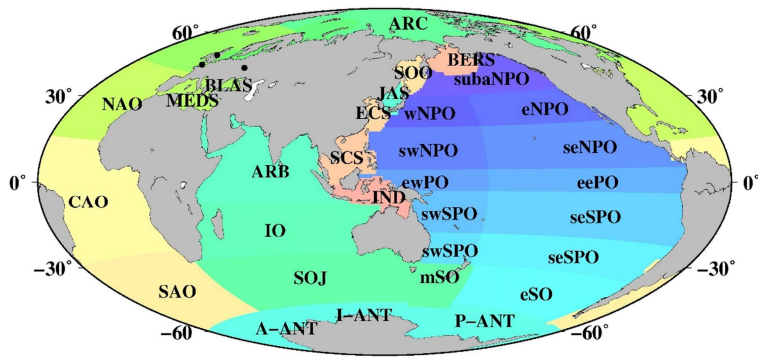
(b)
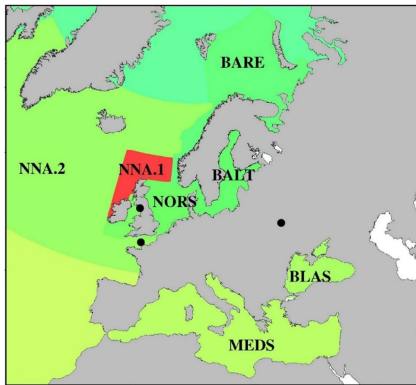
215

(c)
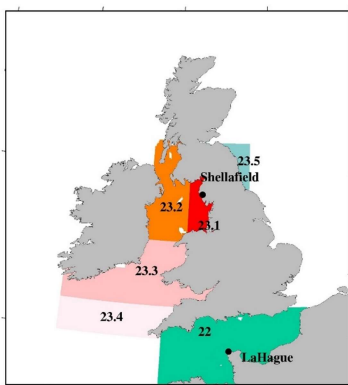
Figure 1: Boxes dividing the global ocean. (a) Global, (b) North Atlantic Ocean and its marginal Sea, and

220   (c) Irish Sea (Box23) and English Chanel (Box22).

225

Table 1. Detail of each box in the global ocean.

Box	subbox	Area	Code	Lon_w	Lon_e	Lat_s	Lat_n	Data No
1		subarctic North Pacific Ocean	subarctic NPO	140.5	240	40	62	2182
2	0	western North Pacific Ocean	western NPO	128	180	25	27	3744
2	0	western North Pacific Ocean	western NPO	129	180	27	28	
2	0	western North Pacific Ocean	western NPO	130	180	28	31	
2	0	western North Pacific Ocean	western NPO	131	180	31	34	
2	0	western North Pacific Ocean	western NPO	132	180	34	35	
2	0	western North Pacific Ocean	western NPO	145	180	35	38.25	
2	0	western North Pacific Ocean	western NPO	141	180	38.25	40	
2	1	western North Pacific Ocean	western NPO	140	141.35	37.15	37.69	7466
2	2	western North Pacific Ocean	western NPO	139.5	141.75	37.69	38.25	2566
2	2	western North Pacific Ocean	western NPO	141.35	141.75	37.15	37.69	
2	2	western North Pacific Ocean	western NPO	140.5	141.75	36.85	37.15	
2	3	western North Pacific Ocean	western NPO	141.75	143.5	36.85	38.25	234
2	4	western North Pacific Ocean	western NPO	140.5	143.5	36	36.85	1365
2	5	western North Pacific Ocean	western NPO	143.5	145	36	38.25	89
2	6	western North Pacific Ocean	western NPO	140	145	35	36	2682
3		eastern North Pacific Ocean	eastern NPO	180	255	25	40	953
4		western subtropical North Pacific Ocean	subtropical western NPO	121	180	5	25	497
5		eastern subtropical North Pacific Ocean	subtropical eastern NPO	180	283	5	25	671
6		western equatorial Pacific Ocean	equatorial western PO	117	180	-5	5	65
7		eastern equatorial Pacific Ocean	equatorial eastern PO	180	285	-5	5	156
8		western subtropical South Pacific Ocean	subtropical western SPO	142	180	-25	-5	52
9		eastern subtropical South Pacific Ocean	subtropical eastern SPO	180	290	-25	-5	220
10		western South Pacific Ocean	subtropical western SPO	149	180	-40	-25	43
11		eastern South Pacific Ocean	subtropical eastern SPO	180	290	-40	-25	109
12		eastern Southern Ocean	eastern SO	180	291.93	-60	-40	25
13		Pacific sector of Antarctic	Pacific ANT	147	291.93	-90	-60	3
14		Japan Sea	JAS	127	142	33.4	52	2806
15		Arabian Sea	ARB	32	119	-10	30	60
16		Indian Ocean	IO	20	129	-35	-10	76
17		Southern Ocean	SOJ	20	147	-60	-31	34
18		Arctic Ocean	ARC	0	360	70	90	651
19		Middle Southern Ocean	middle SO	147	180	-60	-31	16
20		Barents Sea and Coast of Norway	BARE	2	71	58	80	836
21		Baltic Sea	BALT	9	30	53	66	6450
22		North Sea	NORS	0	360	50	58	5555

230

235

Table 1. Detail of each box in the global ocean. (Continued)

Box	subbox	Area	Code	Lon_w	Lon_e	Lat_s	Lat_n	
23	1	Irish Sea	IRIS	356	358	53	55	3744
23	2	Irish Sea	IRIS	353	356	53	56	2505
23	3	Irish Sea	IRIS	352	357	52	53	1487
23	3	Irish Sea	IRIS	350	358	51	52	
23	4	Irish Sea	IRIS	350	357	50	51	90
23	5	Irish Sea	IRIS	356	359	55	56	
23	5	Irish Sea	IRIS	358	359	54	55	
24		English Channel	ENGC	0	360	49	50.5	3059
25	1	northern North Atlantic Ocean	NNA	350	360	59	62	2287
25	1	northern North Atlantic Ocean	NNA	350	355	55	59	
25	1	northern North Atlantic Ocean	NNA	350	352	54	55	
25	1	northern North Atlantic Ocean	NNA	350	351	52	54	
25	1	northern North Atlantic Ocean	NNA	0	3	59	62	
25	2	northern North Atlantic Ocean	NNA	295	350	45	70	1628
25	2	northern North Atlantic Ocean	NNA	350	360	62	70	
25	2	northern North Atlantic Ocean	NNA	350	355	45	50	
25	2	northern North Atlantic Ocean	NNA	0	3	62	64	
25	2	northern North Atlantic Ocean	NNA	355	0	45	46	
25	2	northern North Atlantic Ocean	NNA	355	359	46	47	
25	2	northern North Atlantic Ocean	NNA	355	358	47	48	
25	2	northern North Atlantic Ocean	NNA	0	3	62	64	
25	2	northern North Atlantic Ocean	NNA	0	4	64	65	
25	2	northern North Atlantic Ocean	NNA	0	5	65	66	
25	2	northern North Atlantic Ocean	NNA	0	6	66	67	
25	2	northern North Atlantic Ocean	NNA	0	7	67	68	
25	2	northern North Atlantic Ocean	NNA	0	8	68	69	
25	2	northern North Atlantic Ocean	NNA	0	9	69	70	
26		Black Sea	BLAS	27	42	41	48	88
27		Mediterranean Sea	MEDS	0	360	30	46	211
28		North Atlantic Ocean	NAO	262	360	15	45	154
29		Central Atlantic Ocean	CAO	0	360	-30	15	97
30		South Atlantic Ocean	SAO	290	360	-60	-30	35
31		Sea of Okhotsk	SOO	135	165	43	63	72
32		Eastern China Sea	ECS	117	131	25	41	1189
33		South China Sea	SCS	99	125	-2	25	90
34		Berigng Sea	BERS	162	203	52	66	71
35		Indonesian Archipelago	IND	105	142	-18	4	27
36		Atlantic sector of Antarctic	Atlantic ANT	0	360	-90	-60	3
37		Indian sector of Antarctic	Indian ANT	20	147	-90	-60	4

2.2 The 0.5-yr median values of ^{137}Cs the surface ^{137}Cs activity concentrations in each box

The 0.5-yr median values of the surface ^{137}Cs activity concentrations in each box were calculated and shown in the dataset (Inomata and Aoyama, 2022c, doi: 10.34355/Ki-net.KANAZAWA-U.00151). These 0.5-yr median values of the surface ^{137}Cs activity concentrations are useful to verify the general ocean circulation models (Tsumune et al., 2011; Tsubono et al., 2016) and assess the radiation doses delivered to humans through the ingestion of marine food (Aarklog et al., 1997; IAEA, 2005; UNSCEAR, 2013). The 0.5-yr median values of the surface ^{137}Cs concentrations in each box were produced by the grid value producing command of block median programs (Wessel et al., 2013). The block median reads the arbitrary data (x, y, z) and calculates the median value in a grid defined in the setting range. In the case of t-year, the data within t-year±0.5 years were used to calculate the median values. We produced the dataset (box number, year, and ^{137}Cs activity concentrations)

for each box. These gridded data were recalculated to continuous curvature splines with adjustable tension, and these values are regarded as the 0.5-yr median value. In the case of Box 2, significantly higher concentrations were observed only near the F1NPS (Box 2.1-2.6) because of the direct release of ^{137}Cs. We used only the ^{137}Cs activity data in Box 2.0 for the analysis of the 0.5-yr median values because the significantly higher values are localized and do not reflect concentrations throughout Box 2.

2.3 Estimates of apparent half residence times in global surface seawater

The ^{137}Cs activity concentrations are mainly dominated by fallout into the surface seawater, radioactive decay with a 30.17-yr half-life, horizontal transport, and downwards transport below the mixed layer. Based on the long-term measurement of ^{90}Sr deposition by the global monitoring network, the cumulative ^{90}Sr deposition reached a maximum in the late 1960s to the early 1970s (UNSCEAR, 2000). This suggests that the atmospheric deposition of ^{137}Cs had a minor contribution to the surface seawater ^{137}Cs activity concentrations after 1970 (UNSCEAR, 2000; Hirose and Aoyama, 2003a; Aoyama et al., 2006). The decrease in ^{137}Cs activity concentrations in the surface seawater in each box is approximated by the corresponding fitting of the exponentially decreasing curves. This decreasing rate of ^{137}Cs activity concentrations is controlled by radionuclide decay as well as physical ocean circulation because the contribution from large-scale deposition by atmospheric nuclear tests was negligible after 1970 (UNSCEAR, 2000). The regression line of the 0.5-yr median value of ^{137}Cs for each box was determined and apparent half residence time (Tap) due to the radioactive decay and ocean physical processes were estimated. The Tap of ^{137}Cs was calculated using the following equations:

$$^{137}Cs = {}^{137}Cs_0 exp(-\lambda_{cs,\ apparent}) \qquad (1)$$

$$\lambda_{Cs,apparent} = \lambda_{Cs,ocean} + \lambda_{Cs,decay} \qquad (2)$$

$$Tap = 0.693/(\lambda_{Cs,apparent}) \qquad (3)$$

$$Tpo = 0.693/(\lambda_{Cs,ocean}) \qquad (4)$$

where $\lambda_{Cs,apparent}$, $\lambda_{Cs,ocean}$, and $\lambda_{Cs,decay}$ are the decay constants for apparent decay, physical oceanographic decay, and radioactive decay, respectively. $\lambda_{Cs,apparent}$ is estimated by using the regression line of the 0.5-yr median value of ^{137}Cs as shown in (1). Tpo is the apparent half residence time by causing the oceanic physical processes and $\lambda_{Cs,ocean}$ was estimated $\lambda_{Cs,apparent}$ and $\lambda_{Cs,decay}$ in equation (2). Considering that the half-life of ^{137}Cs ($T_{1/2}$) is 30.17 years, the Tap should be shorter than the half-life if no source of ^{137}Cs exists in the region of interest. A shorter Tap means that ^{137}Cs is removed quickly in the area and/or the ^{137}Cs inflow amount is small in the area compared with the ^{137}Cs outflow amount. In other words, a Tap shorter than the radioactive decay time indicates that the variations in the ^{137}Cs activity concentrations are strongly controlled by physical ocean processes. In contrast, a longer Tap as well as a negative Tpo value means that ^{137}Cs is preserved in the region for a longer time and/or there is an influx of water mass with higher ^{137}Cs in the region compared to the ^{137}Cs outflow from the region.

However, the exponentially decreasing trend from 1970 to 2010, before the F1NPS accident, did not estimate for all boxes. Tap from 1970 to 2010 were estimated for the western North Pacific Ocean, Japan Sea, and Eastern China Sea. For other boxes, Tap, therefore, was estimated for several periods, taking into account the source contribution as follows. Tap1 is before 1970 (periods with nuclear weapon tests at a global scale), Tap2 is the period from 1970 to 1986-1990 (until the Chernobyl accident), Tap3 is from 1990 to 2010 (after the Chernobyl accident), and Tap4 is after 2011 (after F1NPS accident). There were some regions, where did not estimate to Tap, such as the northern North Atlantic and surrounding waters, because decreasing trend of ^{137}Cs could not be approximated by Equation (1).

2.4 F1NPS contribution to the 0.5-yr ^{137}Cs median values in the North Pacific Ocean

After several years following the F1NPS accident, ^{137}Cs activity concentrations in surface seawater gradually increased in the Japan Sea, Eastern China Sea, subarctic North Pacific Ocean, and Bering Sea (Aoyama et al., 2016a, 2017;

Inomata et al., 2018; Smith et al., 2017, Kumamoto et al., 2019). To estimate the contribution of the F1NPS accident, ^{137}Cs

295 derived from the F1NPS accident ([F1NPS-^{137}Cs]) in 2011 was estimated using the following equation.

[F1NPS-^{137}Cs]each box = [0.5-yr average ^{137}Cs values]each box – [Global-^{137}Cs]each box   (5)

The "[Global-^{137}Cs]each box" in 2011 was estimated by extrapolating the exponential regression line from 1990 to 2010 under the assumption that the apparent half residence time of ^{137}Cs activity concentrations were the same value.

2.5 Reconstruction with the 2-minute latitude/longitude ^{137}Cs deposition amount in the global ocean

300   To estimate the ^{137}Cs inventory in each box in the global ocean, we reconstructed the ^{137}Cs global fallout distribution with a two-minute latitude/longitude grid based on the 10° latitude/longitude grid data of ^{137}Cs deposition, which was constructed using ^{137}Cs data measured in rainwater, seawater, and soil by Aoyama et al. (2006). Topography–bathymetry information were based on the two-minute Gridded Global Relief Data (ETOPO2) (Earth Topography; NOAA National Geophysical Data Center, 2006), taking into account the ellipticity of the Earth (Oki et al., 1997; Suga et al., 2013).

305

2.6 Estimate of the ^{137}Cs inventory in the surface mixed layer in the global ocean

We estimated the ^{137}Cs inventory in the surface mixed layer in each box and compared it with the ^{137}Cs fallout amount until 1970 because a major input of ^{137}Cs into surface seawater occurred in the early 1960s and reached a maximum in 1970 (IAEA, 2000; Aoyama et al., 2006). The ^{137}Cs deposition in the surface seawater after 1970 was negligible compared to the

310 activity concentrations in the surface seawater. Therefore, the behaviour of ^{137}Cs in the surface seawater after 1970 is mainly controlled by radioactive decay and ocean physical transport processes. In this study, the ^{137}Cs inventory was estimated under the assumption that ^{137}Cs was mixed and homogeneously distributed within each box, with a 0.5-yr timescale in the surface mixed layer. However, the Irish Sea (Box 23) was subdivided into five regions (Boxes 23.1-23.5) because significantly higher values were observed around the directly discharged area from the Sellafield plant. It is noted that there were no available data

315 in Box 23.5. In the northern North Atlantic Ocean, higher ^{137}Cs activity concentrations were observed in the region close to the Irish Sea or the North Sea. In this case, the northern North Atlantic Ocean was also divided into two boxes (Box 25.1 and Box 25.2). Box 2 is also divided into 7 subboxes, because of significantly higher concentrations were observed near the F1NPS.

The ^{137}Cs surface mixed layer inventory (unit: PBq) was estimated using the following equation, assuming that ^{137}Cs activity concentrations are almost constant in the surface mixed layer.

320    $[^{137}\text{Cs inventory}]_{\text{box}} = \sum_{i=1}^{grid\ number}([\ ^{137}\text{Cs median value}]_{\text{box}} \times [\text{sea area}]_{\text{box}} \times [\text{averaged mixed layer depth}]_{\text{box}})$ (6)

The sea area in each box was calculated using the basin mask assigned to each two-minute latitude/longitude square, which was created based on the two-minute Gridded Global Data (NOAA National Geophysical Data Center, 2006). The average mixed layer depth in each box was calculated using the two-degree latitude/longitude gridded "Mixed Layer Climatology" data constructed by the French Research Institute for the Exploitation of the Sea (IFREMER) (Montegut et al., 2004; Mignot

325 et al., 2007). These data were regridded as the two-minute latitude/longitude data to set the same scale as the sea area dataset. In this dataset, the mixed layer depth was defined as the depth at which the surface temperature decreases by 0.2 °C and the density decreases by 0.03 kg m^{-3}. The mixed layer depths were estimated by 780000 profiles recorded in the World Ocean Database 09-National Oceanographic Data Center (NODC); Conductively, Temperature and Depth Profile (CTD) (1961–2008); World Ocean Circulation Experiment-3.0 Profiling Float Data (PFL) CTD (1990–2002) and ARGO PFL (1995–2008).

330 The mixed layer depth was the monthly time interval with seasonal variation that is deeper in winter and shallower in summer. It is recognised that sea water subducted from the ocean surface in the mode water formation region associated with the winter convective mixing because of the lower buoyancy from the ocean surface (Hanawa and Tally, 2001). The flow through the winter mixed layer ventilate the sea water into the ocean interior. The maximum monthly mixed layer depth in each box, mainly winter month, was used to calculate the ^{137}Cs inventory in the mixed layer. The mixed layer depths used to estimate

the inventory ranged from 33 to 182 m. In the western North Pacific Ocean (Box 2), significantly higher ^{137}Cs values around the F1NPS causes the higher 0.5-yr median value after 2011. Then, our previous estimated inventory by statistical optical interpretation analysis in the subarctic North Pacific Ocean and western and eastern North Pacific Ocean (Inomata et al., 2016).

The ^{137}Cs density in the surface seawater (unit: kBqm^{-2}) was also estimated by using the following equation.

$$[{}^{137}\text{Cs density in the surface seawater}]_{box} = [{}^{137}\text{Cs inventory}]_{box}/[\text{sea area}]_{box} \qquad (7)$$

2.7. Mass balance; inflow and outflow of ^{137}Cs from each box

In the marine environment, ^{137}Cs activity concentrations after 1970 were dominantly controlled by radioactive decay and physical ocean processes, except for the release by accident and reprocessing plants. As the physical oceanographic processes, ^{137}Cs in the surface seawater in each box receive inflow from the upstream box, outflow to the downstream box, and downward transport below the surface mixed layer. In fact, estimates of ^{137}Cs transport amount in these processes were very difficult in this study. Therefore, outflowed ^{137}Cs by these processes were represented as net outflowed ^{137}Cs in each box. Mass balance of ^{137}Cs in the surface mixed layer was considered as following equations.

$$[{}^{137}\text{Cs inventory}]_{box,\ ti+5} = [{}^{137}\text{Cs inventory}]_{box,ti} - [\text{radioactive decayed } {}^{137}\text{Cs}]_{box,\ \Delta t} - [\text{net outflowed } {}^{137}\text{Cs}]_{box,\ \Delta t} \qquad (8)$$

$$[\text{radioactive decay}]_{box,\ \Delta t} = [{}^{137}\text{Cs inventory} \times \exp(-0.693/T_{1/2} \times \Delta t)]_{box} \qquad (9)$$

$$[\text{net outflowed } {}^{137}\text{Cs}]_{box,\ ti+5} = [\text{inflowed } {}^{137}\text{Cs}]_{box,\ ti} + [\text{outflowed } {}^{137}\text{Cs}]_{box,\ ti} \qquad (10)$$
$$+ [\text{downwards transport of } {}^{137}\text{Cs below the surface mixed layer}]_{box,ti}$$

where,

Δt : 5 years

ti : 1970+i×5 (i=0,1,···, 9).

$[{}^{137}\text{Cs inventory}]_{box,\ ti}$ is the value at initial year and $[{}^{137}\text{Cs inventory}]_{box,\ ti+5}$ is the ^{137}Cs inventory after the Δt year in each box. In this study, this mass balance was estimated to every 5 years from 1970 to 2015. In the case of 1970, ^{137}Cs deposition amount until 1970 was used as the value of the initial year in each box. In the northern North Atlantic Ocean and Arctic Ocean, an extremely large inflow was estimated in 2000 due to the extremely large values included in the dataset. These data in 2000 and 2005 were removed from the figures.

3 Results

Figure 2 shows the temporal variations in the 0.5-yr median value of ^{137}Cs in each box. Table 2 lists the 0.5-yr median values of the surface ^{137}Cs in the global ocean from 1960 to 2020 every 5 years. The 0.5-yr median values of ^{137}Cs in each box are also listed in Inomata and Aoyama (2022c). In this section, temporal variations in the 0.5-yr average ^{137}Cs values in each box are described.

370
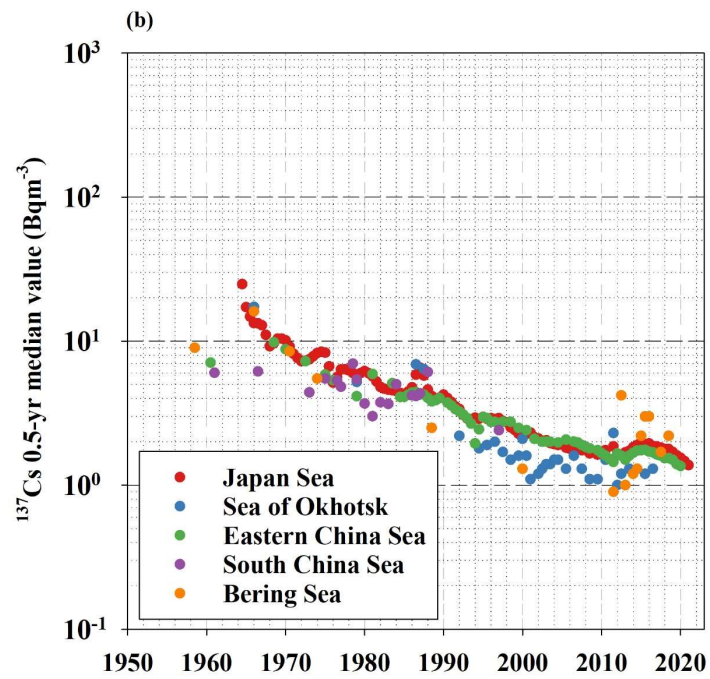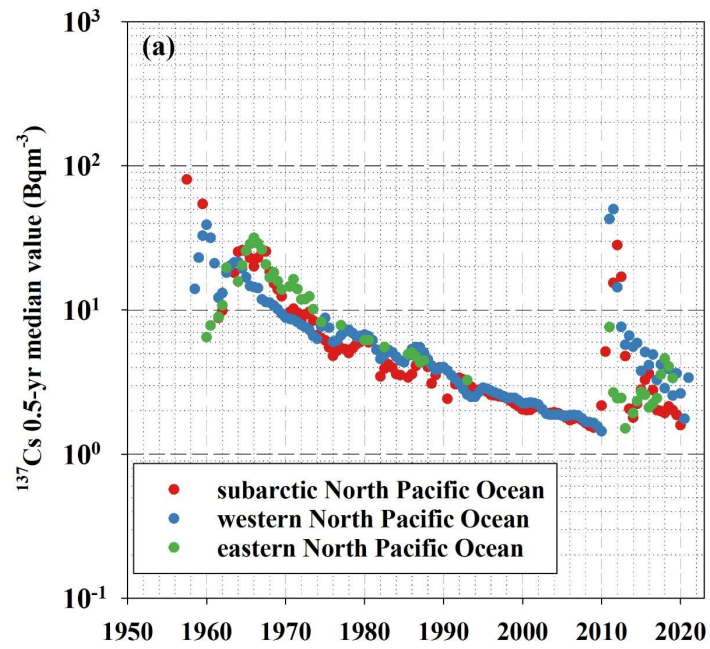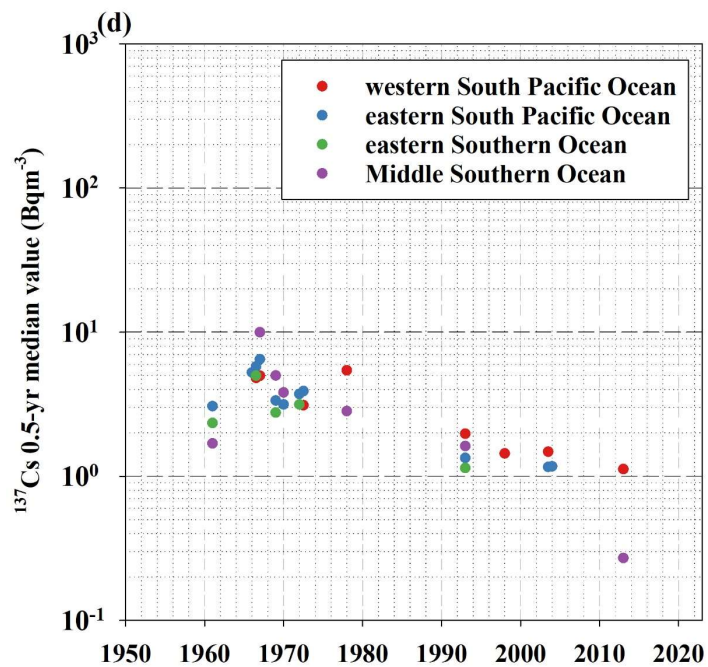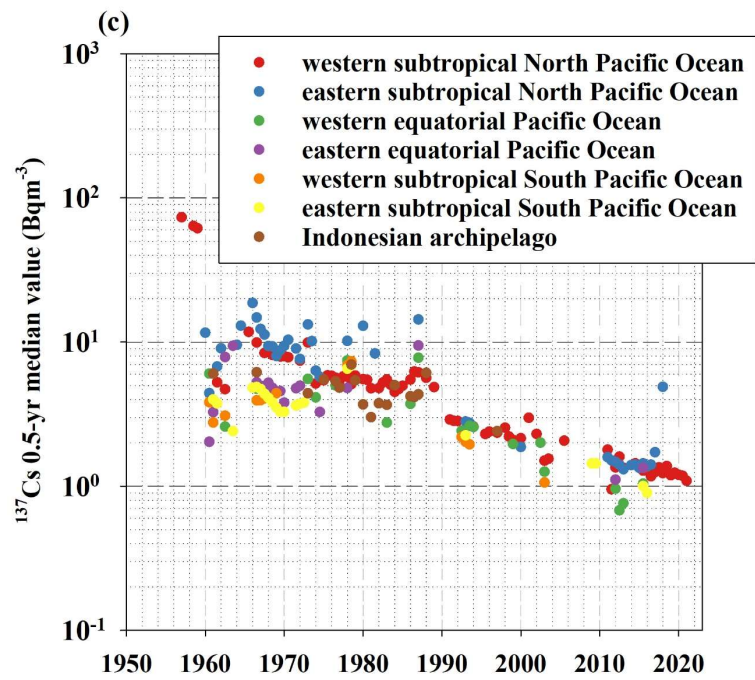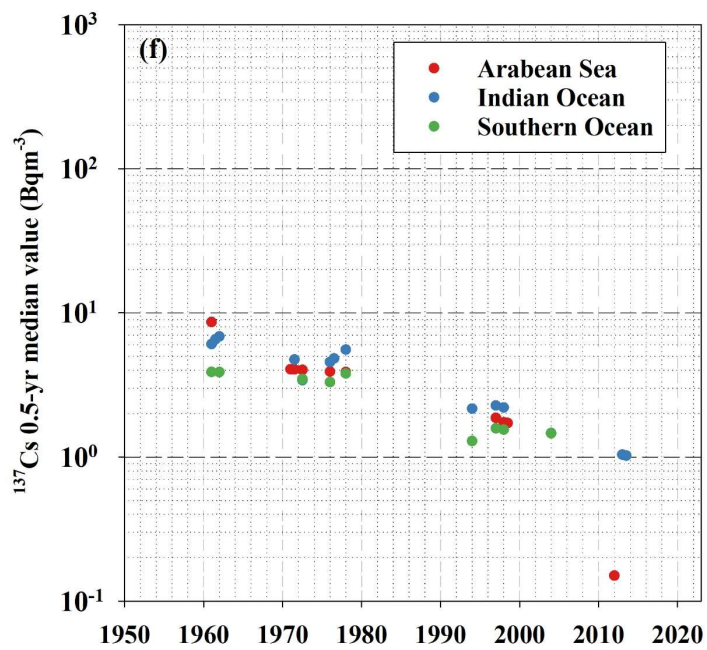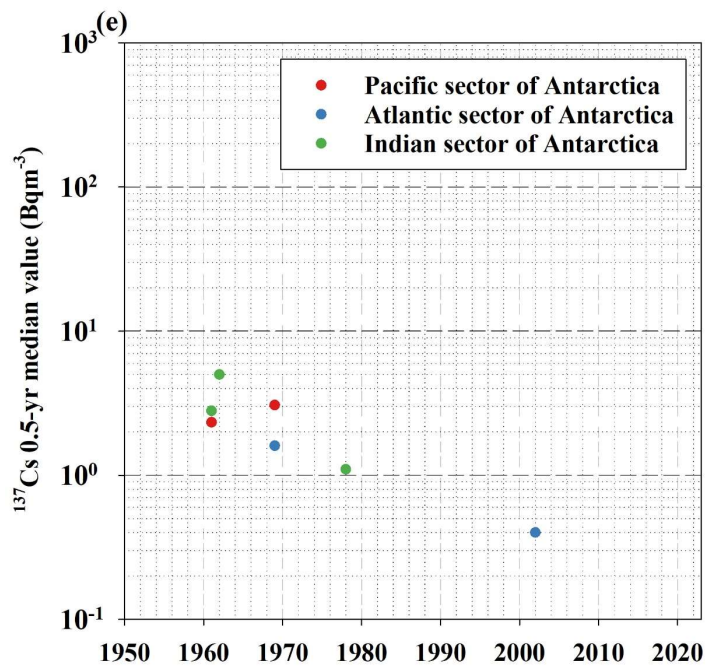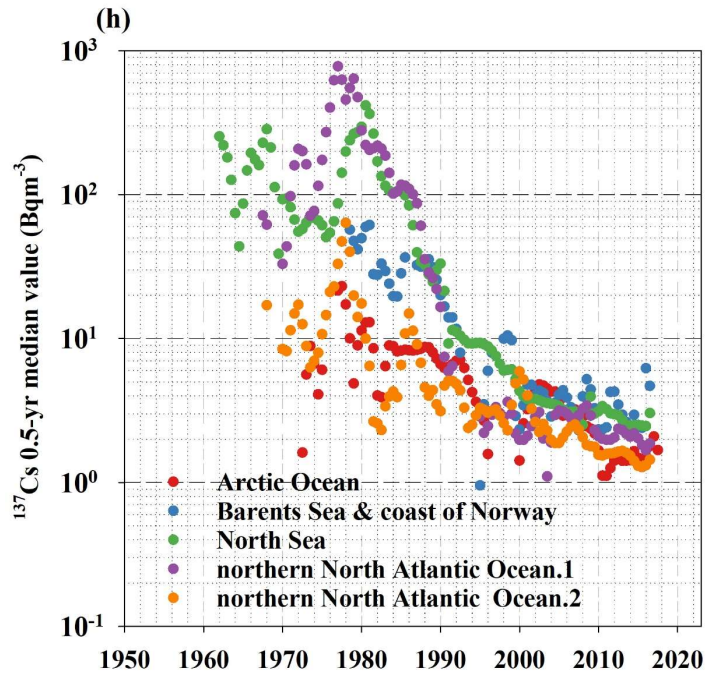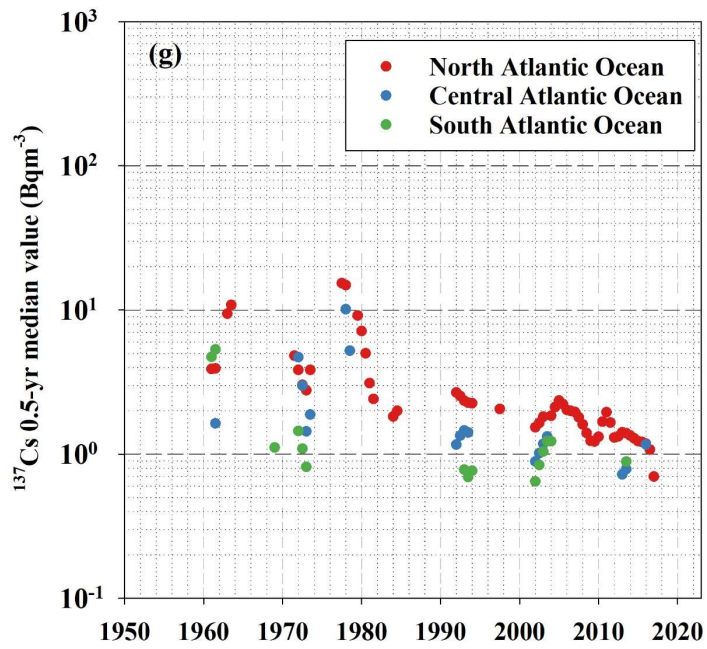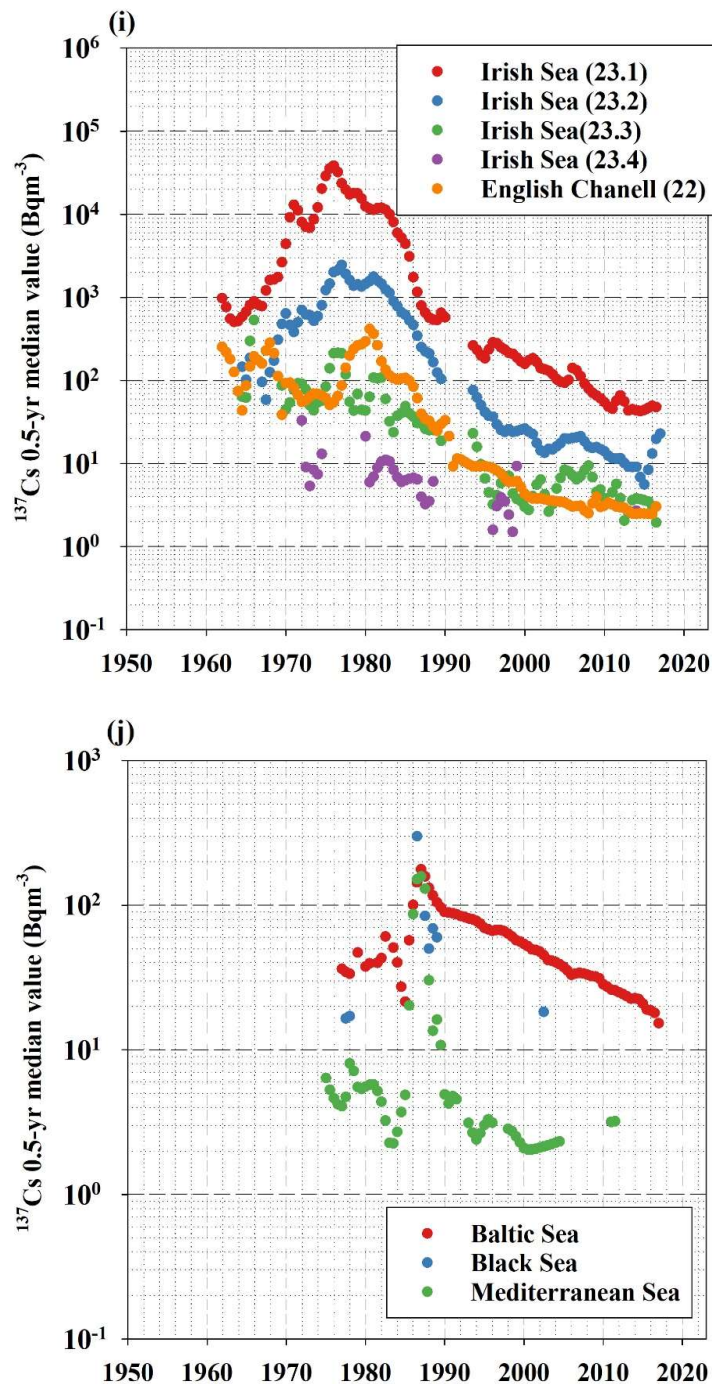
380

Figure 2: 0.5-yr median ^{137}Cs values of each box for (a) Boxes 1–3 (subarctic North Pacific Ocean, western North Pacific Ocean, and eastern North Pacific Ocean), (b) Boxes 14 and 31–34 (Japan Sea, Sea of Okhotsk, Eastern China Sea, South China Sea, and Bering Sea), (c) Boxes 4-9 (western subtropical North Pacific Ocean, eastern subtropical North Pacific Ocean, western equatorial Pacific Ocean, eastern equatorial Pacific Ocean, eastern subtropical South Pacific Ocean, and western subtropical South Pacific Ocean), (d) Boxes 10–12 and 19 (western subtropical South Pacific Ocean, eastern subtropical South Pacific Ocean, eastern Southern Ocean, and middle Southern Ocean), (e) Boxes 13, 36 and 37 (Pacific sector of the Antarctic Ocean, Atlantic sector of the Antarctic Ocean, and Indian sector of the Antarctic Ocean), (f) Boxes 15–17 (Arabian Sea, Indian Ocean, and Southern Ocean), (g) Boxes 28–30 (North Atlantic Ocean, Central Atlantic Ocean, and South Atlantic Ocean), (h) Boxes 18, 20, 22 and 25 (Arctic Ocean, Barents Sea and coast of Norway, North Sea, and northern North Atlantic Ocean), (i) Boxes 23 and 24 (Irish Sea and English Channel), (j) Boxes 21, 26 and 27 (Baltic Sea, Black Sea and Mediterranean Sea).

385

390

Table 2. 0.5-yr ^{137}Cs median value in each box.

box	0.5-yr ^{137}Cs median value											
	1960	1965	1970	1975	1980	1985	1990	1995	2000	2005	2010	2015
	(Bq m^{-3})	(Bq m^{-3})	(Bq m^{-3})	(Bq m^{-3})	(Bq m^{-3})	(Bq m^{-3})	(Bq m^{-3})	(Bq m^{-3})	(Bq m^{-3})	(Bq m^{-3})	(Bq m^{-3})	(Bq m^{-3})
1 subarctic North Pacific Ocean	38	25	10	7.0	4.8	3.4	3.3	2.7	2.2	1.8	1.5	2.4
2 western North Pacific Ocean	24	16	8.8	7.2	5.9	4.8	3.4	2.8	2.3	1.9	1.5	4.7
3 eastern North Pacific Ocean	6.5	26	15	10	6.7	4.5	3.7	3.0	2.5	2.1	1.7	2.7
4 western subtropical North Pacific Ocean	-	-	7.0	6.4	5.7	5.2	2.9	2.5	2.2	1.9	1.7	1.3
5 eastern subtropical North Pacific Ocean	12	-	9.8	9.8	9.8	9.8	3.0	2.5	2.2	1.8	1.6	1.4
6 western equatorial Pacific Ocean	4.6	4.3	5.4	5.4	5.4	5.4	3.0	2.4	1.9	1.5	1.2	0.9
7 eastern equatorial Pacific Ocean	13	7.1	4.3	4.3	4.3	4.3	2.4	2.1	1.8	1.6	1.4	1.2
8 western subtropical South Pacific Ocean	3.1	3.7	14	9.1	6.1	4.1	2.8	1.9	1.2	0.8	0.6	0.4
9 eastern subtropical South Pacific Ocean	5.0	4.8	3.0	5.2	5.2	2.4	2.4	2.1	1.9	1.6	1.4	1.0
10 western South Pacific Ocean	-	13	9.3	4.2	4.7	3.4	2.4	1.8	1.6	1.4	1.2	1.1
11 eastern South Pacific Ocean	2.5	5.1	3.2	3.3	2.6	2.0	1.6	1.3	1.2	1.2	1.1	1.0
12 eastern Southern Ocean	3.0	3.2	3.5	2.7	2.1	1.7	1.3	1.0	0.8	0.6	0.5	0.4
13 Pacific sector of Antarctic	2.2	2.7	2.7	1.4	0.7	0.4	0.2	0.1	0.1	0.0	0.0	0.0
14 Japan Sea	44	19	9.0	7.1	5.6	4.4	3.7	3.0	2.4	1.9	1.6	2.0
15 Arabian Sea	8.6	-	4.1	4.0	3.8	3.5	2.9	2.4	1.9	-	-	-
16 Indian Ocean	6.5	5.5	4.6	5.5	4.4	3.6	2.9	2.3	1.8	1.5	1.2	1.0
17 Southern Ocean	-	-	3.5	3.5	3.5	2.6	2.1	1.6	1.3	1.0	0.8	0.6
18 Arctic Ocean	-	-	1.2	6.1	11.3	8.2	6.7	3.2	1.4	3.6	1.7	1.5
19 Middle Southern Ocean	0.3	7.2	4.4	3.3	2.4	1.8	1.4	1.0	0.8	0.6	0.4	0.3
20 Barents Sea and Coast of Norway	-	-	-	-	45.5	32.7	23.5	16.9	5.1	4.4	3.7	3.2
21 Baltic Sea	-	-	-	30.0	37.6	21.6	95.9	71.0	52.5	38.9	28.8	21.3
22 North Sea	-	86.6	92.8	61.3	295.5	107.3	33.2	9.3	3.9	3.4	3.0	2.6
23.1 Irish Sea	-	669.6	4410.7	28847.0	12468.5	4424.7	587.1	184.8	158.5	94.1	54.8	44.1
23.2 Irish Sea	-	102.0	638.8	1224.6	1457.3	615.7	96.3	41.7	26.5	20.1	14.0	5.6
23.3 Irish Sea	-	62.1	44.9	84.3	43.3	49.0	18.8	6.6	3.0	8.4	3.8	3.6
23.4 Irish Sea	-	-	11.9	9.5	7.5	6.0	4.8	3.8	3.0	2.4	1.9	1.5
23.5 Irish Sea	-	-	-	-	-	-	-	-	-	-	-	-
24 English Channel	-	11.3	47.5	49.1	17.5	22.6	15.1	5.9	3.3	2.1	1.8	1.6
25.1 northern North Atlantic Ocean	-	-	46.3	174.1	279.5	116.8	16.5	2.9	2.0	3.2	2.1	2.0
25.2 northern North Atlantic Ocean	-	-	8.4	10.7	17.5	6.6	3.1	3.3	5.9	1.9	1.6	1.3
26 Black Sea	-	-	-	-	-	-	56.4	36.2	23.2	14.8	9.5	6.1
27 Mediterranean Sea	-	-	6.4	5.6	4.9	4.9	3.0	2.1	2.1	2.3	3.2	-
28 North Atlantic Ocean	-	-	6.3	6.0	5.6	3.4	2.8	2.4	2.1	1.7	1.5	1.3
29 Central Atlantic Ocean	-	-	3.1	4.8	6.4	4.6	1.4	1.3	1.2	1.1	1.0	0.9
30 South Atlantic Ocean	5.6	-	5.4	4.6	3.9	3.3	2.8	2.4	1.9	1.5	1.2	0.9
31 Sea of Okhotsk	-	19.0	12	7.5	4.7	3.0	2.1	1.9	1.6	1.4	1.2	1.2
32 Eastern China Sea	7.1	-	7.9	6.4	5.2	4.2	3.3	2.8	2.4	2.0	1.7	1.8
33 South China Sea	-	-	5.6	7.8	10	3.9	2.5	1.6	1.0	0.6	0.4	0.3
34 Beringg Sea	-	-	7.8	6.0	4.6	3.5	2.7	2.0	1.5	1.2	0.9	2.2
35 Indonesian Archipelago	6.0	6.0	5.8	5.3	4.8	4.3	4.0	3.6	3.3	3.0	2.7	2.5
36 Atlantic sector of Antarctic	-	-	1.5	1.2	1.0	0.8	0.7	0.5	0.4	0.4	0.3	0.2
37 Indian sector of Antarctic	4.3	3.0	2.1	1.4	1.0	0.7	0.5	0.3	0.2	0.2	0.1	0.1

395

3.1 North Pacific Ocean (Box 1-3)

Figure 2a shows the temporal variations in the 0.5-yr median ^{137}Cs values in the subarctic North Pacific Ocean (Box 1), western North Pacific Ocean (Box 2), and astern North Pacific Ocean (Box 3). The ^{137}Cs in this region largely originated
400 from atmospheric deposition due to large-scale weapons tests (e.g., Aoyama et al., 2006; Inomata et al., 2012), the Chernobyl accident in 1986 (Miyao et al., 1989), and the F1NPS accident after 2011 (e.g., Aoyama et al., 2016a, b; Inomata et al., 2016). The temporal variations in the 0.5-yr median values of ^{137}Cs were the highest in the middle and late 1950s. In the 1960s, the 0.5-yr median values of ^{137}Cs increased gradually and reached a maximum in 1968. Then, the values decreased exponentially.

The 0.5-yr median values of ^{137}Cs after approximately 1970 became even smaller than those in the 1960s because the
405 supply due to ^{137}Cs deposition was negligible. This implies that the variations in the ^{137}Cs activity concentrations after 1970 strongly depended on the physical processes in the ocean. Until the early 1960s, the 0.5-yr median values of ^{137}Cs in the subarctic North Pacific Ocean and western North Pacific Ocean were higher than those in the eastern North Pacific Ocean. However, the 0.5-yr median values of ^{137}Cs in the eastern North Pacific Ocean increased in the 1960s and were slightly higher than those in the western North Pacific Ocean in the 1970s. A small peak that occurred in 1986 was caused by the deposition

of ^{137}Cs from the Chernobyl accident. The supply of ^{137}Cs due to Chernobyl fallout in the western and eastern North Pacific Ocean was larger than that in the subarctic North Pacific Ocean. After 2011, the 0.5-yr average ^{137}Cs values increased in this region. However, the maximum values in the eastern North Pacific Ocean were several years later than those observed in the subarctic and western North Pacific Ocean due to the basin-scale transport of ^{137}Cs in the North Pacific Ocean.

3.2 Marginal seas of the western North Pacific Ocean (Box 14, 31-34)

The temporal variations in the 0.5-yr ^{137}Cs values in the marginal seas of the North Pacific Ocean (the Japan Sea (Box 14), Sea of Okhotsk (Box 31), Eastern China Sea (Box 32), South China Sea (Box 33), and Bering Sea (Box 34)) are displayed in Fig. 2b. The 0.5-yr ^{137}Cs values in the marginal seas of the North Pacific Ocean also decreased exponentially. In 1986, a small peak due to ^{137}Cs fallout from the Chernobyl accident was observed in the Japan Sea and Sea of Okhotsk. In the 1980s, the 0.5-yr median value of ^{137}Cs was also high in the South China Sea. After the 1990s, the 0.5-yr median value of ^{137}Cs in the Sea of Okhotsk was smaller than those in the other boxes (the Japan Sea, Eastern China Sea, and South China Sea) in this region. An increase in the 0.5-yr average ^{137}Cs values in 2011 occurred in the Japan Sea, Sea of Okhotsk, and Bering Sea because of ^{137}Cs deposition originating from the F1NPS. In the Japan Sea and Eastern China Sea, the 0.5-yr median values of ^{137}Cs gradually increased after the F1NPS accident. In addition, an increase in the 0.5-yr median values of ^{137}Cs derived from the F1NPS occurred gradually in the Sea of Okhotsk and the Bering Sea.

3.3 Subtropical, equatorial Pacific Ocean and Indonesian Archipelago (Box 4-9, 35)

The 0.5-yr median values of ^{137}Cs in the western subtropical North Pacific Ocean (Box 4) in the late 1950s were significantly high (62-73 Bam^{-3}) due to local fallout (Fig. 2c). In the 1970s and 1980s, the 0.5-yr median values of ^{137}Cs almost constantly varied in the eastern subtropical North Pacific Ocean (Box9) and higher than those in other region. The values in the western subtropical North Pacific Ocean and western equatorial Pacific Ocean were almost constant in the 1970s and 1980s. In the eastern equatorial Pacific Ocean (Box 7) and eastern subtropical South Pacific Ocean (Box 9), the values increased gradually. After the mid-1980s or the 1990s, the 0.5-yr median ^{137}Cs values showed an exponential decrease until 2011. The 0.5-yr median values of ^{137}Cs in the Indonesian Archipelago (Box 35) showed almost the same range as those in the western subtropical and equatorial Pacific Ocean.

3.4 South Pacific Ocean (Boxes 10-12 and 19)

In the South Pacific Ocean (the western South Pacific Ocean (Box 10), eastern South Pacific Ocean (Box 11), eastern Southern Ocean (Box 12), and middle Southern Ocean (Box 19)), as shown in Fig. 2d, the 0.5-yr median ^{137}Cs activity concentrations in 1961 ranged from 1.4 to 2.5 Bq m^{-3}, whereas in 1967, the 0.5-yr median of ^{137}Cs increased to 4.5–9.9 Bq m^{-3}. Afterwards, the 0.5-yr median value of ^{137}Cs decreased exponentially, although the available data were limited. Moreover, substantially lower 0.5-yr median ^{137}Cs values of less than 1 Bq m^{-3} were observed in the middle Southern Ocean in 2013.

3.5 Antarctic Ocean (Boxes 13, 36, and 37)

The 0.5-yr median ^{137}Cs activity concentrations in the Antarctic Ocean were the lowest in the global ocean, although the measurements data were very limited (Fig. 2e). The 0.5-yr median ^{137}Cs activity concentrations from the 1960s to the 2010s decreased from 3.3 to 0.01 Bq m^{-3} in the Pacific sector of the Antarctic Ocean (Box 13) and from 1.6 to 0.4 Bq m^{-3} in the Atlantic sector of the Antarctic Ocean (Box 36). In the Indian sector of the Antarctic Ocean, the 0.5-yr median ^{137}Cs activity concentrations decreased from 5.0 to 1.1 Bq m^{-3} during the period from 1961.5 to 1978 (Box 37). The decreasing rate in the

Antarctic region was larger than those in the other regions. These lowest 0.5-yr median ^{137}Cs values and larger decreasing rates

450 were due to the long distance from the dominant ^{137}Cs fallout area. The transport of ^{137}Cs from the Southern Ocean would be prevented by the Antarctic Circumpolar circulations. The upwelling of seawater from the deeper layers in the Antarctic Ocean may also have caused dilution of the ^{137}Cs activity concentrations, resulting in the lowest ^{137}Cs values (Kumamoto et al., 2016).

3.6 Indian Ocean (Boxes 15, 16, and 17)

In the 1960s, the 0.5-yr median ^{137}Cs activity concentration was higher in the Arabian Sea (Box 15, 8.9 Bq m^{-3}) than

455 those in the Indian Ocean (Box 16, 5.6-6.6 Bq m^{-3}) and the Southern Ocean (Box 17, 2.7-4.0 Bq m^{-3}) (Fig. 2f). The median ^{137}Cs activity concentrations in the 1960s showed a latitudinal gradient, with higher values in the northern areas and lower values in the southern areas. The 0.5-yr median ^{137}Cs activity concentrations in the Arabian Ocean and Southern Ocean were almost constant in the 1970s, whereas those in the Indian Ocean increased slightly (3.4-5.6 Bq m^{-3}) in the 1970s. These values in the three boxes decreased to approximately 1.3-2.3 Bq m^{-3} in the late 1990s and the early 2000s, although there were no

460 available data in the 1980s. The 0.5-yr median ^{137}Cs activity concentrations in the Indian Ocean were higher than those in the Arabian Ocean and the Southern Ocean. Note that the lowest values (0.15 Bq m^{-3}) were observed in 2012 in the Arabian Sea.

3.7 Atlantic Ocean (Boxes 28-30)

The Atlantic Ocean (the North Atlantic Ocean, Box 28; the Central Atlantic Ocean, Box 29; and the South Atlantic

465 Ocean, Box 30) had a north–south gradient of 0.5-yr median ^{137}Cs values, with higher values in the North Atlantic Ocean and lower values in the South Atlantic Ocean (Fig. 2g). In the North Atlantic Ocean, relatively high values were observed in the 1970s but then rapidly decreased after 1980. After 2000, an exponentially decreasing trend was not observed in the North Atlantic Ocean. The values slightly increased and reached the maximum value (2.4 Bq m^{-3}) in 2005, after which they gradually decreased. In the Central Atlantic Ocean, the temporal variations in the 0.5-yr median values of ^{137}Cs exponentially decreased,

470 although the data were very limited. In the South Atlantic Ocean, the 0.5-yr median values also decreased exponentially after 1970. Notably, the 0.5-yr median values in 2003 in the Central and South Atlantic Oceans slightly increased compared to those in 2002.

3.8 Arctic, northern North Atlantic Ocean and its marginal seas (Boxes 18, 20, 22, and 25)

475 Fig. 2h shows the temporal variations in the 0.5-yr median values of ^{137}Cs in the Arctic Ocean (Box 18), Barents Sea and coast of Norway (Box 20), North Sea (Box 22) and northern North Atlantic Ocean (Box 25.1, 25.2). The dominant sources of ^{137}Cs in this area are the global-scale atmospheric deposition in the 1960s by large-scale nuclear weapons tests and two nuclear fuel reprocessing plants after the 1970s. In these regions, the 0.5-yr median values of ^{137}Cs did not decrease exponentially due to the ^{137}Cs discharged from the nuclear fuel reprocessing plants. In the mid-1970s, the 0.5-yr median ^{137}Cs

480 activity concentrations in the North Sea and northern North Atlantic Ocean increased rapidly, and reached to the maximum in 1977 and 1980.5, respectively. Thereafter, the 0.5-yr median ^{137}Cs activity concentrations in these regions rapidly decreased, and the decreasing rate became small after 1990, which was associated with the reduced amount of released ^{137}Cs.

In the Arctic Ocean, the 0.5-yr median ^{137}Cs activity concentrations increased until the middle 1970s and then decreased. The overall 0.5-yr median ^{137}Cs activity concentrations until the 1970s in the Arctic Ocean were lower than those in the

485 surrounding oceans.

3.9 Irish Sea and English Chanel (Boxes 23 and 24)

The ^{137}Cs activity concentrations in the Irish Sea (Box 23) and English Channel (Box 24) were primarily affected by the discharge from the nuclear fuel reprocessing plants (Fig. 2i). Because the 0.5-yr median value of ^{137}Cs is significantly higher than those in other regions, the scale of the y-axis changes from 10^{-1} to 10^6 Bq m^{-3}. In the Irish Sea (Box 23.1), which is the discharge region, the 0.5-yr median ^{137}Cs activity concentrations increased rapidly and reached 38533 Bq m^{-3} in 1976 and then decreased rapidly. The 0.5-yr median ^{137}Cs activity concentration decreased with increasing distance from the discharge region. In Box 23.2, the maximum value (2453 Bq m^{-3}) was observed in 1977. The ^{137}Cs activity concentrations in the Celtic Sea (Box 23.4) were the lowest in this box. The decreasing gradient of the 0.5-yr median ^{137}Cs values reflected the controlled discharge amount.

In the English Chanel, the 0.5-yr median ^{137}Cs activity concentrations reached a maximum in 1980.5, and these also decreased over time. The 0.5-yr median ^{137}Cs activity concentrations in 2017 in the English Chanel were 1.9 Bq m^{-3}.

3.10 Baltic Sea (Box 21), Black Sea (Box 26) and Mediterranean Sea (Box 27)

In the Baltic Sea (Box 21), the 0.5-yr median values of ^{137}Cs increased gradually in the 1970s due to the inflow of the ^{137}Cs released from reprocessing plants (Fig. 2j). In 1986, the 0.5-yr median values of ^{137}Cs increased rapidly (177 Bq m^{-3}) due to the deposition of ^{137}Cs derived from the Chernobyl accident. The 0.5-yr ^{137}Cs median values in the Baltic Sea decreased over time. The 0.5-yr median ^{137}Cs activity concentration in the Baltic Sea in 2017 was estimated to be 15.3 Bq m^{-3}.

The 0.5-yr median value of ^{137}Cs in the Black Sea (Box 26) in 1977 and 1978.5 was approximately 17 Bq m^{-3}, and in 1986, it increased to 299 Bq m^{-3}, which was at least 18 times higher than that before the Chernobyl accident (Fig. 2j). The 0.5-yr median value of ^{137}Cs decreased rapidly to 60 Bq m^{-3} in 1989. The 0.5-yr median ^{137}Cs value in 2002 was almost equal (18.3 Bq m^{-3}) to that before the Chernobyl accident. The rapid decrease in surface ^{137}Cs could be due to the strong intrusion of surface waters to the deep layers, ^{137}Cs inflow into the Mediterranean Sea after passing through the Bosporus Strait, and radioactive decay (Egorov, 1999; Delfanti et al., 2014). However, Black Sea continues to receive ^{137}Cs derived from Chernobyl by the runoff from rivers (Gulin et al., 2013).

In the Mediterranean Sea (Box 27), the 0.5-yr median value of ^{137}Cs varied from 0.8 to 12 Bq m^{-3} before the Chernobyl accident (Fig. 2j). After the accident, it increased to 142 and 155 Bq m^{-3} in 1986.5 and 1987.5, respectively. In the following years, the 0.5-yr median value of ^{137}Cs decreased rapidly and became almost the same as that before the Chernobyl accident. This rapid decrease could have been due to the stronger intrusion of bottom water from the surface (Delfanti et al., 2000; Delfanti and Papucci, 2010).

3.11. Comparison with the 0.5-yr median ^{137}Cs values in the Pacific Ocean, Indian Ocean, and Atlantic Ocean

Fig. 3 shows a comparison of the 0.5-yr median ^{137}Cs values in the Pacific Ocean, Indian Ocean, and Atlantic Ocean. A significant feature is that the highest values were observed in the western North Pacific Ocean, and the values decreased exponentially over time until 2011. In contrast, the values in the western equatorial Pacific Ocean, western subtropical South Pacific Ocean, and Indian Ocean increased gradually in the 1970s and 1980s, followed by a decrease after the 1990s. The difference in the 0.5-yr median ^{137}Cs values in the Pacific Ocean and Indian Ocean became very small after 1980. Although the data are very limited, the 0.5-yr median ^{137}Cs values in the South Atlantic Ocean were lower than those in the Pacific Ocean and the Indian Ocean. In the 2000s, the 0.5-yr median ^{137}Cs values in the South Atlantic Ocean was increased and the values were close to those in the Pacific Ocean and Indian Ocean.
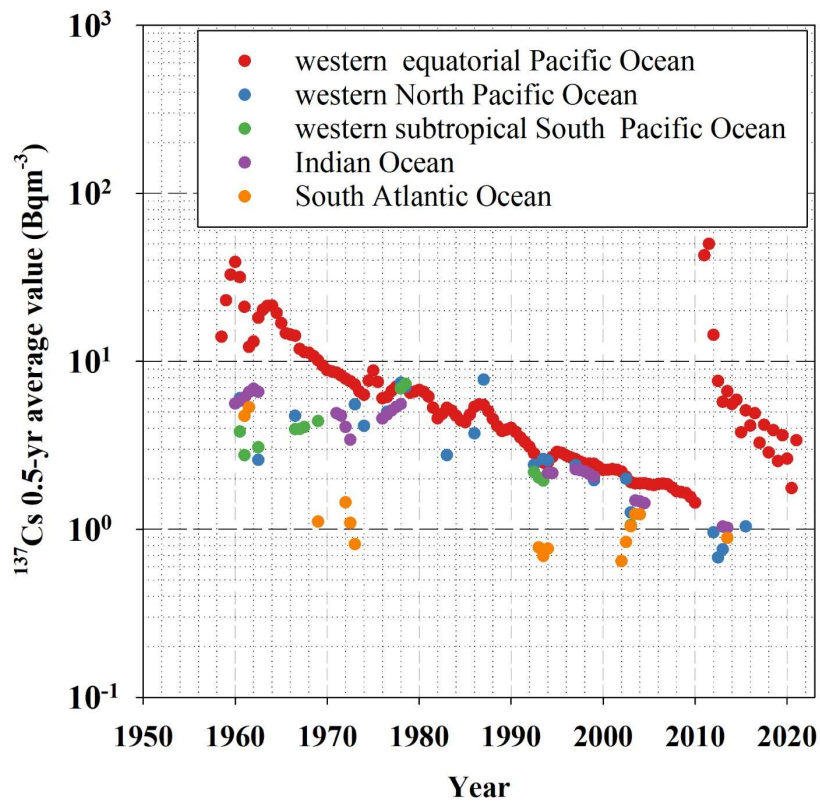
Figure 3: Comparison with 0.5-yr median ^{137}Cs values in the Pacific Ocean, Indian Ocean, and Atlantic Ocean.

3.12. Tap of the 0.5-yr median ^{137}Cs values in the surface mixed layer

530   Fig. 4 shows the temporal variation in the 0.5-yr median ^{137}Cs values in the western North Pacific Ocean and the Japan Sea as a typical case because the sequential time series are available in these boxes. Estimated Tap on the western North Pacific Ocean was 15.0 years, whereas Tap in the Japan Sea was estimated to be 16.4 years. Although we did not show that Figures, Tap in the Eastern China Sea was estimated to be 17.7 years. The longer Tap in the Japan Sea and Eastern China Sea compared with those in the western North Pacific Ocean suggest that ^{137}Cs provided into the Japan Sea and the Eastern China
535   Sea from the western North Pacific Ocean.

        The Tap estimated in all boxes until 2010 are listed in Table 3. For Tap1, which is the longest, at 52.0 years, is estimated in the western equatorial Pacific Ocean, and Tpo in this box is negative. The shorter Tap1, which is approximately 4 years, is in the Japan Sea. In the case of Tap2, the longer Tap values are in the Indonesian Archipelago (36.7 years) with negative Tpo (-169.2 years) and western subtropical North Pacific Ocean (34.1 years) with negative Tpo (-260.7 yeras). In
540   Tap3, longer Tap occurs in 38.0 years for the Central Atlantic Ocean, 15.4 years for the South Atlantic Ocean, 25.2 years for western subtropical North Pacific Ocean, and 15.6 years for western equatorial Pacific Ocean. In the several boxes with the longer Tap, Tpo is estimated to be negative as shown in Table 3..The negative Tpo   suggests that the physical oceanographic processes were controlled the variation of ^{137}Cs activity concentrations.

545

550

(a)
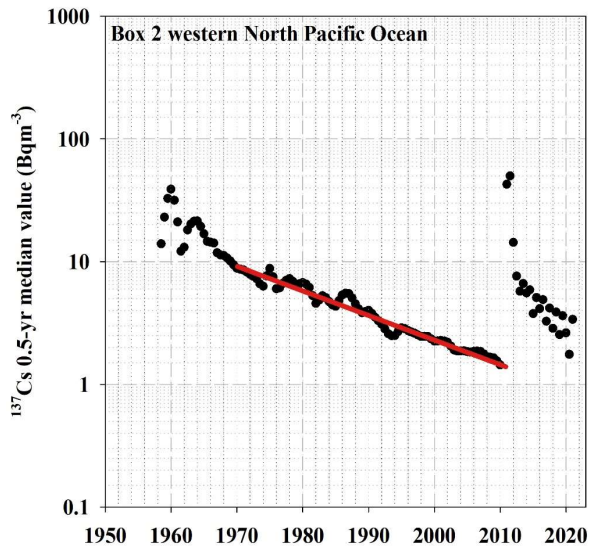
(b)
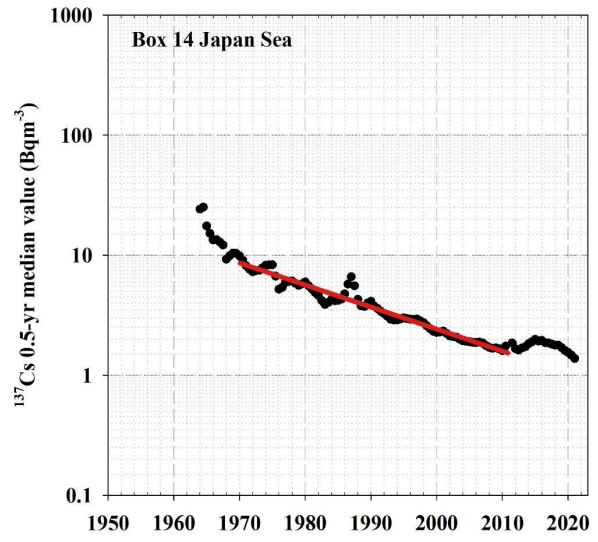
Figure 4: Temporal variation in the 0.5-yr median ^{137}Cs values. (a) Western North Pacific Ocean, (b) Japan Sea. The lines represent the exponential decay of the 0.5-yr ^{137}Cs median value between 1970 and 2010.

Table 3. Tap and Tpo in the global ocean.

		Start	End	Tap	Tpo
Tap	western North Pacific Ocean	1970	2010	15.0	29.9
	Eastern China Sea	1970	2010	17.7	42.8
	Japan Sea	1970	2010	16.4	35.9
Tap1	subarctic North Pacific Ocean	1957.5	1969.5	8.6	12.1
	western subtropical North Pacific Ocean	1957	1970	4.3	5.0
	western equatorial Pacific Ocean	1960.5	1966.5	52.0	-71.8
	eastern equatorial Pacific Ocean	1963.5	1969.5	5.8	7.2
	eastern subtropical South Pacific Ocean	1966	1970	6.0	7.5
Tap2	subarctic North Pacific Ocean	1970.5	1984.5	9.6	14.0
	eastern North Pacific Ocean	1970.5	1985	8.8	12.4
	western subtropical North Pacific Ocean	1970	1989	34.1	-260.7
	Indonesian Archipelago	1973	1997	36.7	-169.2
Tap3	subarctic North Pacific Ocean	1990.5	2009.5	18.2	45.8
	Sea of Okhotsk	1992	2010	24.0	117.0
	western subtropical North Pacific Ocean	1990	2011	25.2	153.0
	western equatorial Pacific Ocean	1992	2003	15.6	32.5
	Indonesian Archipelago	1973	1997	36.7	-169.2
	Baltic Sea	1990	2017	11.5	18.6
	North Atlantic Ocean	1992	2017	21.3	72.3
	Central Atlantic Ocean	1992	2016	38.0	-146.5
	South Atlantic Ocean	1994	2013.5	15.4	31.4

3.13 Horizontal distribution of ^{137}Cs in the surface mixing layer in the global ocean

3.13.1 Horizontal distribution of ^{137}Cs deposition as of the 1st of January 1970

The atmospheric deposition of ^{137}Cs due to the nuclear weapons tests in the global earth as of the 1st of January 1970 is estimated to be 874±90 PBq, with a two-minute latitude/longitude grid resolution. The global fallout of ^{137}Cs in the Northern Hemisphere is 773±80 PBq. At this time, the deposition in the global ocean is estimated to be 577±60 PBq, which is an initial value in this study. These results are good agreement with the estimation of the ten degree latitude/longitude grid by Aoyama et al. (2006), in which the atmospheric deposition of ^{137}Cs derived from nuclear weapons tests in the Northern Hemisphere was 765 PBq and 866 PBq in the global earth on the 1st of January 1970.

Fig. 5 shows the horizontal distributions of ^{137}Cs deposition density in each box in the global ocean. These values are also listed in Table 4. The ^{137}Cs deposition density is high in the midlatitude region in the North Pacific Ocean (the Japan Sea, subarctic North Pacific Ocean, Okhotsk Sea, western North Pacific Ocean, and eastern North Pacific Ocean) and the northern North Atlantic Ocean. In the North Pacific Ocean, these regions correspond to the area in which the Kuroshio Current and Kuroshio Extension are transported. In the northern North Atlantic Ocean, the higher ^{137}Cs deposition area influences the Gulf Stream flow. The dominant features of these regions in the North Pacific Ocean and northern North Atlantic Ocean have received larger precipitation amounts and the occurrence of stratosphere–troposphere air mass exchange (Aoyama et al., 2006). The larger air mass exchange between the stratosphere and troposphere means that the ^{137}Cs injected into the stratosphere by the large-scale weapons tests is transported into the troposphere and deposited on the surface by precipitation. South of 5°N,

the ^{137}Cs deposition density is lower than that in the northern region and there is no significant difference between the open oceans (Pacific, Atlantic, and Indian Oceans). Distribution of ^{137}Cs deposition a two-minute latitude/longitude grid resolution is also well reproduced in the ten degree latitude/longitude grid deposition.

However, these estimations were almost 1.4 times larger than those in the estimation by using a model simulation (UNSCEAR, 1993), with an estimated value of 545 PBq (Aoyama, 2019). The large difference occurred in the meridional distribution in the mid-latitude. These corresponds to have larger ^{137}Cs fallout region, where Kuroshio Current and its extension areas (latitude 20-40°N) in the Pacific Ocean and Gulf stream transport area (latitude 30-50°N) in the Atlantic Ocean. It was also reported that the ^{137}Cs water column inventory in the North Pacific Ocean was 2-3 times larger than those in the cumulative ^{137}Cs fallout amount in the same latitude in the modelling results in UNSCEAR (1993) (Aoyama, 2019). Because reconstructed ^{137}Cs deposition in Aoyama et al. (2006) was based on the historical observed data, uncertainty of model would cause the underestimation of ^{137}Cs deposition amount.
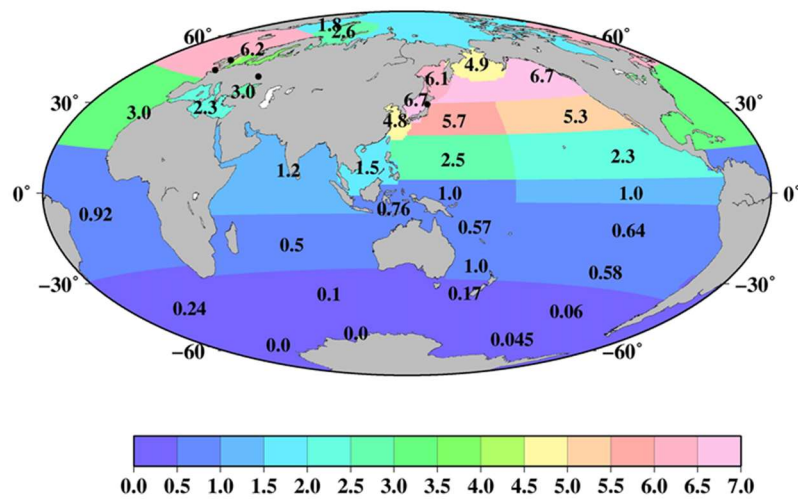
 (b)
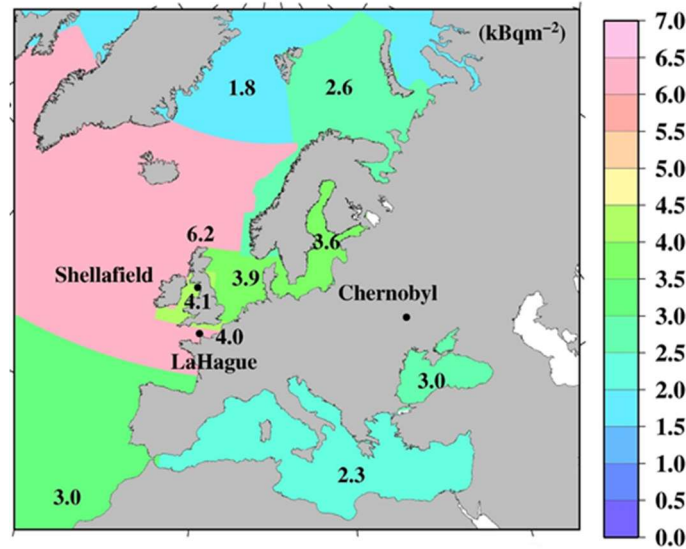
Figure 5: Horizontal distributions of ^{137}Cs deposition density (KBq m^{-2}) as of the 1st of January 1970. (a) Global Ocean, (b) Northern North Pacific Ocean and its marginal seas. Black circles are locations of the F1NPS, Sellafield, La Hague, and Chernobyl power plants.

655

Fig. 6 shows the horizontal distribution of the ^{137}Cs deposition amount as of the 1st of January 1970 in the surface mixed layer in the global ocean. These data are also listed in Table 4. In the Pacific Ocean, a higher ^{137}Cs deposition amount occurs in the subarctic North Pacific Ocean (71.6 PBq), western North Pacific Ocean (40.8 PBq), eastern North Pacific Ocean (52.4 PBq), and subtropical eastern North Pacific Ocean (47.9 PBq). In the Atlantic Ocean, a higher ^{137}Cs deposition amount

660 is found in the northern North Atlantic Ocean (sum of Boxes 25.1 and 25.2; 56.1 PBq) and North Atlantic Ocean (69.8 PBq). The ^{137}Cs deposition amount in the Atlantic Ocean shows a significant latitudinal gradient, which is 27.3 PBq for the Central Atlantic Ocean and 5.1 PBq for the South Atlantic Ocean. In the Indian Ocean, the ^{137}Cs deposition amount also has a north–south gradient. The ^{137}Cs deposition amount is the lowest in the Pacific sector (0.05 PBq), Atlantic sector (0.0 PBq), and Indian sector (0.0 PBq) of the Antarctic Ocean.

665 (a)   (b)
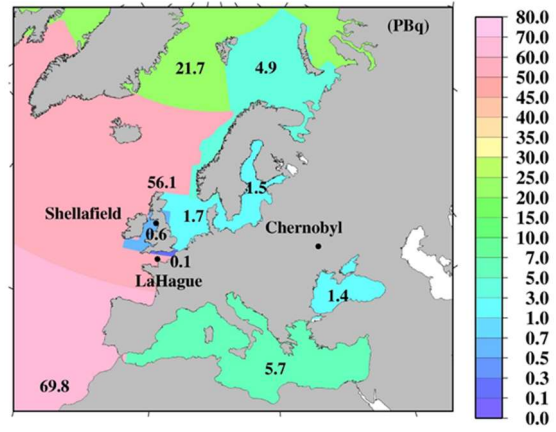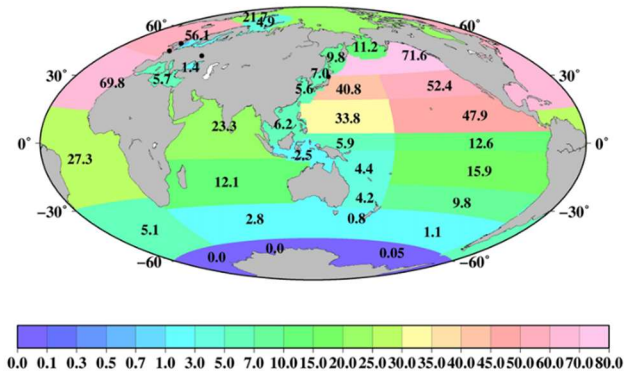
Figure 6: Horizontal distributions of the ^{137}Cs deposition amount (PBq) in each box as of the 1st of January 1970. (a) Global Ocean, (b) Northern North Pacific Ocean and its marginal seas. Black circles are locations of the F1NPS, Sellafield, La Hague,
670 and Chernobyl power plants.

675

680

685

690

695

Table 4. ^{137}Cs deposition density and inventory as 1 January, 1970.

box	^{137}Cs deposition density, 1970	^{137}Cs deposition inventory, 1970
	(kBq m^{-2})	(PBq)
1 subarctic North Pacific Ocean	6.7	71.6
2 western North Pacific Ocean	5.7	40.8
3 eastern North Pacific Ocean	5.3	52.4
4 western subtropical North Pacific Ocean	2.5	33.8
5 eastern subtropical North Pacific Ocean	2.3	47.9
6 western equatorial Pacific Ocean	1.0	5.9
7 eastern equatorial Pacific Ocean	1.0	12.6
8 western subtropical South Pacific Ocean	0.6	4.4
9 eastern subtropical South Pacific Ocean	0.6	15.9
10 western South Pacific Ocean	1.0	4.2
11 eastern South Pacific Ocean	0.6	9.8
12 eastern Southern Ocean	0.1	1.1
13 Pacific sector of Antarctic	0.005	0.05
14 Japan Sea	6.7	7.0
15 Arabian Sea	1.2	23.3
16 Indian Ocean	0.5	12.1
17 Southern Ocean	0.1	2.8
18 Arctic Ocean	1.8	21.7
19 Middle Southern Ocean	0.2	0.8
20 Barents Sea and Coast of Norway	2.6	4.9
21 Baltic Sea	3.6	1.5
22 North Sea	3.9	1.7
23.1 Irish Sea	4.1	0.03
23.2 Irish Sea	4.1	0.1
23.3 Irish Sea	4.1	0.2
23.4 Irish Sea	4.1	0.2
23.5 Irish Sea	4.1	0.02
24 English Channel	4.0	0.3
25.1 northern North Atlantic Ocean	5.5	2.0
25.2 northern North Atlantic Ocean	6.2	53.6
26 Black Sea	3.0	1.4
27 Mediterranean Sea	2.3	5.7
28 North Atlantic Ocean	3.0	69.8
29 Central Atlantic Ocean	0.9	27.3
30 South Atlantic Ocean	0.2	5.1
31 Sea of Okhotsk	6.1	9.8
32 Eastern China Sea	4.8	5.6
33 South China Sea	1.5	6.2
34 Berigng Sea	4.9	11.2
35 Indonesian Archipelago	0.8	2.5
36 Atlantic sector of Antarctic	0.0	0.0
37 Indian sector of Antarctic	0.0	0.0

700

3.13.2. Horizontal distribution of 0.5-yr median ^{137}Cs values in the global ocean

Fig. 7 shows the spatial variations in the 0.5-yr median ^{137}Cs values in the global ocean every 5 years. In 1970, the 0.5-year median ^{137}Cs values were higher in the North Pacific Ocean and lower in the South Pacific Ocean. In particular, the highest value (14.8 Bq m^{-3}) was observed in the eastern North Pacific Ocean. In the South Pacific Ocean, relatively high values

705 occurred in the western and western subtropical South Pacific Ocean (9.3 and 13.6 Bq m^{-3}) compared to those in the eastern region (3-4.3 Bq m^{-3}). The 0.5-yr median ^{137}Cs values in the Indonesian Archipelago (5.8 Bq m^{-3}) and the South China Sea (5.6 Bq m^{-3}) were almost the same or slightly higher than those in the western equatorial Pacific Ocean (5.4 Bq m^{-3}). In 1975, the 0.5-yr median ^{137}Cs values in the South China Sea were higher than those in the Indonesian Archipelago (Fig. 7b). In 1980 and 1985 (Fig. 7c, 7d), in the Pacific Ocean, higher values were found in the eastern subtropical Pacific Ocean (9.8 Bq m^{-3}).

710   In the North Pacific Ocean, the 0.5-yr median ^{137}Cs values were higher in the eastern region, whereas higher values in the South Pacific Ocean were found in the western region. In 1990, the 0.5-yr median ^{137}Cs values decreased, although the concentration distribution was similar to that of the 1980s (Fig. 7e). In particular, after 1990, the Indonesian Archipelago became the hot spot region, with relatively high 0.5-yr median ^{137}Cs activity values in the Pacific Ocean and Indian Ocean. Higher values in this region were still observed in 2015 (Fig. 7j). The latitudinal gradient, which was higher in the North

715 Pacific Ocean and lower in the South Pacific Ocean, became small, which lasted until 2010. In 2015, an increase in the 0.5-year median ^{137}Cs values was found in the western and subarctic North Pacific Ocean due to the release of ^{137}Cs from the F1NPS accident (Fig. 7j). The lowest value occurred in the Antarctic Ocean in the global ocean after 1970 (Fig. 7).

     In the Atlantic Ocean, a latitudinal gradient that was higher in the northern North Atlantic Ocean and North Atlantic Ocean (north of 30°N) than in the Central and South Atlantic Ocean occurs. In 2015, the values in the South Atlantic Ocean

720 (0.7 Bq m^{-3}) were almost equal to those in the Southern Ocean (0.6 Bq m^{-3}) (Fig. 7j). In the Atlantic Ocean, because of the discharged ^{137}Cs in the surface seawater from the nuclear reprocessing plants, i.e., the Sellafield plant, significantly higher 0.5-yr ^{137}Cs median values occurred in the Irish Sea, particularly at ^{137}Cs discharge points (Box 23.1), as shown in Figs. 8 and 9. The discharged ^{137}Cs was transported to the northern North Pacific Ocean (Box 25.1) and North Sea from the Irish Sea (Box 23.2). The 0.5-yr median ^{137}Cs values after 1985 (Fig. 8d) decreased gradually in accordance with the discharged amount of

725 ^{137}Cs (Fig. 9c). The increase in the 0.5-yr median ^{137}Cs values in the Baltic Sea (96 Bq m^{-3}) and Black Sea (56 Bq m^{-3}) in 1990 was caused by the deposition of ^{137}Cs from the Chernobyl accident (Figs. 8e, f). Contamination due to the Chernobyl accident continued in the Baltic Sea and Black Sea until 2015 (Fig. 8j).

730

735

740

745

750

(a)

(b)
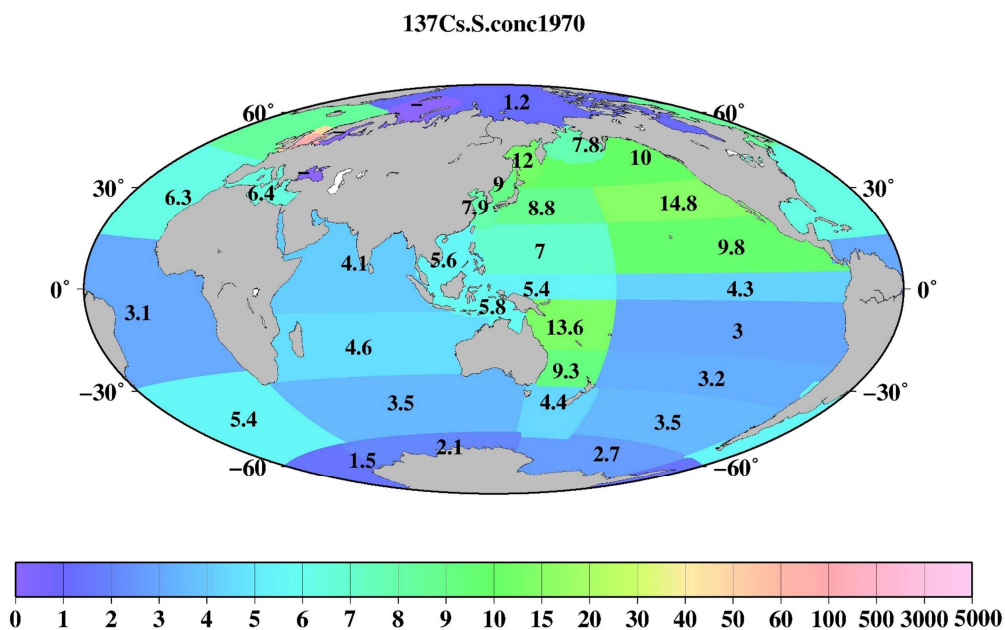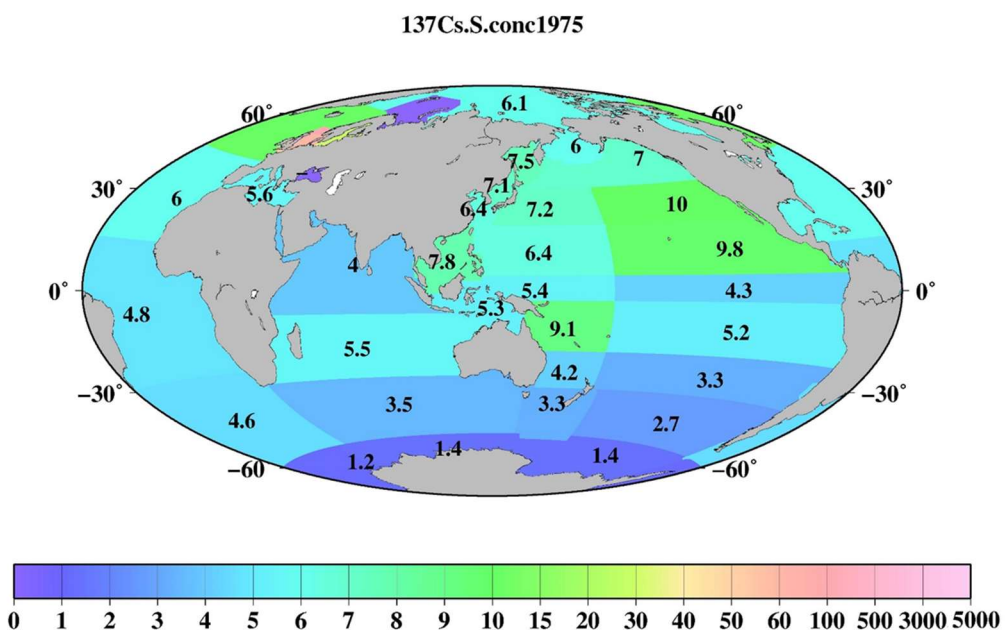
(c)
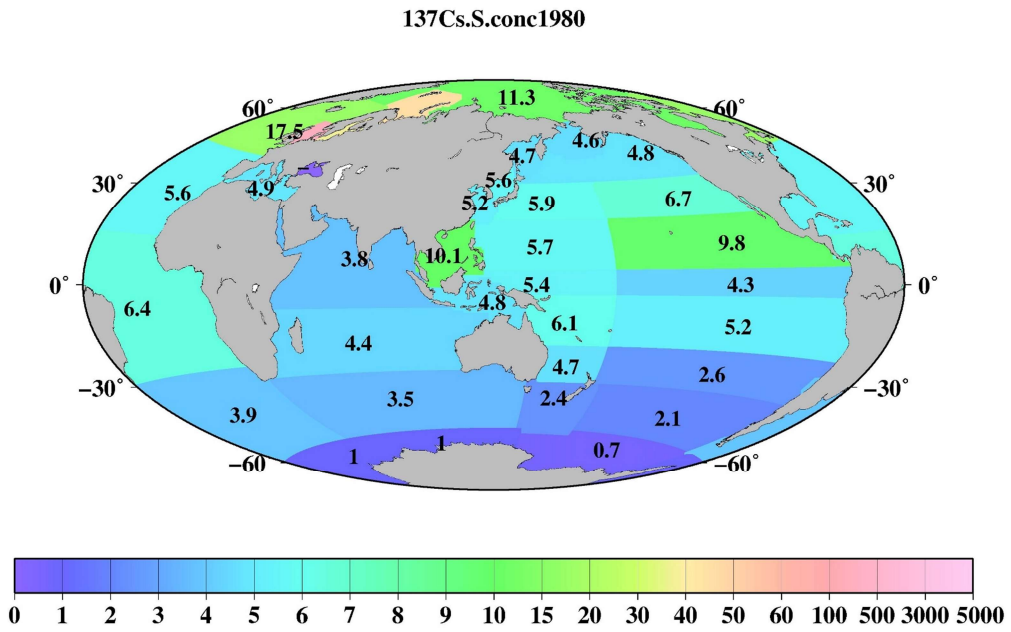
(d)
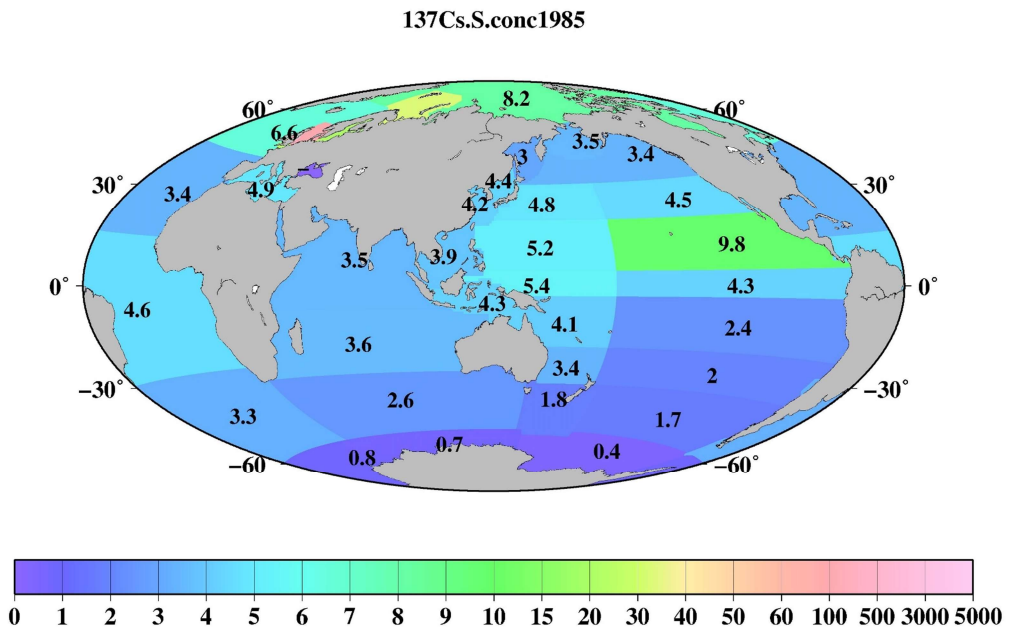
770

775

(e)
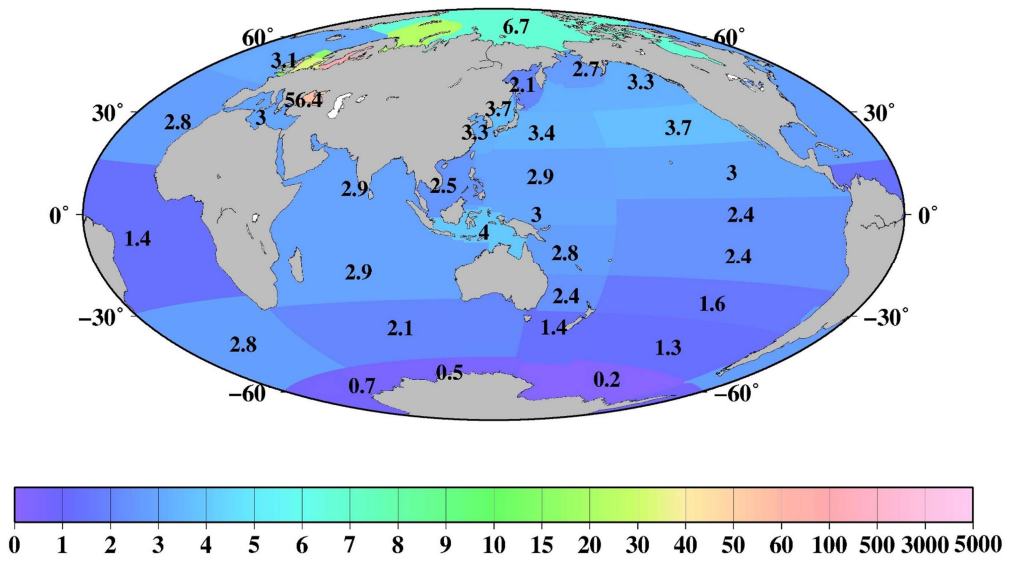
137Cs.S.conc1990

(f)

137Cs.S.conc1995

(g)

(h)

(i)

(j)
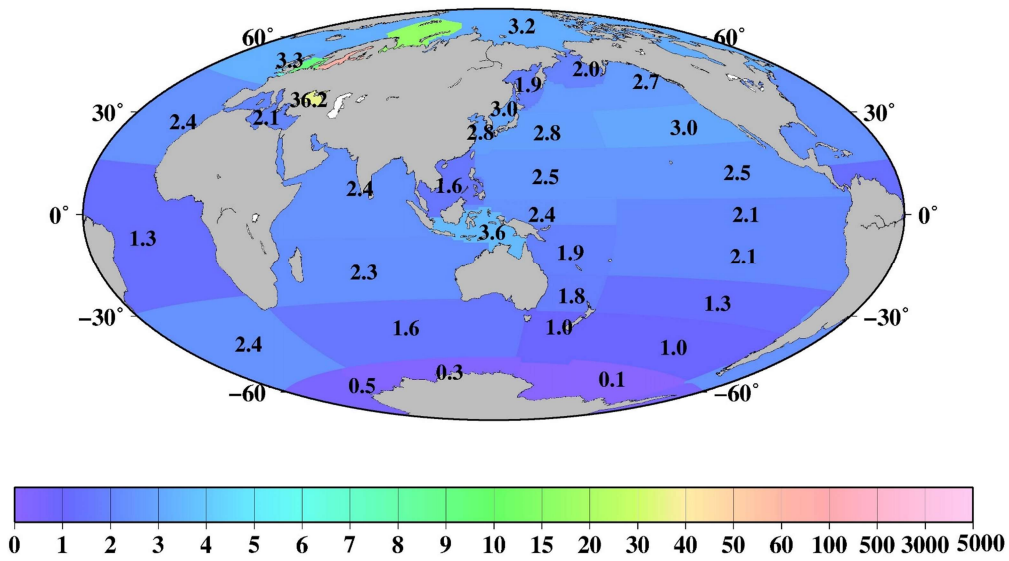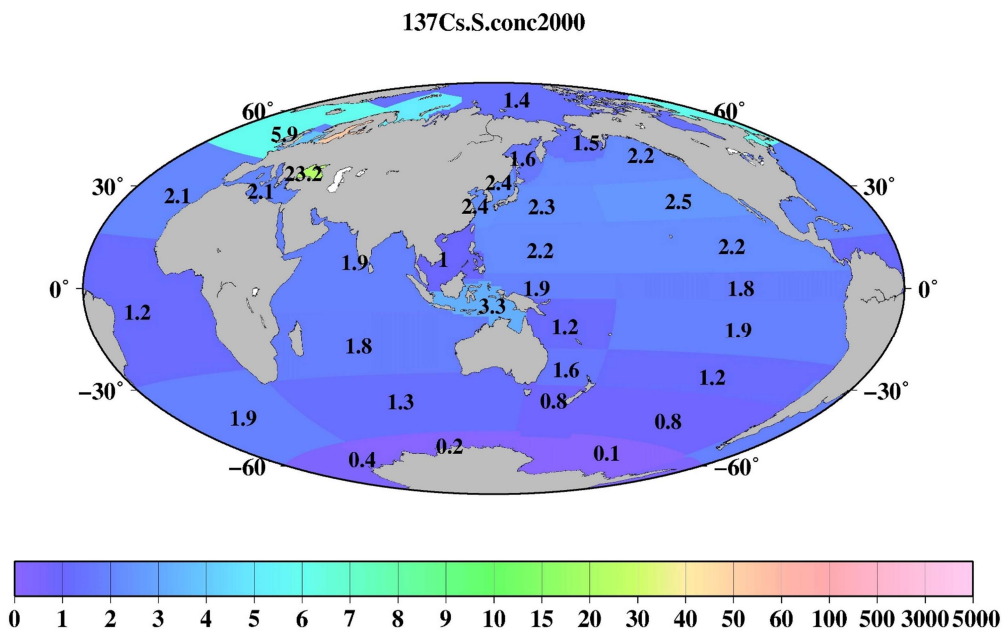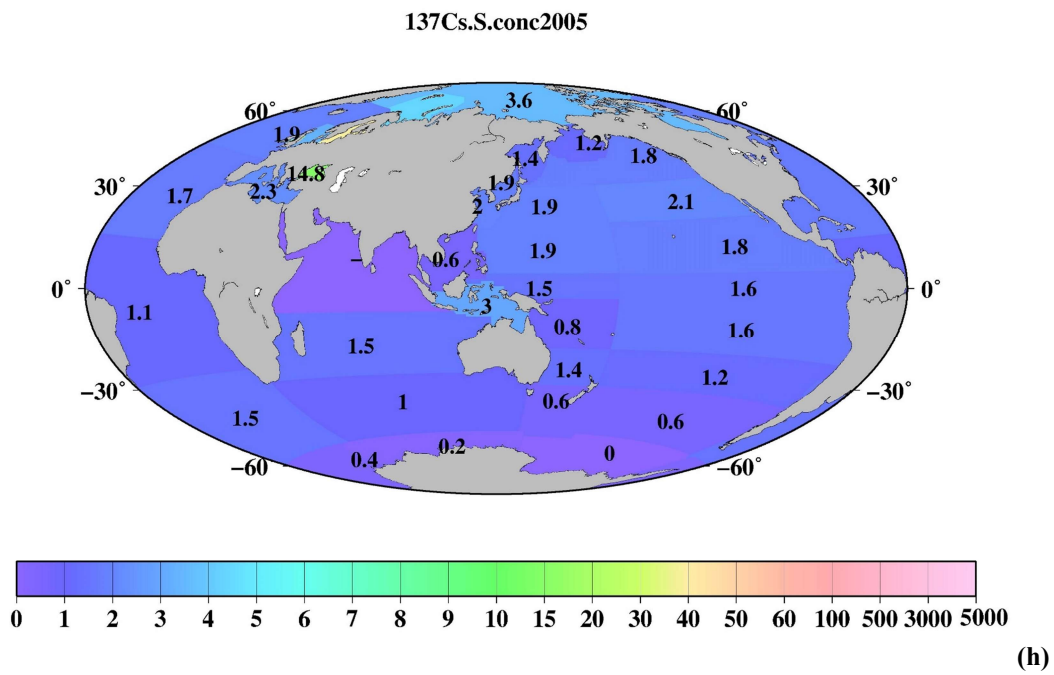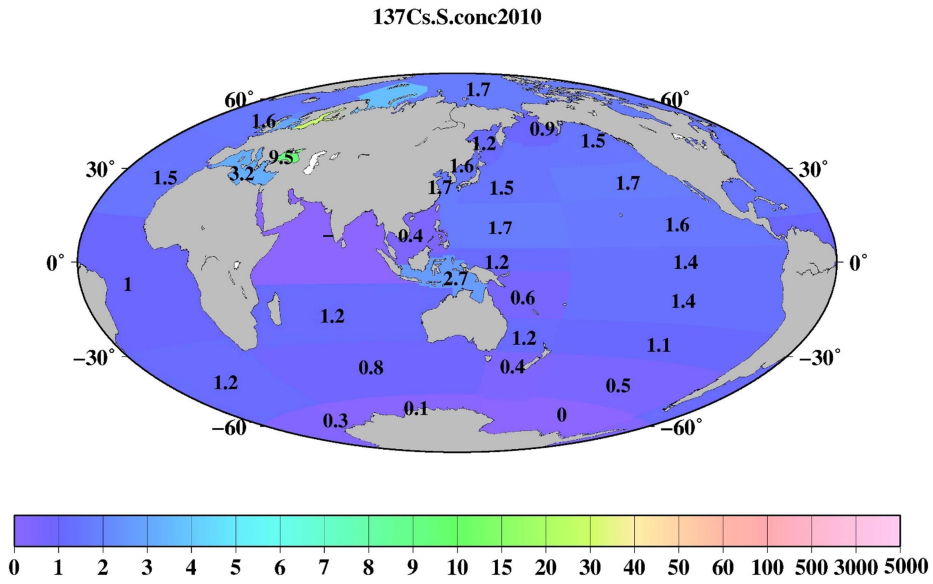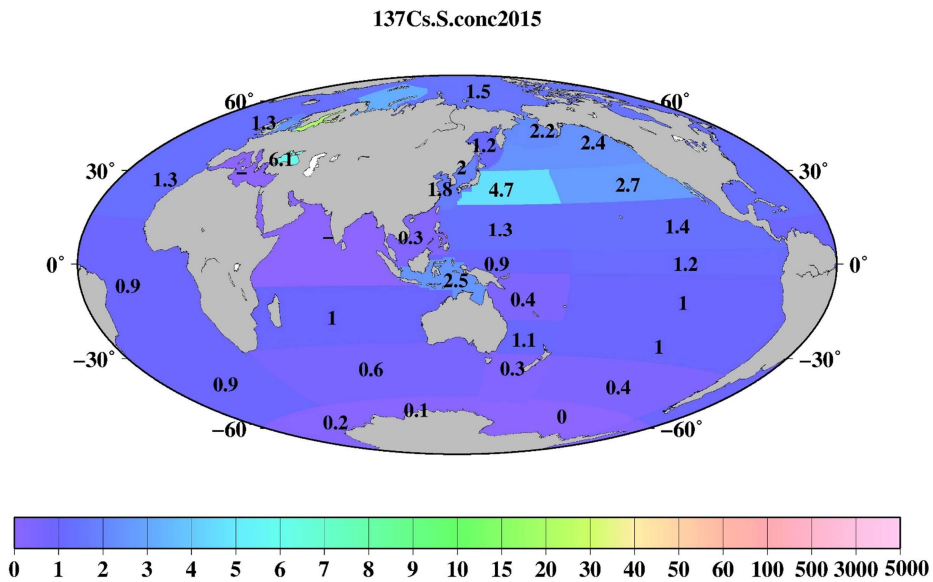
Figure 7: Horizontal distributions of the 0.5-yr median ^{137}Cs value in the surface mixed layer in the global ocean. The unit is Bqm^{-3}. (a) 1970, (b) 1975, (c) 1980, (d) 1985, (e) 1990, (f) 1995, (g) 2000, (h) 2005, (i) 2010, and (j) 2015.

(a)

1970

(b)
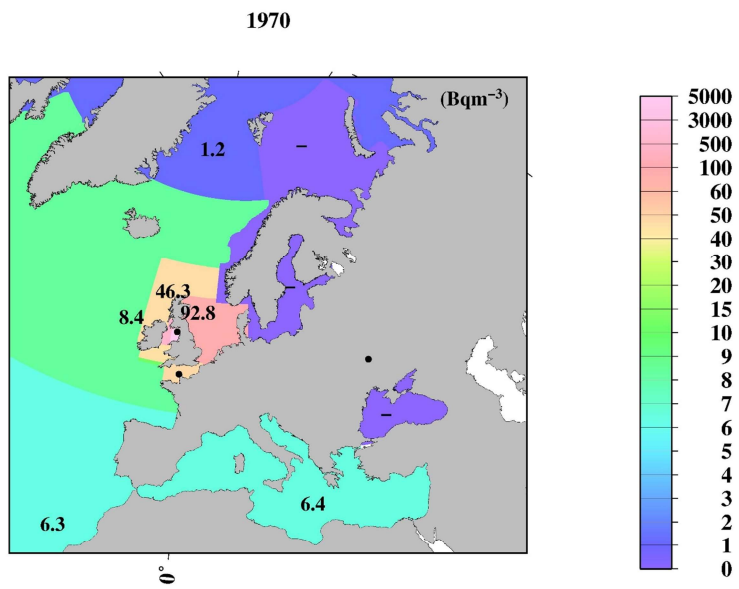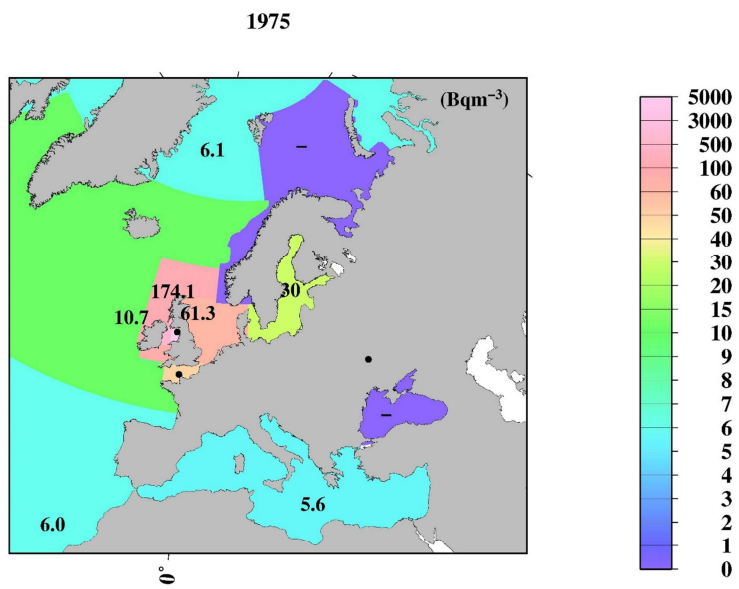
1975

825

830

835

(c)

(d)

840

845

850

(e)

1990

855

(f)
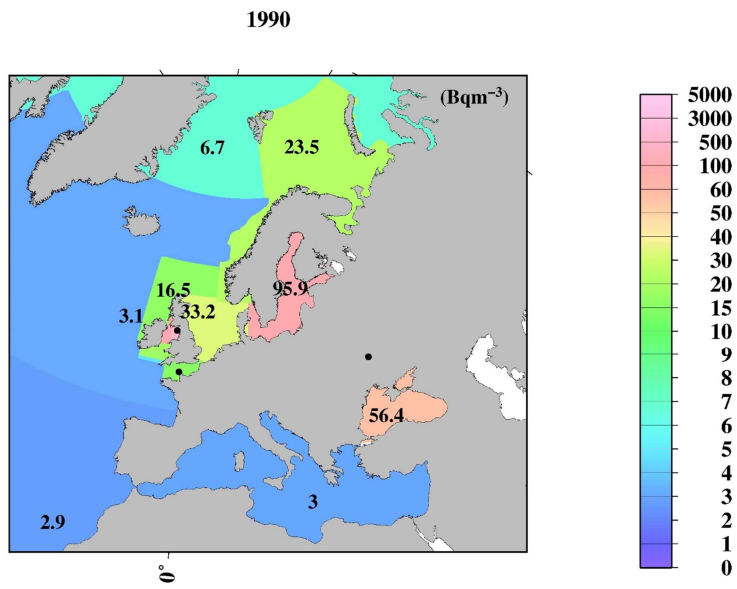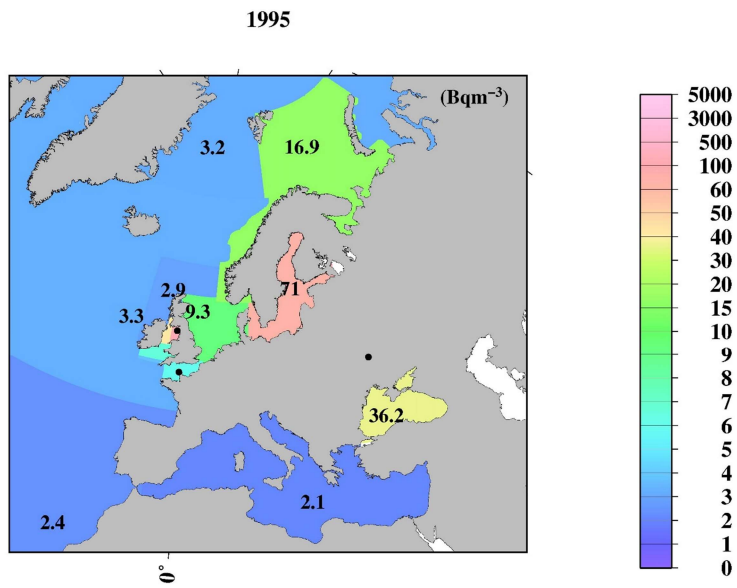
1995

860

865

(g)

870

(h)

875

880

(i)
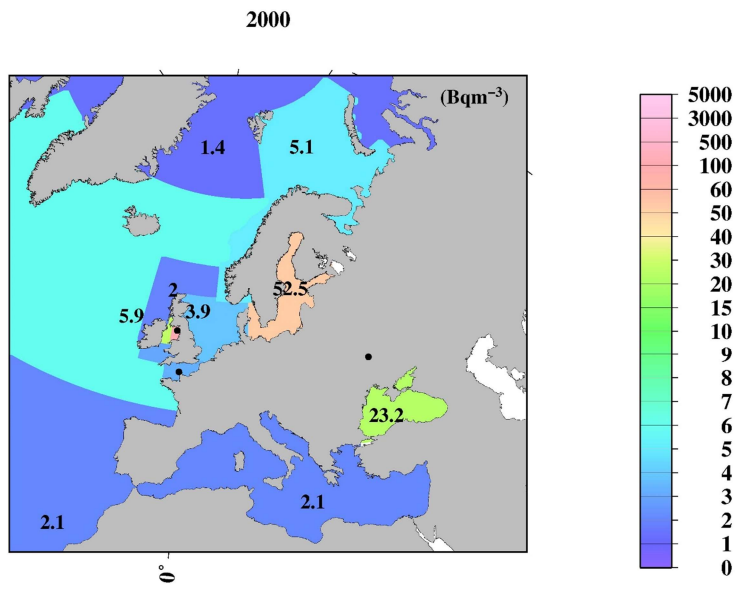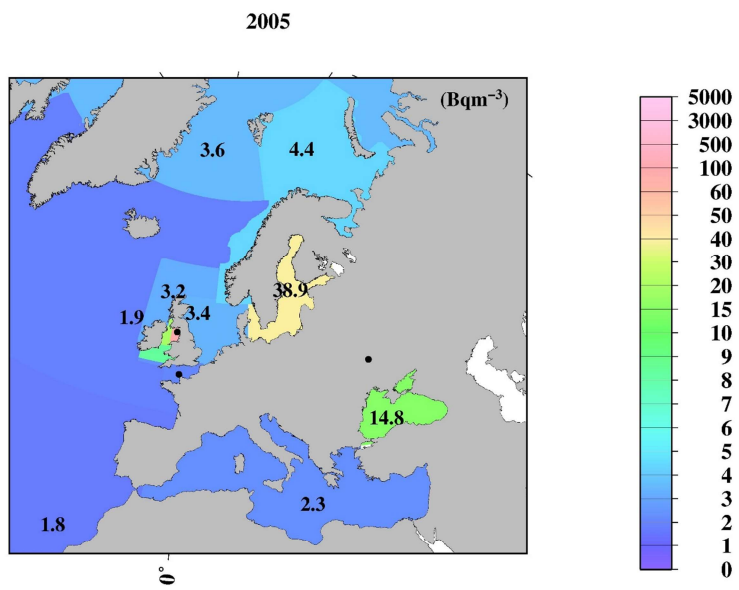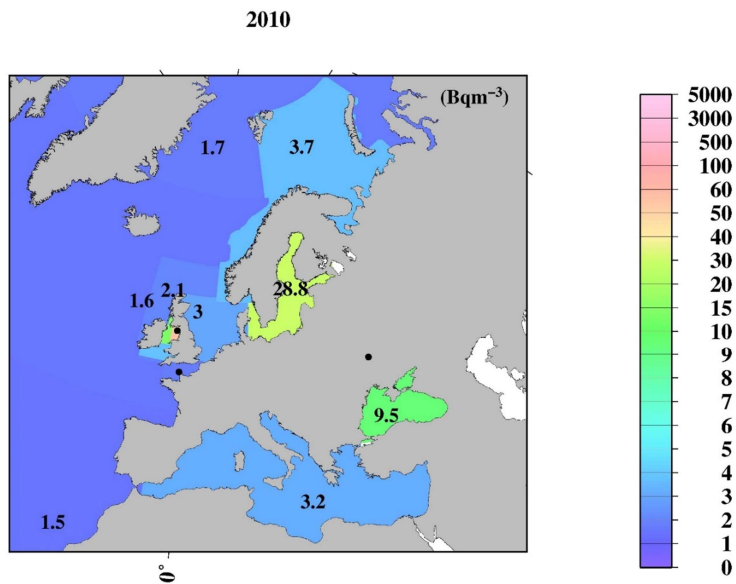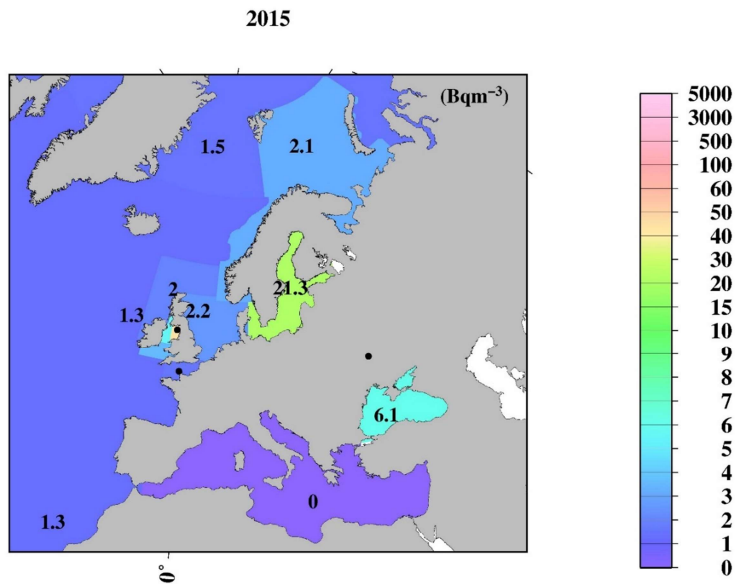
Figure 8: Horizontal distributions of the 0.5-yr median ^{137}Cs value in the surface mixed layer in the northern North Atlantic Ocean and its marginal seas. The unit is Bqm^{-3}. (a) 1970, (b) 1975, (c) 1980, (d) 1985, (e) 1990, (f) 1995, (g) 2000, (h) 2005, (i) 2010, and (j) 2015.

(a)

1970

(b)

1975

905

910

(c)

(d)
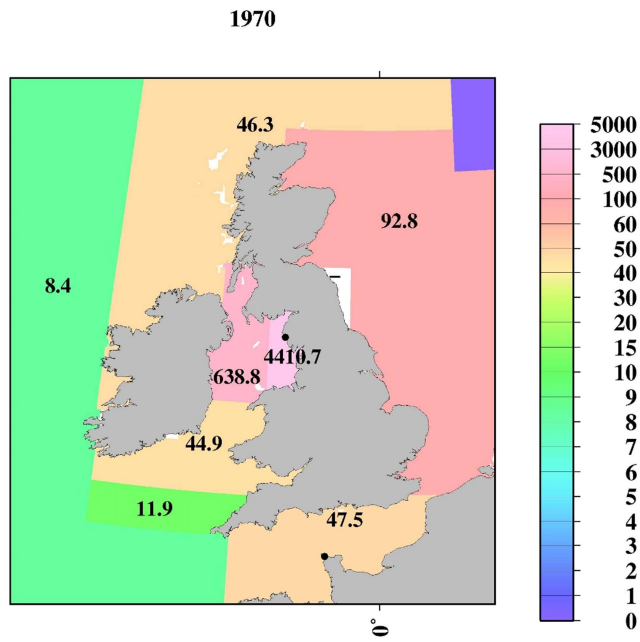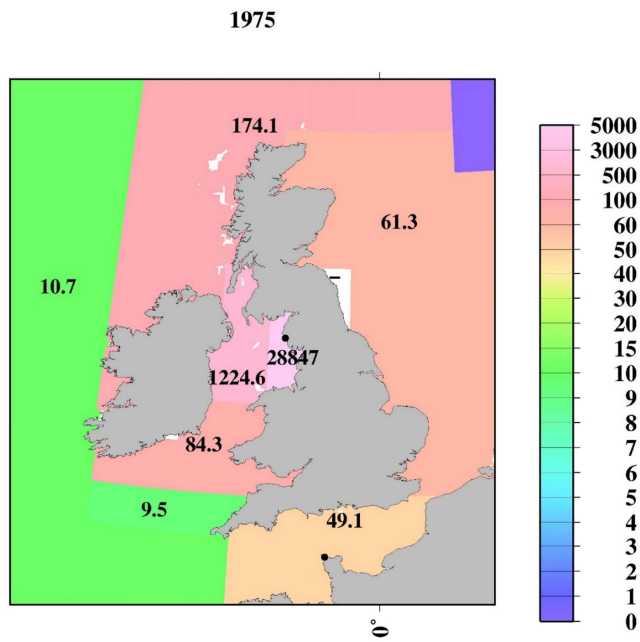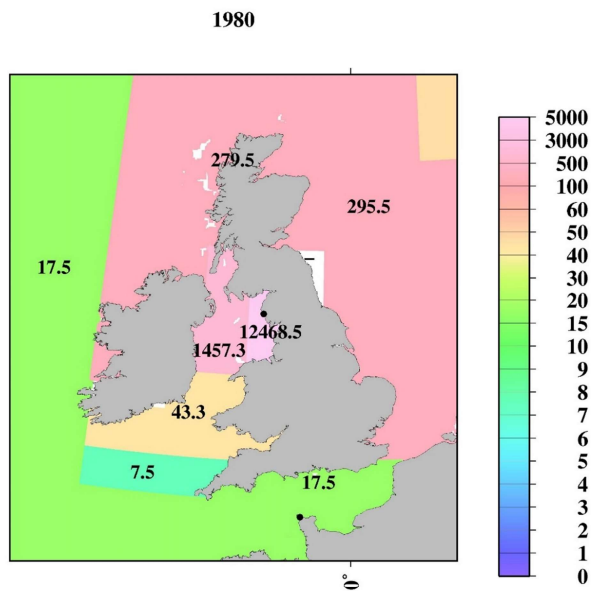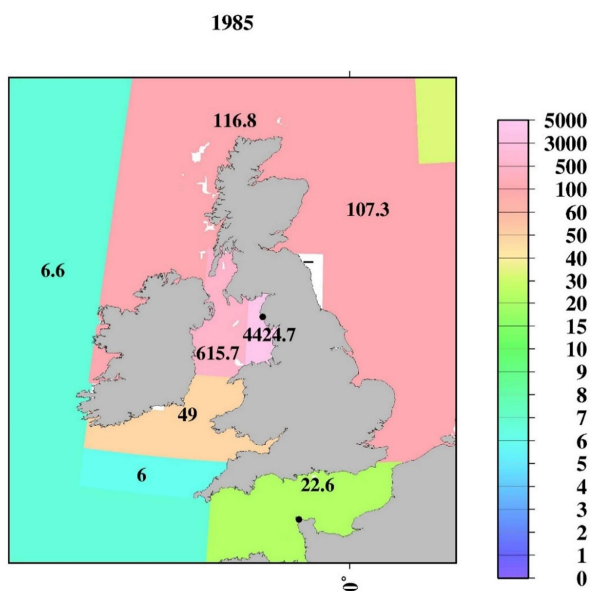
(e)
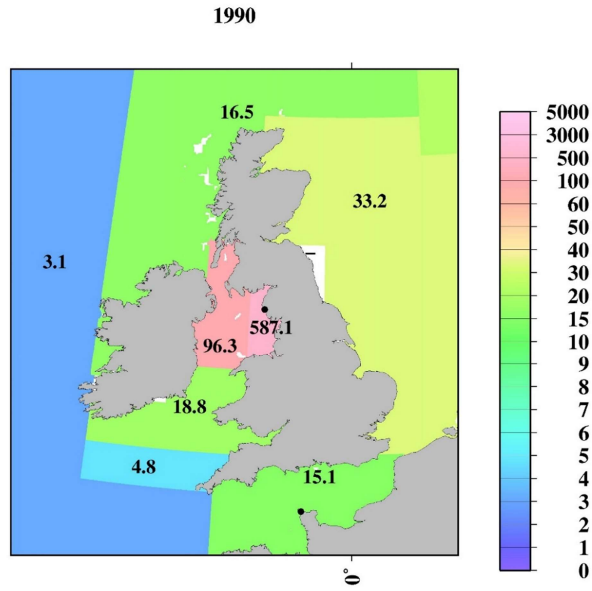
(f)
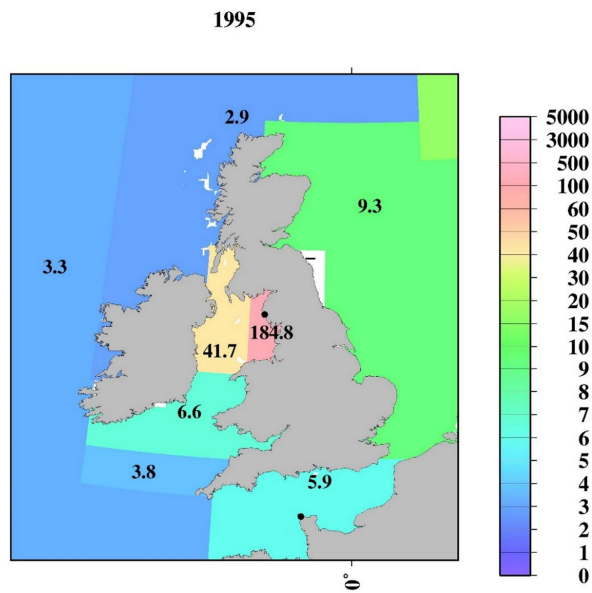
935

940

945

(g)

(h)

950

955

960

(i)
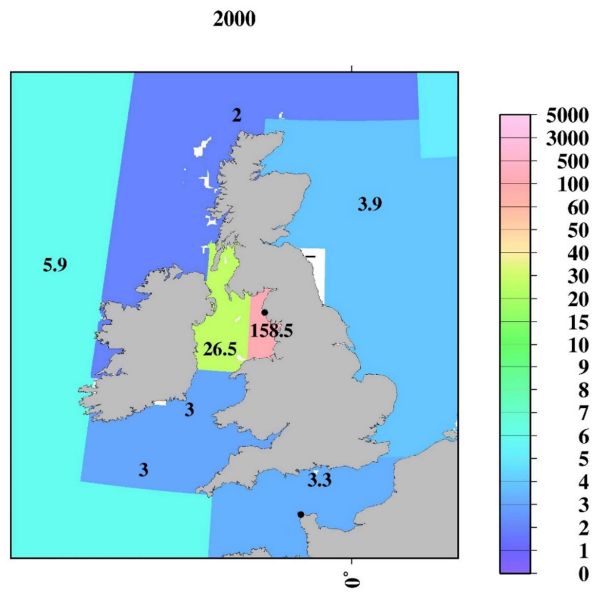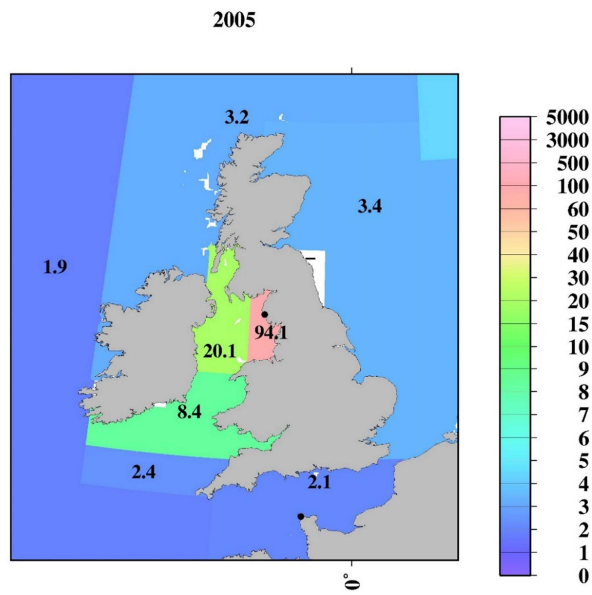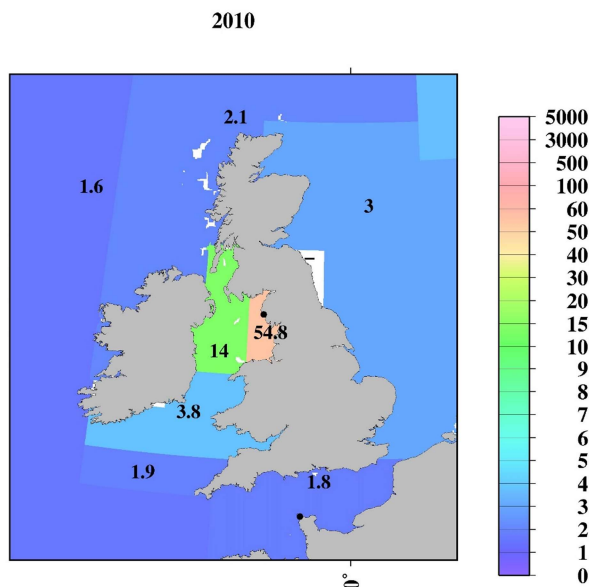
(j)
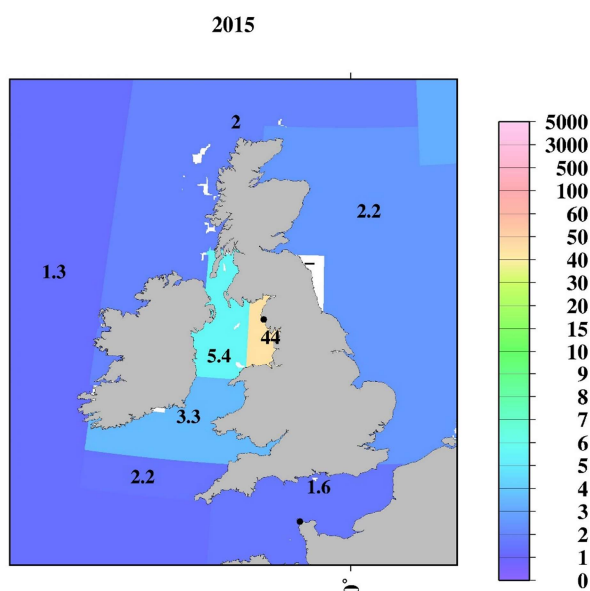
Figure 9: Horizontal distributions of the 0.5-yr median ^{137}Cs value in the surface mixed layer in the Irish Sea. The unit is Bqm^{-3}. (a) 1970, (b) 1975, (c) 1980, (d) 1985, (e) 1990, (f) 1995, (g) 2000, (h) 2005, (i) 2010, and (j) 2015. The "-" mean that there is no available data.

3.14 ^{137}Cs inventory in the surface mixing layer in the global ocean after 1970

The horizontal distribution of the surface mixed layer depth in the global ocean are shown in Fig. 10. The mixed layer depth in the open ocean shows a clear latitudinal distribution of deeper (~182 m) in the higher latitudes and shallower in the lower latitudes, particularly in the equatorial Pacific Ocean (48 m for the eastern equatorial Pacific Ocean and 58 m for the western equatorial Pacific Ocean). In the coastal sea, the mixed layer depths are shallower (33-76 m) than those in the open ocean. The mixed layer depth in each box is also listed in Table 5.

(a)
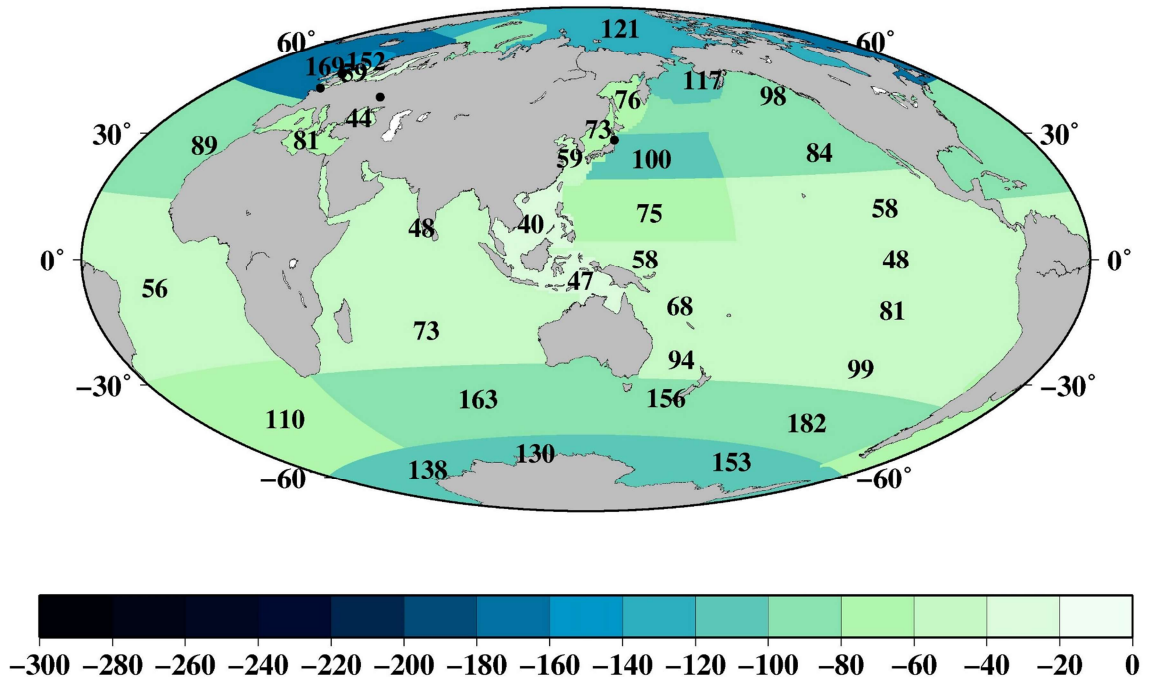
980

(b)
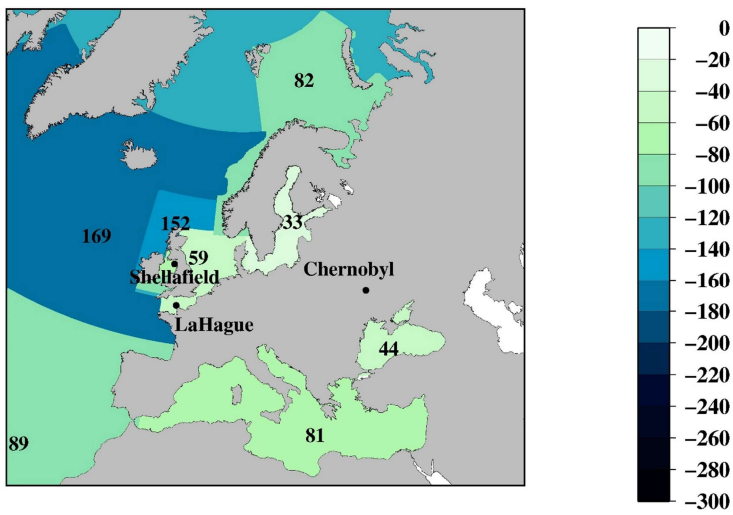
985

(c)
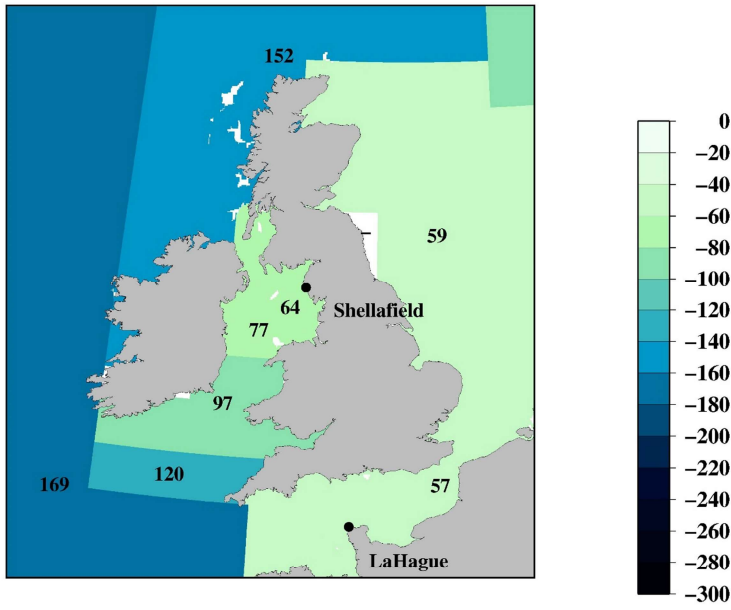
990

Figure 10: Median mixed layer depth in each box in the global ocean. (a) Global, (b) North Atlantic Ocean and its marginal sea, and (c) Irish Sea. The unit is m. The "-" means that there is no mixed layer depth data.

995

1000

1005

1010

1015

Table 5. ^{137}Cs inventory in each box in the global ocean.

Box Area	Area (10⁶km²)	Mixed Layer Depth (m)	¹³⁷Cs inventory (PBq)									
			1970	1975	1980	1985	1990	1995	2000	2005	2010	2015
1 subarctic North Pacific Ocean	10.66	98	10.4	7.3	5.1	3.5	3.4	2.8	2.3	1.9	1.6	2.5
2 western North Pacific Ocean	7.14	100	6.3	5.2	4.2	3.4	2.4	2.0	1.6	1.4	1.1	3.3
3 eastern North Pacific Ocean	9.85	84	12.2	8.2	5.5	3.7	3.0	2.5	2.0	1.7	1.4	2.2
4 western subtropical North Pacific Ocean	13.41	75	7.1	6.4	5.8	5.2	2.9	2.6	2.2	1.9	1.7	1.3
5 eastern subtropical North Pacific Ocean	20.46	58	11.6	11.6	11.6	11.6	3.5	3.0	2.6	2.2	1.9	1.6
6 western equatorial Pacific Ocean	6.12	58	1.9	1.9	1.9	1.9	1.1	0.8	0.7	0.5	0.4	0.3
7 eastern equatorial Pacific Ocean	12.34	48	2.6	2.6	2.6	2.6	1.4	1.3	1.1	0.9	0.8	0.7
8 western subtropical South Pacific Ocean	7.81	68	7.2	4.8	3.2	2.2	1.5	1.0	0.7	0.4	0.3	0.2
9 eastern subtropical South Pacific Ocean	24.91	81	6.0	10.5	10.5	4.9	4.9	4.3	3.7	3.3	2.8	2.0
10 western South Pacific Ocean	4.31	94	3.8	1.7	1.9	1.4	1.0	0.7	0.6	0.6	0.5	0.4
11 eastern South Pacific Ocean	16.86	99	5.2	5.5	4.3	3.3	2.6	2.2	2.0	1.9	1.8	1.7
12 eastern Southern Ocean	16.92	182	10.7	8.4	6.6	5.2	4.0	3.2	2.5	2.0	1.5	1.2
13 Pacific sector of Antarctic	9.87	153	4.1	2.1	1.1	0.6	0.3	0.2	0.1	0.0	0.0	0.0
14 Sea of Japan	1.04	73	0.7	0.5	0.4	0.3	0.3	0.2	0.2	0.1	0.1	0.2
15 Arabian Sea	20.23	48	4.0	3.8	3.7	3.4	2.8	2.3	1.9	-	-	-
16 Indian Ocean	23.25	73	7.7	9.3	7.5	6.0	4.8	3.9	3.1	2.5	2.0	1.6
17 Southern Ocean	26.55	163	15.2	15.2	15.2	11.4	8.9	7.0	5.5	4.3	3.4	2.7
18* Arctic Ocean	12.03	121	1.7	8.8	16.5	12.0	9.7	4.7	2.1	5.3	2.4	2.2
19 Middle Southern Ocean	5.09	156	3.5	2.6	1.9	1.5	1.1	0.8	0.6	0.5	0.3	0.3
20* Barents Sea and Coast of Norway	1.85	81	-	-	6.8	4.9	3.5	2.5	0.8	0.7	0.6	0.5
21* Baltic Sea	0.41	33	-	0.4	0.5	0.3	1.3	1.0	0.7	0.5	0.4	0.3
22* North Sea	0.43	59	2.4	1.6	7.5	2.7	0.8	0.2	0.1	0.1	0.1	0.1
23.1* Irish Sea	0.01	64	2.3	15.2	6.6	2.3	0.3	0.1	0.1	0.05	0.03	0.02
23.2*	0.03	77	1.5	2.8	3.3	1.4	0.2	0.1	0.1	0.05	0.03	0.01
23.3*	0.05	97	0.2	0.4	0.2	0.3	0.1	0.03	0.02	0.0	0.02	0.02
23.4*	0.04	120	0.1	0.0	0.0	0.03	0.02	0.02	0.01	0.01	0.01	0.01
23.5*	0.01	-	0.0	0.0	0.0	0.0	0.0	0.0	0.0	0.0	0.0	0.0
24* English Channel	0.08	57	0.2	0.2	0.1	0.1	0.1	0.0	0.0	0.0	0.0	0.0
25.1* Northern North Atlantic Ocean	0.36	152	2.5	9.5	15.2	6.4	0.9	0.2	0.1	0.2	0.1	0.1
25.2*	8.59	169	12.2	15.5	25.4	9.5	4.5	4.8	8.6	2.7	2.3	1.9
26 Black Sea	0.46	44	-	-	-	-	1.1	0.7	0.5	0.3	0.2	0.1
27* Mediterranean Sea	2.51	81	1.3	1.1	1.0	1.0	0.6	0.4	0.4	0.5	0.6 -	
28 North Atlantic Ocean	23.03	89	12.8	12.1	11.5	6.8	5.8	4.9	4.2	3.6	3.0	2.6
29 Central Atlantic Ocean	29.58	56	5.1	7.9	10.7	7.7	2.3	2.1	1.9	1.8	1.6	1.5
30 South Atlantic Ocean	21.48	110	12.7	10.8	9.1	7.8	6.6	5.6	4.4	3.5	2.8	2.2
31 Sea of Okhotsk	1.61	76	1.5	0.9	0.6	0.4	0.3	0.2	0.2	0.2	0.1	0.1
32 East China Sea	1.18	59	0.5	0.4	0.4	0.3	0.2	0.2	0.2	0.1	0.1	0.1
33 South China Sea	4.02	40	0.9	1.3	1.6	0.6	0.4	0.3	0.2	0.1	0.1	0.0
34 Bering Sea	2.28	117	2.1	1.6	1.2	0.9	0.7	0.5	0.4	0.3	0.2	0.6
35 Indonesian Archipelago	3.27	47	0.9	0.8	0.7	0.7	0.6	0.6	0.5	0.5	0.4	0.4
36 Atlantic sector of Antarctic	5.61	138	1.2	1.0	0.8	0.6	0.5	0.4	0.3	0.3	0.2	0.2
37 Indian sector of Antarctic	5.31	130	1.4	1.0	0.7	0.5	0.3	0.2	0.2	0.1	0.1	0.1

* : 0.5yr average value without curve fitting

-: There is no available data.

By using these mixed layer depths, the estimated ^{137}Cs inventory in the surface seawater from 1970 to 2015 every 5 years is shown in Figs. 11-13. The ^{137}Cs inventory in the surface seawater is also listed in Table 5. In the Pacific Ocean, a higher ^{137}Cs inventory exists in the subarctic North Pacific Ocean (10.4 PBq), western and eastern North Pacific Ocean (6.3 PBq and 12.2 PBq), and subtropical western and eastern North Pacific Ocean (7.1 PBq and 11.6 PBq) in 1970 (Fig.11a). In particular, the ^{137}Cs inventory in the eastern North Pacific Ocean/subtropical eastern North Pacific Ocean is larger than that in the western regions. In the South Pacific Ocean, a higher ^{137}Cs inventory is observed in the western subtropical South Pacific Ocean (7.2 PBq) and eastern Southern Ocean (10.7 PBq) in 1970. After 1975, the ^{137}Cs inventory in the eastern part is larger than that in the western part in the South Pacific Ocean. The ^{137}Cs inventory in the surface seawater in the Southern Hemisphere is the highest in the Pacific Ocean, followed by the Indian Ocean, and it is the lowest in the Atlantic Ocean. In the Indian

Ocean, the ^{137}Cs inventory has a latitudinal gradient with higher in the Southern Ocean (15.2 PBq) and lower in the Arabian

1030   Sea in 1970. These latitudinal gradients of the ^{137}Cs inventory in the surface mixed layer continued until 2015.

In the northern North Atlantic Ocean, its marginal seas, and the Arctic Ocean (Figs. 12, 13), the ^{137}Cs inventory is strongly influenced by the discharged ^{137}Cs from fuel reprocessing plants in the Irish Sea and English Chanel after 1970, as well as the global fallout from large-scale weapon tests in the 1960s and 1960s (Northern North Atlantic Ocean.2 and Arctic Ocean). In the Irish Sea, the maximum ^{137}Cs inventory occurred in the Irish Sea.1 (15.2 PBq) in 1975. The ^{137}Cs discharged

1035   into the Irish Sea.1 was transported into the Irish Sea.2 (3.3 PBq in 1980), followed by transport to the northern North Atlantic Ocean.1 (15.2 PBq in 1980), North Sea (7.5 PBq in 1980), and Barents Sea and coast of Norway (6.8 PBq in 1980). This pattern is also consistent with general pattern of seawater transport in this region (Prandle et al., 1984, 1991 ; Bois et al., 2020). The ^{137}Cs discharged from the La Hague was also transported into the North Sea.

(a)
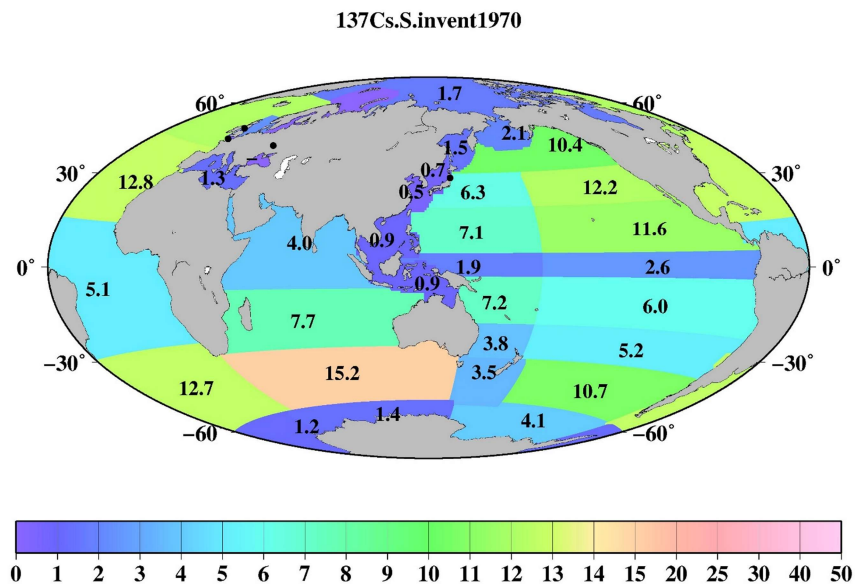
1040

(b)
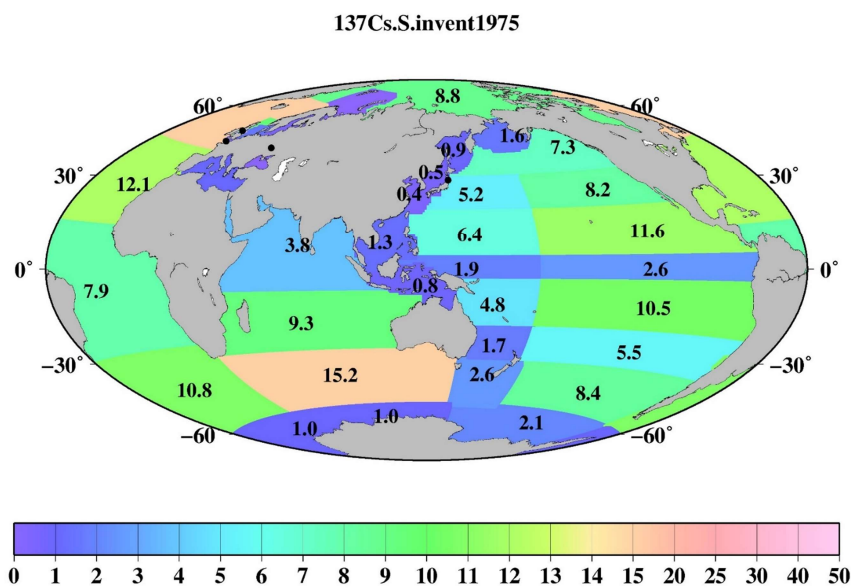
1045   (c)
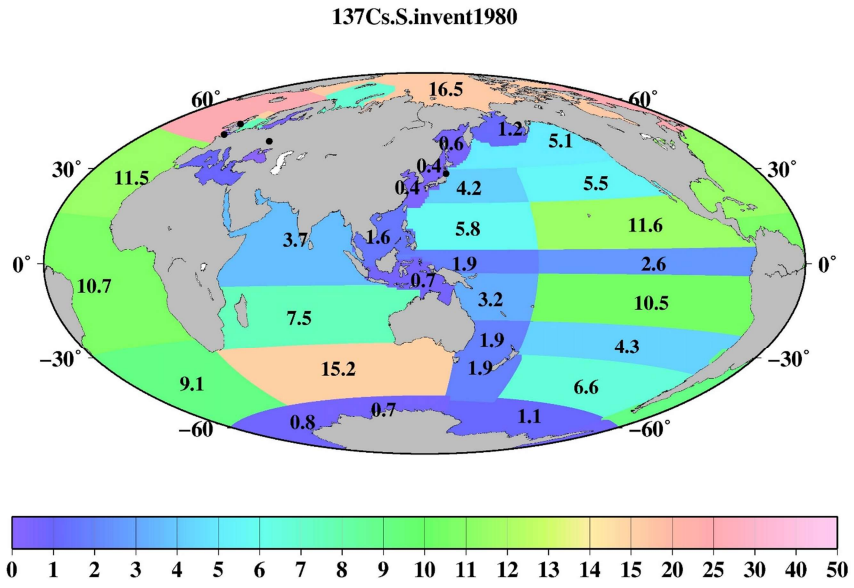
(d)
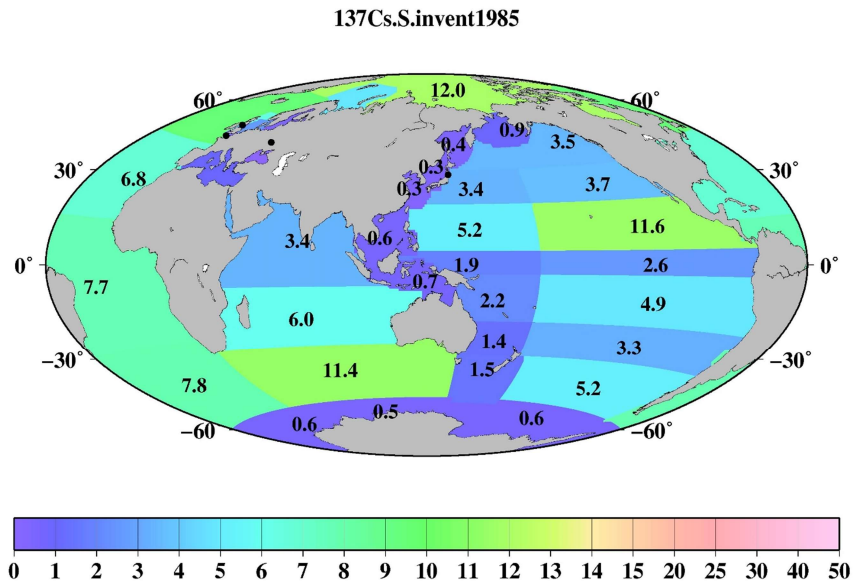
(d)

1050

1055

(e)

1060

(f)

1065

1070

1075 (g)

(h)

1080

1085

1090

(i)

(j)
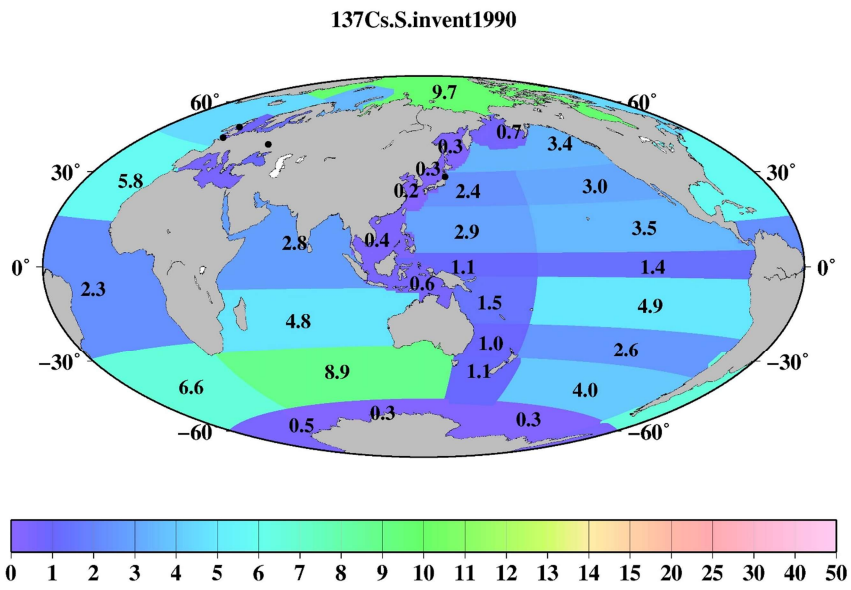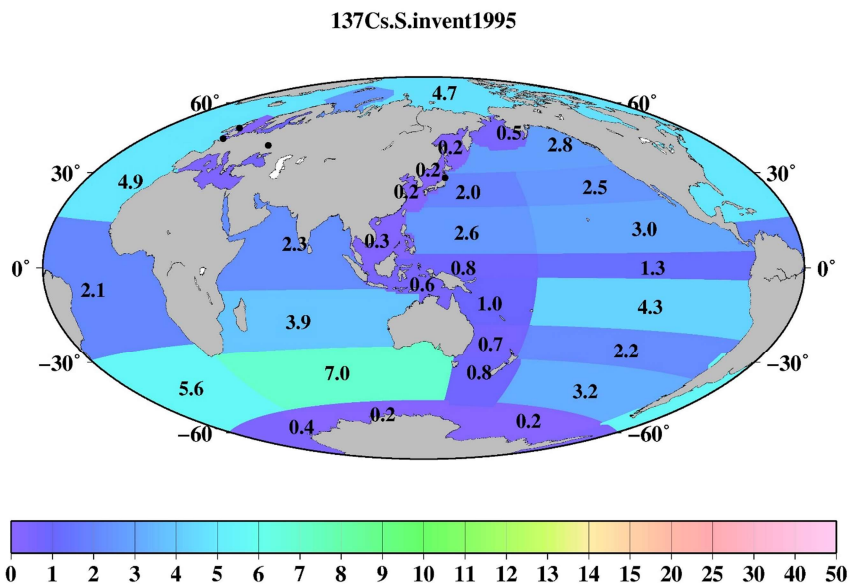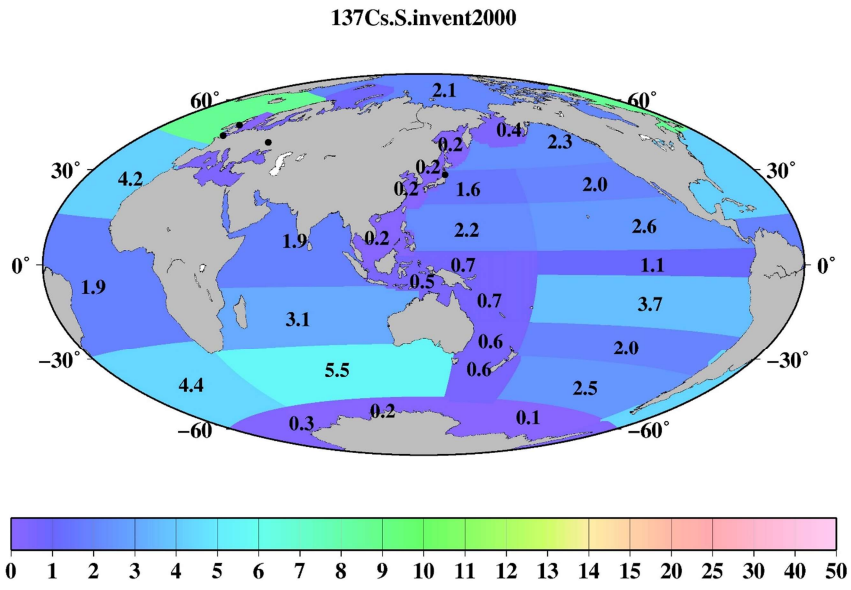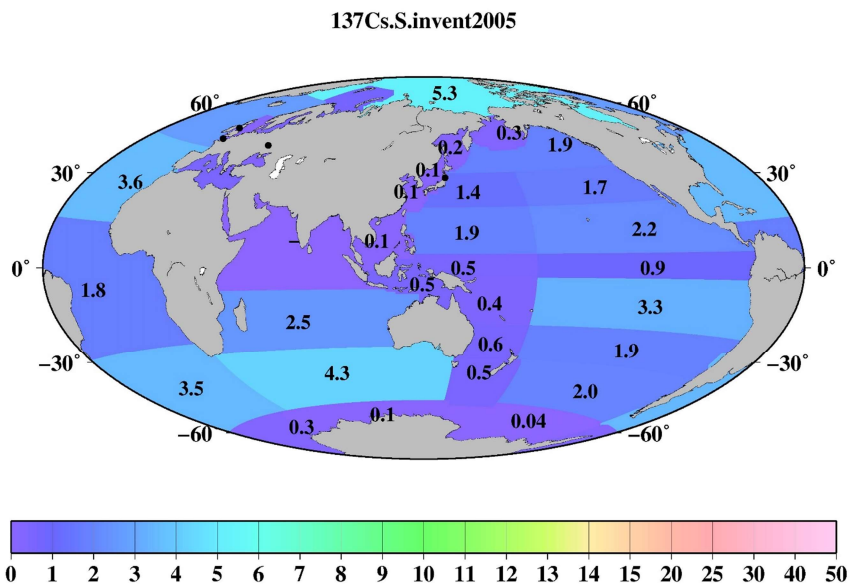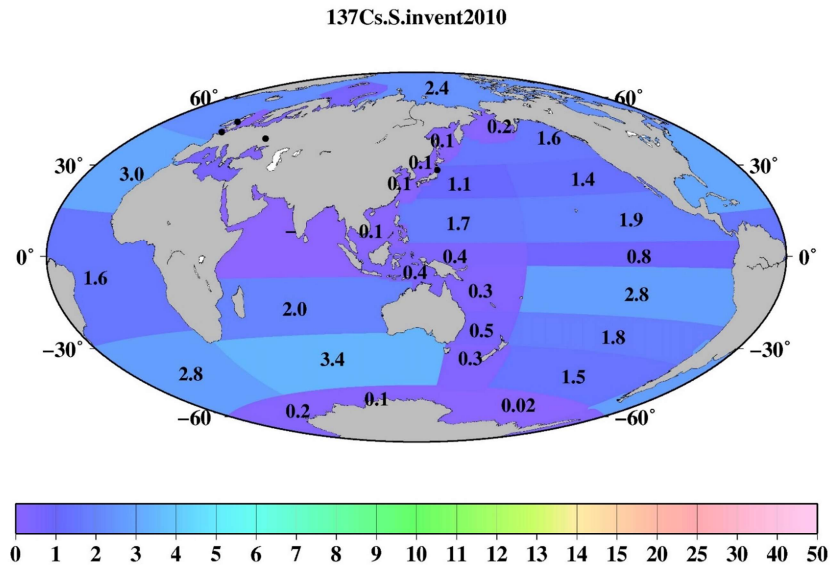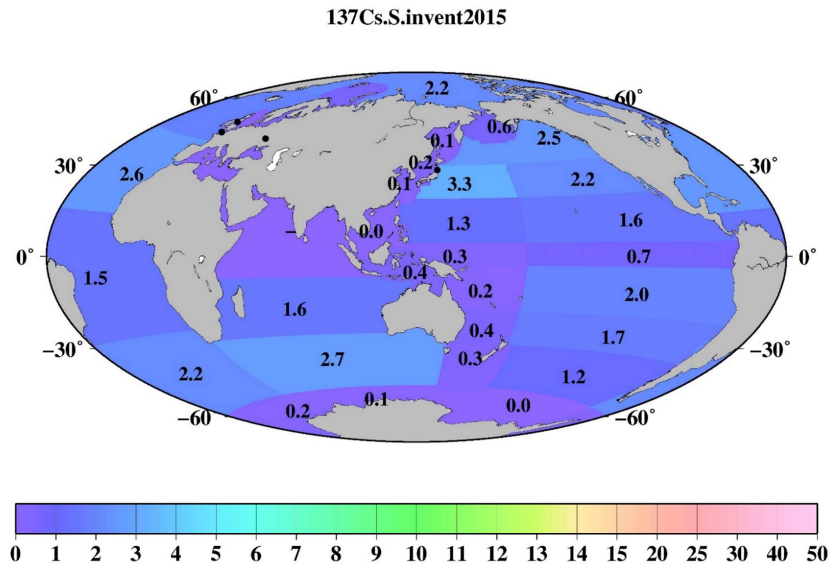
Figure 11: Horizontal distributions of the ^{137}Cs inventory in the surface mixed layer in the global ocean. Unit is PBq. (a) 1970, (b) 1975, (c) 1980, (d) 1985, (e) 1990, (f) 1995, (g) 2000, (h) 2005, (i) 2010, and (j) 2015. The "-" mean that there is no available data.

(a)

1970

 (b)

1975

(c)

1980

(d)
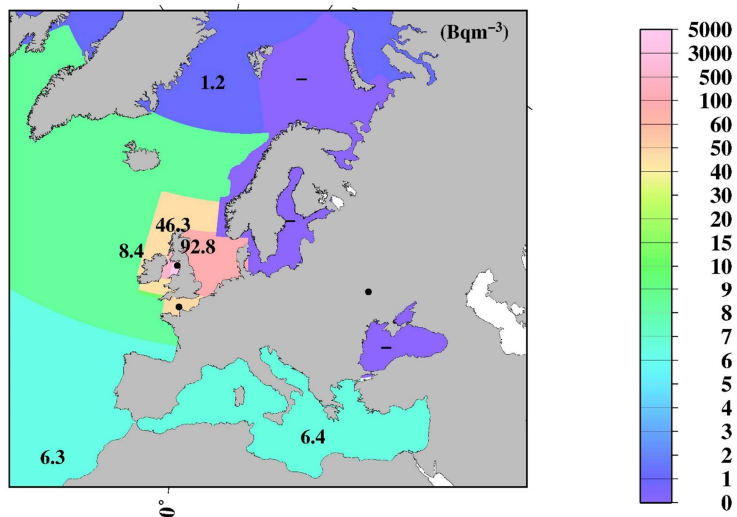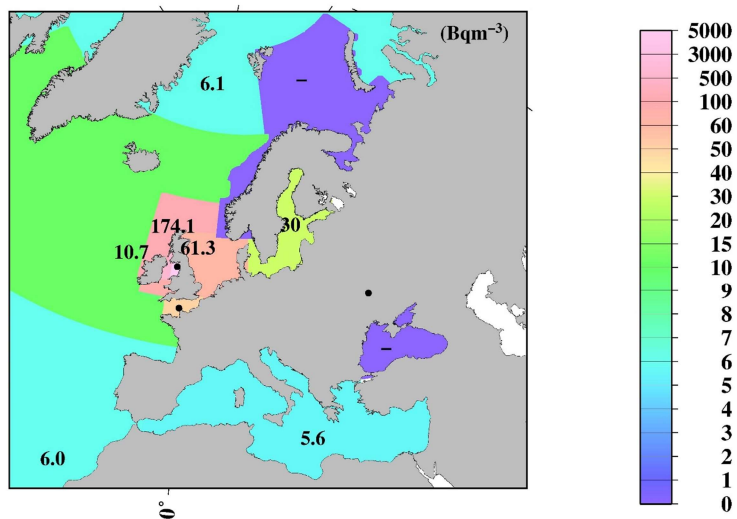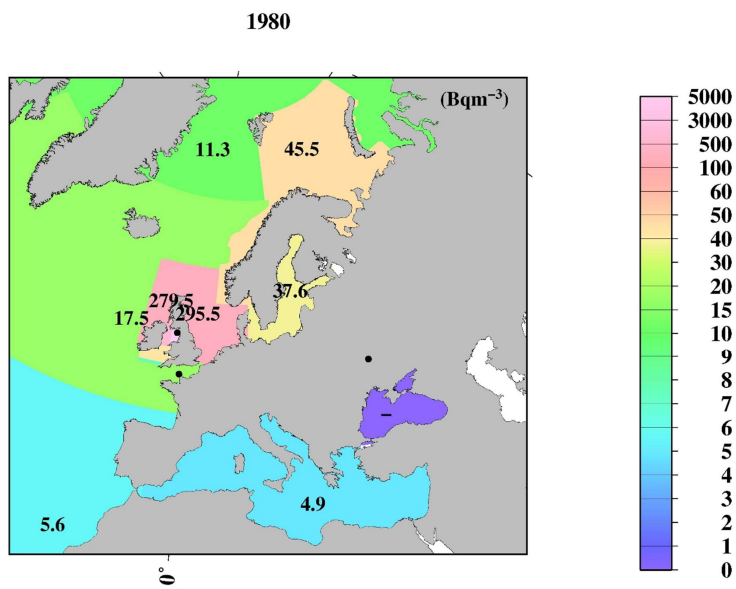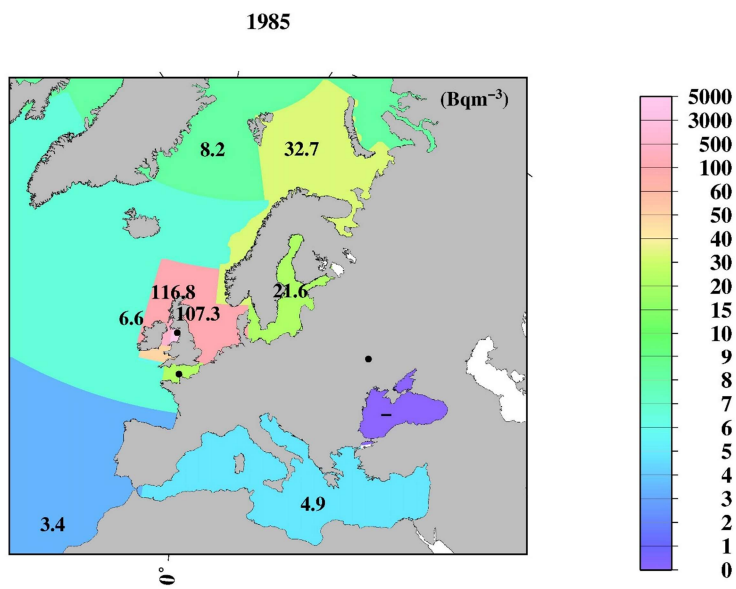
1985

(e)
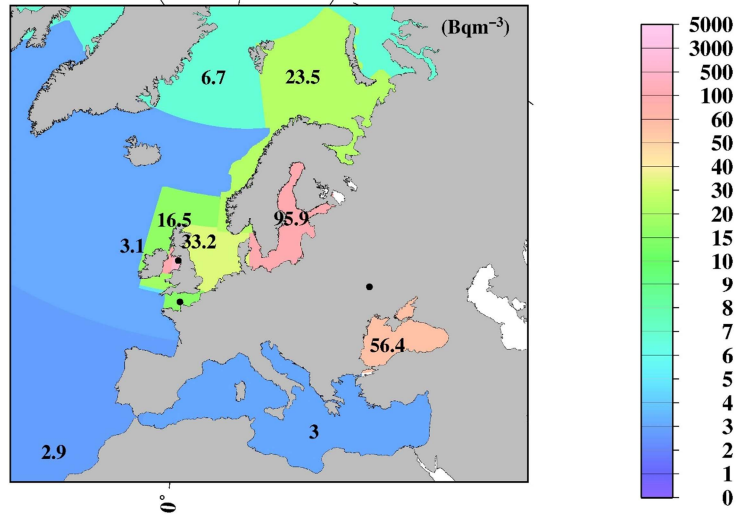
1990

1140

(f)

1995

1145

1150

1155   (g)

(h)

1160

1165

1170

(i)

(j)
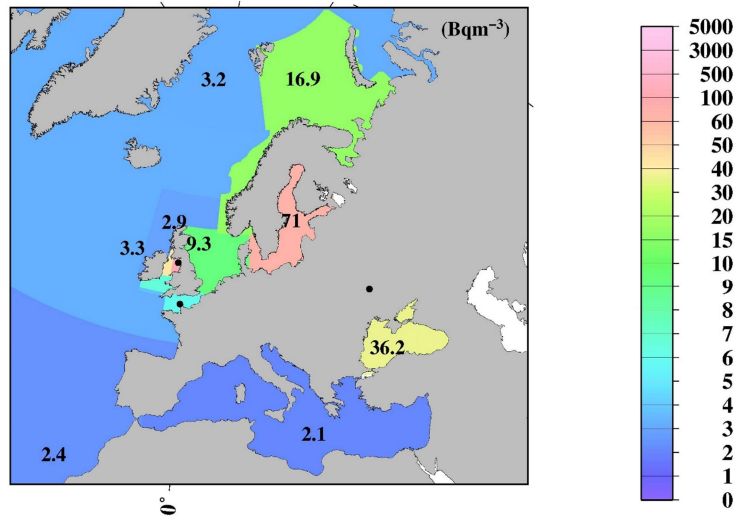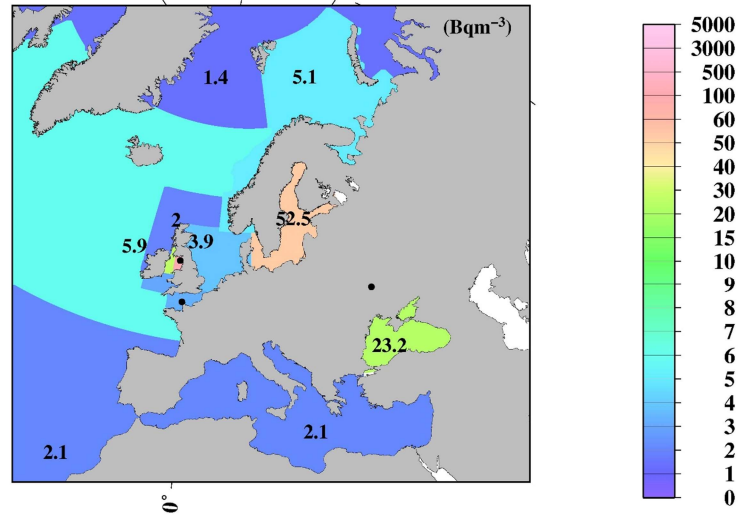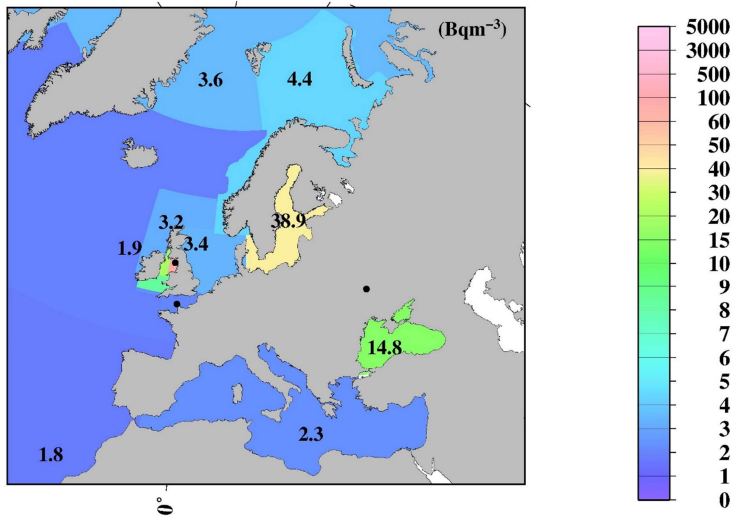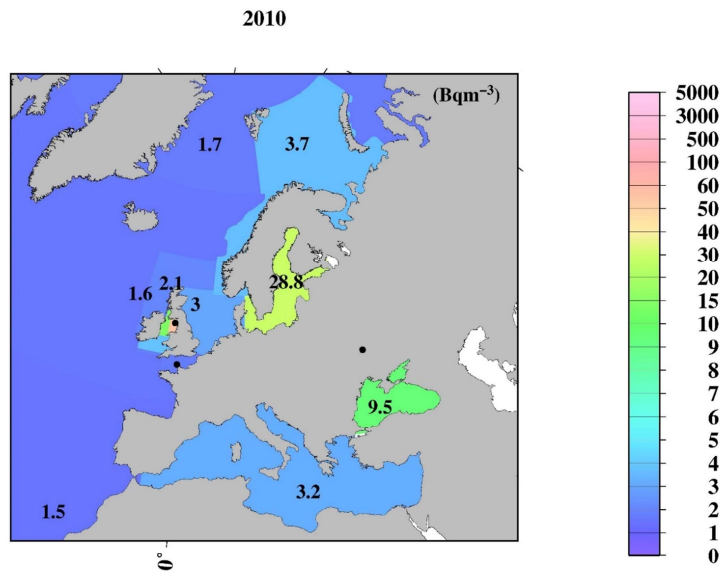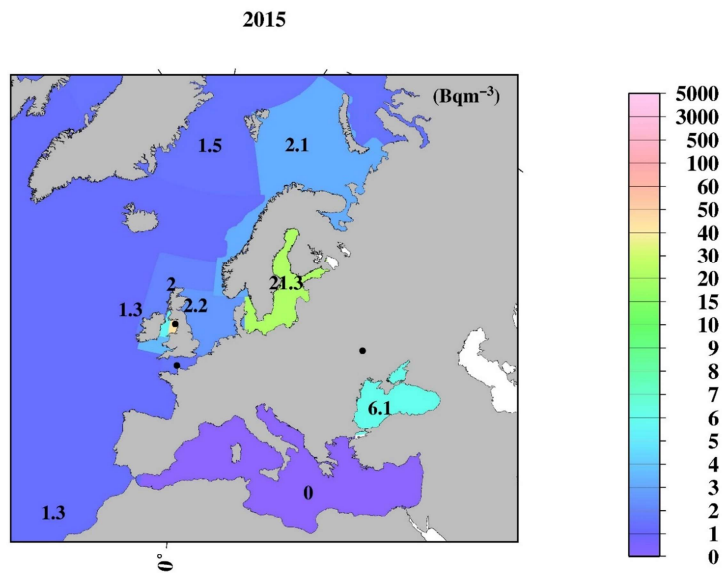
Figure 12: Horizontal distributions of ^{137}Cs inventory in the surface mixed layer in the northern North Pacific Ocean and its marginal seas. Unit is PBq. (a) 1970, (b) 1975, (c) 1980, (d) 1985, (e) 1990, (f) 1995, (g) 2000, (h) 2005, (i) 2010, and (j) 2015. The "-" mean that there is no available data.

1175

1180

1185

(a)

(b)
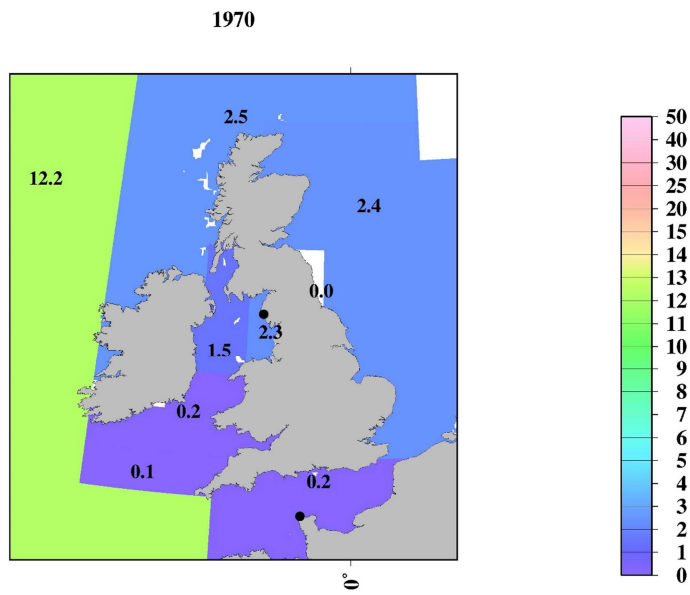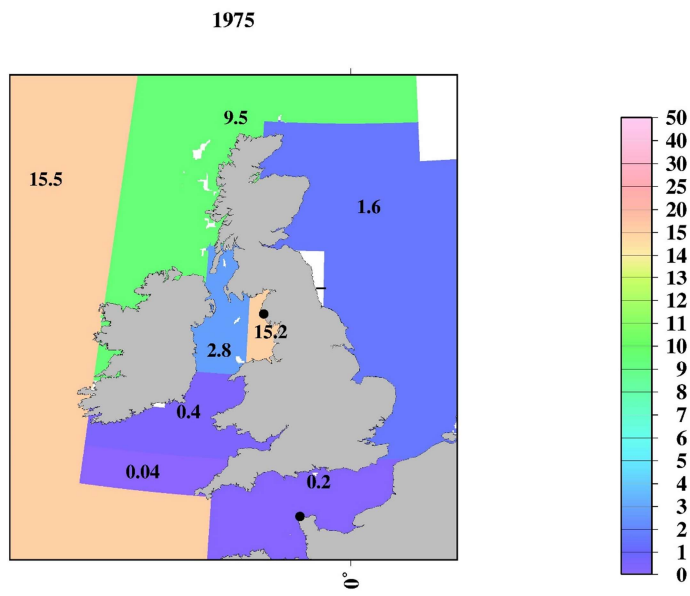
(c)
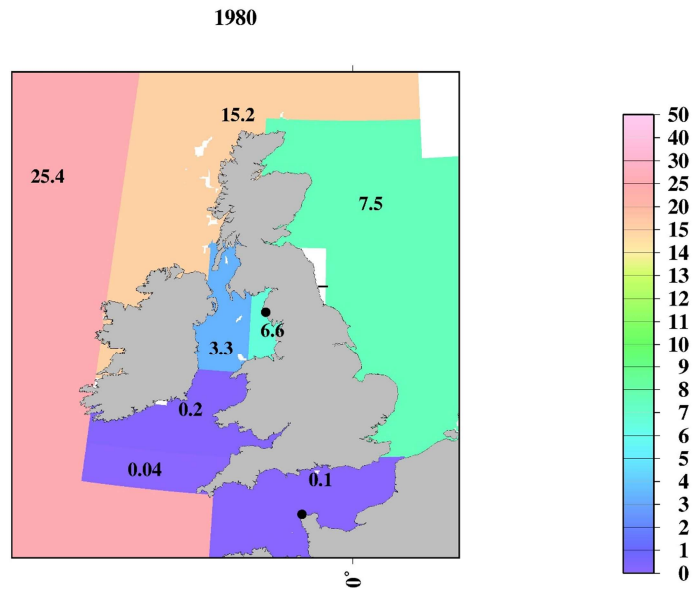
1205

(d)
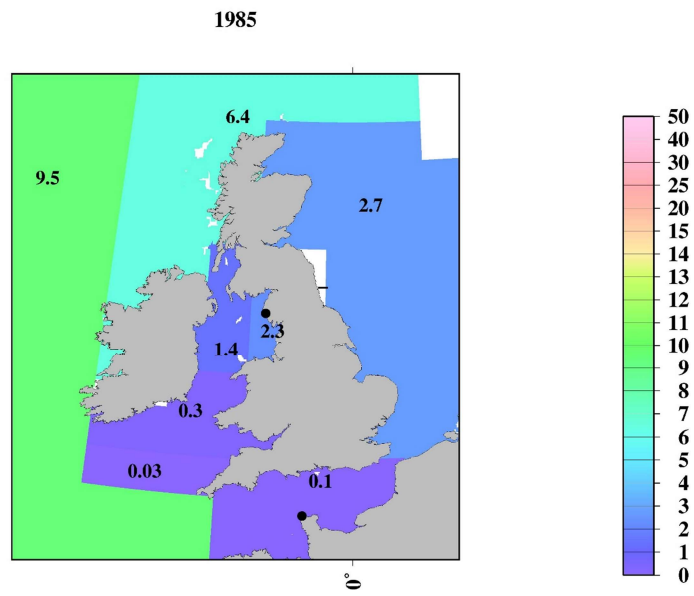
1210

1215

1220

(e)

(f)

1225

1230

1235

(g)

2000

(h)
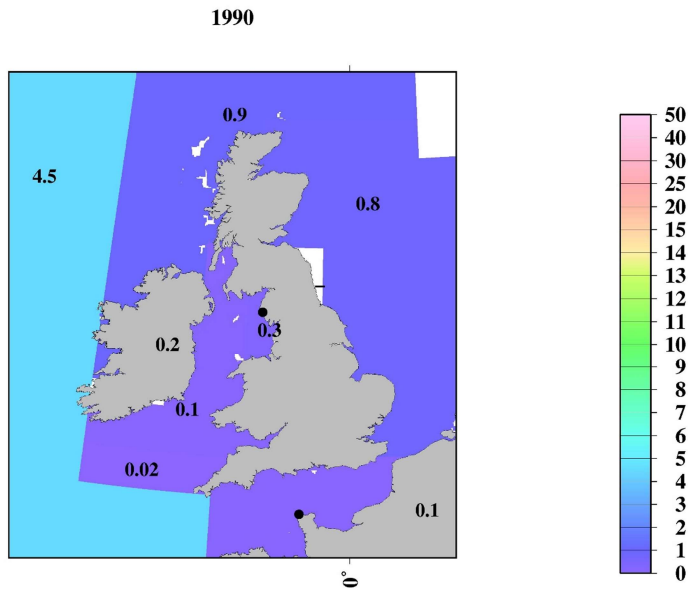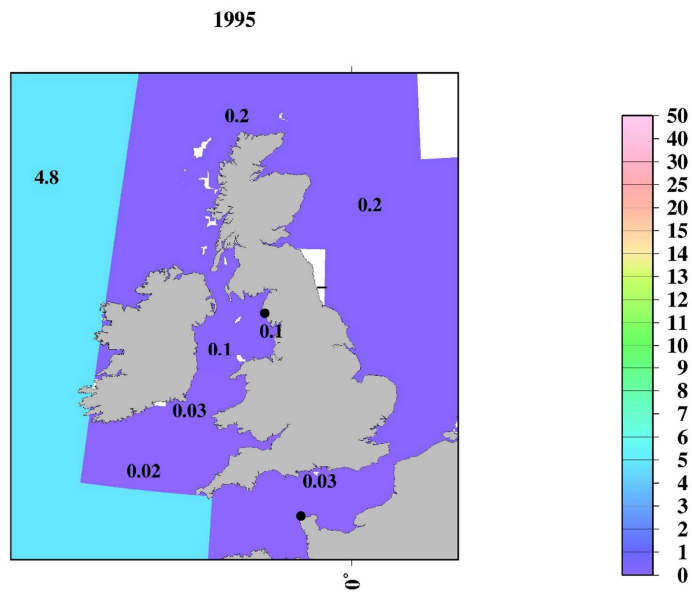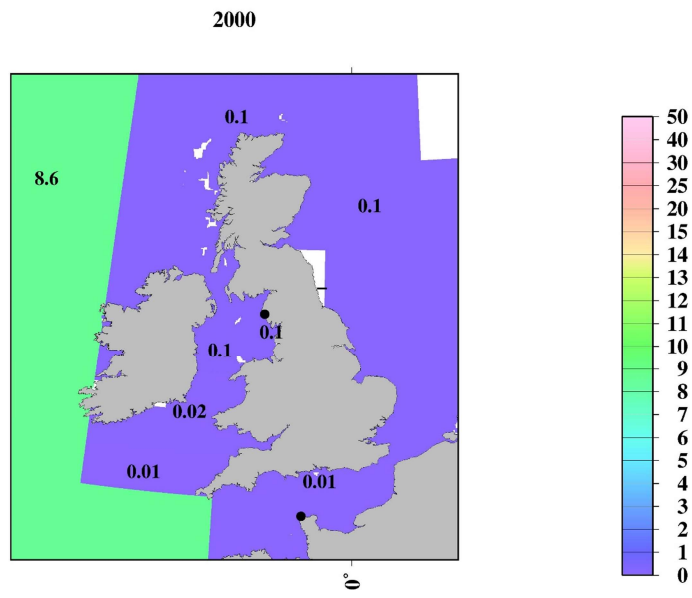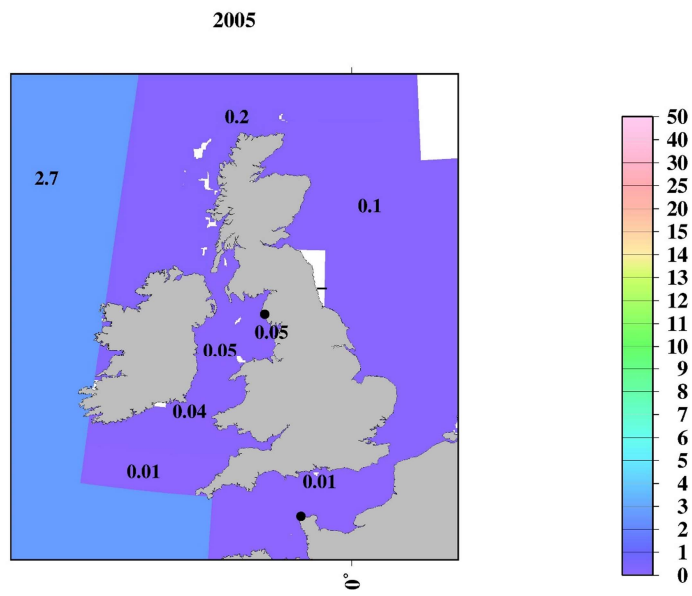
2005

1240

1245

1250

(i)
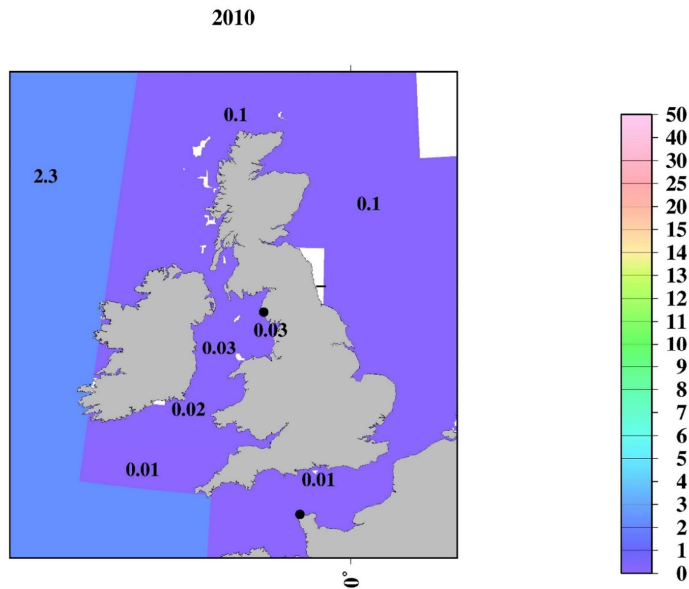
1255 **(j)**
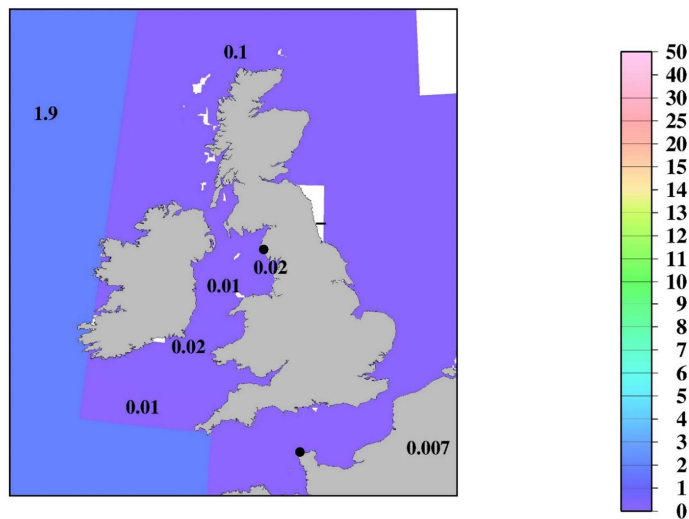
Figure 13: Horizontal distributions of the ¹³⁷Cs inventory in the surface mixed layer in the Irish Sea and English Channel. Unit is PBq. (a) 1970, (b) 1975, (c) 1980, (d) 1985, (e) 1990, (f) 1995, (g) 2000, (h) 2005, (i) 2010, and (j) 2015. The "-" mean that there is no available data.

1260   Fig. 14 shows the time variation in ^{137}Cs inventories in the surface mixed layer during 1970-2015. The ^{137}Cs inventory in the surface mixed layer in the global ocean in 1970 was estimated to be 184±26 PBq. This result indicates that 32% of the deposited ^{137}Cs remained in the surface mixed layer; in other words, 68% of the deposited ^{137}Cs was transported below the surface mixed layer on a decadal scale in 1970. In 1970, the ^{137}Cs inventory was the largest in the North Pacific Ocean, followed by the North Atlantic Ocean and the marginal sea, Atlantic Ocean, and South Pacific Ocean. The ^{137}Cs inventories

1265 increase until 1980, and the inventory is estimated to be 201±27 PBq in 1975 and 214±11 PBq in 1980 due to the discharge of ^{137}Cs from the Sellafield and La Hague reprocessing plants. According to the estimation by OSPAR (2021), approximately 41.4 PBq (32 PBq until 1980, Aarklog, 2003) and 1.04 PBq (0.70 PBq until 1980; Aarkrog, 2003) of ^{137}Cs were discharged from the Sellafield and La Hague plants from 1970 to 1998, respectively. The contribution from the nuclear fuel reprocessing plants and large-scale nuclear weapons tests (39%) observed in the Arctic Ocean and the northern North Atlantic Ocean and

1270 its marginal sea (the Arctic Ocean, Barents Sea and coast of Norway, Baltic Sea, North Sea, northern North Atlantic Ocean, Irish Sea, and the English Channel) resulted in a large ^{137}Cs inventory in 1980. After 1980, the ^{137}Cs inventory decreased gradually and was estimated to be 37.2±3.6 PBq in 2010, immediately before the F1NPS accident. Although the ^{137}Cs inventory decreased over time after 1980 until 2010, immediately before the F1NPS accident, the relative contributions of the ^{137}Cs inventory in the South Pacific Ocean, Indian Ocean, and Atlantic Ocean gradually increased and were estimated to be 20, 15,

1275 and 20% in 2010, respectively. After the F1NPS accident, the ^{137}Cs inventory increased and was estimated to be 50.7 ± 7.3 PBq.
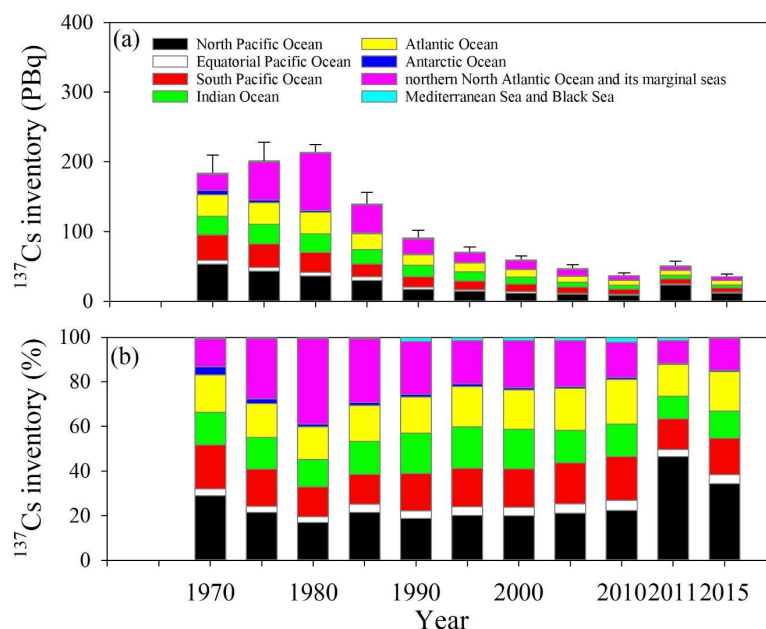
Figure 14: Temporal variations in the ^{137}Cs inventory every 5 years in the global ocean surface seawater.

4 Discussion

1280 **4.1 Basin-scale transport of ^{137}Cs in surface seawater in the North Pacific Ocean, its marginal seas, and the equatorial Pacific Ocean**

Fig. 15 shows the spatiotemporal variations in the ^{137}Cs density in the surface mixed layer in the North Pacific Ocean, subtropical North Pacific Ocean, equatorial Pacific Ocean, and subtropical western South Pacific Ocean. In the western North Pacific Ocean, except for the highest ^{137}Cs density in 1960, ^{137}Cs density increased and reached to 1964, and then decreases

1285 exponentially. However, in the eastern North Pacific Ocean, the ^{137}Cs density increased until 1966 and then decreased exponentially. The 2 years timelag that reached the maximum value was caused by horizontal transport from the western North Pacific Ocean and accumulated in the eastern North Pacific Ocean (Inomata et al., 2012). In the subtropical western and eastern North Pacific Ocean, and eastern equatorial Pacific Ocean, the ^{137}Cs density was almost constant in the 1970s and the 1980s. After the 1990s, the ^{137}Cs density decreased gradually. In the western equatorial Pacific Ocean and western subtropical South

1290 Pacific Ocean, the ^{137}Cs density increased gradually until the 1980s and then decreased after the 1990s. As shown in Table 3, Tap2 in the eastern North Pacific Ocean, which is estimated to be 8.8 years, is shorter than that in the western North Pacific Ocean (16.9 years). This suggests that the outflowed ^{137}Cs amount in the eastern North Pacific Ocean was larger than the inflowed ^{137}Cs amount from the western North Pacific Ocean. The Tap2 in the western subtropical North Pacific Ocean is estimated to be 34.1 years and Tpo is estimated to be -260.7 years. This mean that the ^{137}Cs was accumulated in this region: It

1295 was also reported that seawater with higher ^{137}Cs activity concentrations moved southwards with subsidence associated with the North Pacific subtropical gyre, followed by westwards transport and subduction in the central and eastern subtropical North Pacific Ocean (Inomata et al.,2012). The increased ^{137}Cs density in the western equatorial Pacific Ocean and the western

1300
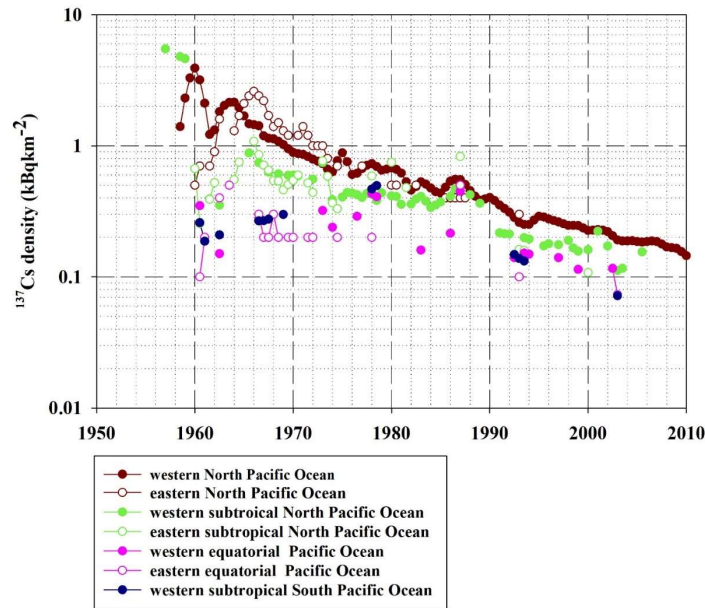
Figure 15: [137]Cs density in the surface mixed layer in the North Pacific Ocean, equatorial Pacific Ocean, and South Pacific Ocean.

1305 **4.2. Transport of ^{137}Cs from the Pacific Ocean to the Indian Ocean via the Indonesian Sea throughflow**

As described in the previous sections, seawater with a relatively large ^{137}Cs density (^{137}Cs activity concentrations) is transported westwards in the equatorial Pacific Ocean and the subtropical western South Pacific Ocean. It is known that the warm seawater in the equatorial Pacific Ocean is transported into the Indian Ocean by the wind-forcing circulation through the Indonesian Archipelago, namely, the Indonesian throughflow (Gordon, 2005; Feng et al., 2018). Reportedly, the median volume of

1310 seawater in the Indonesian throughflow was estimated to be 15 Sv (1 Sv = 10^6 m^{3}s^{-1}) (e.g., Gordon et al., 2010; Feng et al., 2018). The Indonesian throughflow consists of seawater derived from the North Pacific Ocean, South Pacific Ocean, and Antarctic Ocean. Approximately 9 Sv of seawater is transported to the Indian Ocean (Gordon et al., 2005). The transport of seawater from the Pacific Ocean into the Indian Ocean is revealed by the higher tritium concentrations in the seawater transported from the North Pacific Ocean through the Makassae Strait with the Mindanao Current, whereas seawater with

1315 lower tritium concentrations is transported into the Indian Ocean from the South Pacific Ocean via the Hamahera Sea (Fin et al., 1994). This suggests that most of the ^{137}Cs in the surface seawater inflows into the Indian Ocean from the North Pacific Ocean. Furthermore, the South Indian Ocean is connected to the Atlantic Ocean around the Cape of Good Hope via the Agulhas Current (Sanchez-Cabeza et al., 2011) with an median seawater mass transport of 8.7 Sv, according to Stramma and England (1999). Although we used the median box value in this discussion, the signatures of ^{137}Cs inflow from the North Pacific Ocean

1320 to the Indian Ocean via the Indonesian Archipelago were recognized by measurements. Evidently, higher concentrations were found at approximately 100°E in the subsurface layer, whereas lower concentrations were observed at approximately 70°E in the surface seawater (Povinec et al., 2011). In addition, ^{137}Cs in the Indian Ocean is transported westwards at approximately 10–15°S latitude (Sanchez-Cabeza et al., 2011; Povinec et al., 2011).

In this section, we discuss the ^{137}Cs inflow from the Pacific Ocean to the Indian Ocean, followed by the Atlantic

1325 Ocean. In the Indonesian Archipelago, the 0.5-yr median value of ^{137}Cs in 2010 was 2.7 Bq m^{-3} (Table 2, Fig. 7). This value is higher than those in the surrounding sea area, such as in the Eastern China Sea (1.7 Bq m^{-3}), western North Pacific Ocean

(1.5 Bq m^{-3}), western subtropical North Pacific Ocean (1.7 Bqm^{-3}), and western equatorial Pacific Ocean (1.2 Bq m^{-3}). The 0.5-yr median value in the Indonesian Archipelago in 2010 decreased to approximately 53% compared to that in 1970. These decreasing rates are smaller than those in the surrounding sea area (78-93%).

1330    Figure 16 shows the spatiotemporal variations in the ^{137}Cs density in the regions related to the Indonesian throughflow (the South China Sea, Indonesian Archipelago, western subtropical South Pacific Ocean, Arabian Sea, and Indian Ocean). The ^{137}Cs density in each box in the global surface seawater is also listed in Table 6. The ^{137}Cs density in the western subtropical South Pacific Ocean were almost the same as those in the Indonesian Archipelago. This result suggests that ^{137}Cs derived from large-scale weapons tests in the western North Pacific Ocean flowed into the Indian Ocean by basin-scale transport. The ^{137}Cs

1335 densities in the Indian Ocean (the Arabian Sea, Indian Ocean, and Southern Ocean) were almost similar to or higher than those in the Indonesian Archipelago. Furthermore, the ^{137}Cs density in these regions decreased after the 1990s. Tap in the Indonesian Archipelago was estimated to be 36.7 years and those in Tpo was estimated to be -169.2 years. It is likely that the main plume of ^{137}Cs derived from the large-scale weapon tests is transported into the Indian Ocean, with a time scale of 20-30 years.

    Furthermore, several studies have found that ^{137}Cs was transported into the South Atlantic Ocean via the Agulhas

1340 Current and then transported northwards with the Bengella Current (Sanchez-Cabeza et al., 2011; Strama and England, 1999). The transit times from the Pacific Ocean to the Atlantic Ocean via the Indian Ocean were estimated over four decades via model simulations (Tsumune et al., 2011). In this study, a slight increase in the ^{137}Cs median values in the Central Atlantic Ocean and South Atlantic Ocean was detected in 2003, as shown in Fig. 2g. Furthermore, Tap3 in the South and Central Atlantic Ocean (38 and 15.4 years) are longer than those in the surrounding boxes. The difference of ^{137}Cs concentrations in

1345 the Central and South Atlantic Ocean compared with the Pacific Ocean and Indian Ocean become to be small after the 1990s as shown in Figure 3. These results support the interpretation that the ^{137}Cs deposited into the western North Pacific Ocean is transported into the equatorial Pacific Ocean, Indian Ocean, and Atlantic Ocean on an approximately three-four decadal scale.
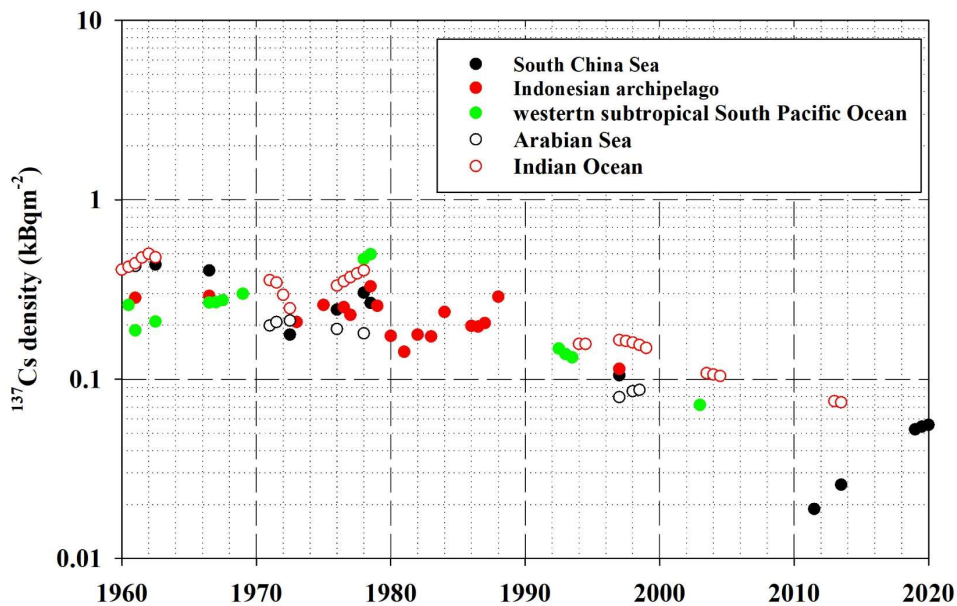
1350

Figure 16: ^{137}Cs density in the Indonesian Archipelago and surrounding sea in the surface mixed layer.

1355

Table 6. ^{137}Cs density in each box in the global ocean.

Box	Area	^{137}Cs density (kBq m^{-2})									
		1970	1975	1980	1985	1990	1995	2000	2005	2010	2015
1	subarctic North Pacific Ocean	0.98	0.68	0.47	0.33	0.32	0.26	0.22	0.18	0.15	0.24
2	western North Pacific Ocean	0.89	0.72	0.59	0.48	0.34	0.28	0.23	0.19	0.16	0.47
3	eastern North Pacific Ocean	1.24	0.84	0.56	0.38	0.31	0.25	0.21	0.17	0.14	0.23
4	western subtropical North Pacific Ocean	0.53	0.48	0.43	0.39	0.22	0.19	0.17	0.14	0.13	0.10
5	eastern subtropical North Pacific Ocean	0.57	0.57	0.57	0.57	0.17	0.15	0.12	0.11	0.09	0.08
6	western equatorial Pacific Ocean	0.31	0.31	0.31	0.31	0.17	0.14	0.11	0.09	0.07	0.05
7	eastern equatorial Pacific Ocean	0.21	0.21	0.21	0.21	0.12	0.10	0.09	0.08	0.07	0.06
8	western subtropical South Pacific Ocean	0.92	0.62	0.42	0.28	0.19	0.13	0.08	0.06	0.04	0.03
9	eastern subtropical South Pacific Ocean	0.24	0.42	0.42	0.20	0.20	0.17	0.15	0.13	0.11	0.08
10	western South Pacific Ocean	0.88	0.39	0.45	0.32	0.23	0.17	0.15	0.13	0.11	0.10
11	eastern South Pacific Ocean	0.31	0.33	0.25	0.20	0.15	0.13	0.12	0.11	0.11	0.10
12	eastern Southern Ocean	0.63	0.49	0.39	0.30	0.24	0.19	0.15	0.12	0.09	0.07
13	Pacific sector of Antarctic	0.41	0.22	0.11	0.06	0.03	0.02	0.01	0.00	0.00	0.00
14	Japan Sea	0.65	0.52	0.41	0.32	0.27	0.22	0.17	0.14	0.11	0.15
15	Arabian Sea	0.20	0.19	0.18	0.17	0.14	0.11	0.09	-	-	-
16	Indian Ocean	0.33	0.40	0.32	0.26	0.21	0.17	0.13	0.11	0.09	0.07
17	Southern Ocean	0.57	0.57	0.57	0.43	0.34	0.26	0.21	0.16	0.13	0.10
18	Arctic Ocean	0.15	0.73	1.37	1.00	0.81	0.39	0.17	0.44	0.20	0.18
19	Middle Southern Ocean	0.68	0.51	0.38	0.29	0.21	0.16	0.12	0.09	0.07	0.05
20	Barents Sea and Coast of Norway	-	-	3.71	2.67	1.92	1.38	0.42	0.35	0.30	0.26
21	Baltic Sea	-	1.00	1.26	0.72	3.21	2.38	1.76	1.30	0.96	0.71
22	North Sea	5.49	3.62	17.49	6.35	1.96	0.55	0.23	0.20	0.18	0.16
23.1	Irish Sea	281.40	1840.44	795.49	282.29	37.46	11.79	10.11	6.00	3.49	2.82
23.2	Irish Sea	49.13	94.19	112.09	47.35	7.41	3.21	2.04	1.54	1.08	0.43
23.3	Irish Sea	4.35	8.17	4.20	4.75	1.82	0.64	0.29	0.82	0.37	0.35
23.4	Irish Sea	1.35	1.07	0.85	0.68	0.54	0.43	0.34	0.27	0.22	0.17
23.5	Irish Sea	-	-	-	-	-	-	-	-	-	-
24	English Channel	2.71	2.80	1.00	1.29	0.86	0.34	0.19	0.12	0.10	0.09
25.1	northern North Atlantic Ocean	7.04	26.45	42.47	17.74	2.51	0.44	0.30	0.48	0.32	0.31
25.2	northern North Atlantic Ocean	1.42	1.81	2.96	1.11	0.53	0.56	1.00	0.32	0.26	0.22
26	Black Sea	-	-	-	-	2.46	1.58	1.01	0.65	0.42	0.27
27	Mediterranean Sea	0.52	0.45	0.40	0.40	0.25	0.17	0.17	0.19	0.26	-
28	North Atlantic Ocean	0.56	0.53	0.50	0.30	0.25	0.21	0.18	0.15	0.13	0.11
29	Central Atlantic Ocean	0.17	0.27	0.36	0.26	0.08	0.07	0.07	0.06	0.05	0.05
30	South Atlantic Ocean	0.59	0.50	0.43	0.36	0.31	0.26	0.20	0.16	0.13	0.10
31	Sea of Okhotsk	0.91	0.57	0.36	0.23	0.16	0.14	0.12	0.11	0.09	0.09
32	Eastern China Sea	0.47	0.38	0.31	0.25	0.20	0.17	0.14	0.12	0.10	0.11
33	South China Sea	0.23	0.32	0.41	0.16	0.10	0.06	0.04	0.03	0.02	0.01
34	Berigng Sea	0.92	0.70	0.53	0.41	0.31	0.24	0.18	0.14	0.11	0.26
35	Indonesian Archipelago	0.27	0.25	0.23	0.21	0.19	0.17	0.15	0.14	0.13	0.12
36	Atlantic sector of Antarctic	0.21	0.17	0.14	0.11	0.09	0.07	0.06	0.05	0.04	0.03
37	Indian sector of Antarctic	0.27	0.19	0.13	0.09	0.06	0.04	0.03	0.02	0.01	0.01

-: There is no available data.

#: Estimated value based on the extrapolation of the trend line.

4.3. Recirculation of F1NPS ^{137}Cs associated with basin-scale transport in the North Pacific Ocean and its marginal sea

1360   In this section, we focus on the temporal variations in the ^{137}Cs activity concentrations in the North Pacific Ocean and its marginal seas after 2011 to investigate the transport of ^{137}Cs from the F1NPS accident. Fig. 17a shows the 0.5-yr ^{137}Cs median values in the western and eastern North Pacific Ocean after 2011. These boxes were selected as typical cases because

the main plume of F1NPS-^{137}Cs is transported in these region and exists in many measurements. As described above, the 0.5-yr median values of ^{137}Cs decreased exponentially before the F1NPS accident. However, significantly high 0.5-yr median ^{137}Cs values were measured in the western North Pacific Ocean (8-59 Bq m^{-3}), where is the major atmospheric fallout region (30-50°N, western North Pacific Ocean), and eastern North Pacific Ocean (2.4-7.6 Bq m^{-3}) in 2011/2012. Increases in ^{137}Cs in the subarctic North Pacific Ocean (15-28 Bq m^{-3}) and Bering Sea (4.2 Bq m^{-3}) were also observed in 2011/2012, although the data did not show due to the limited sample measurements. Slightly higher values were also observed in the Sea of Okhotsk (2.3 Bq m^{-3}; not shown in this figure) and the Japan Sea (1.6-1.9 Bq m^{-3}). These were caused by the atmospheric deposition of ^{137}Cs derived from the F1NPS accident.

After 2013, in the western North Pacific Ocean, the 0.5-yr median ^{137}Cs values decreased exponentially with seasonal variation, in which higher in summer and lower in winter. In the eastern North Pacific Ocean, the 0.5-yr median ^{137}Cs values increased after 2014 and reached a maximum in 2018. It is clear that the 0.5-yr median ^{137}Cs values in the eastern North Pacific Ocean were higher than those in the western region in 2018/2019. With the optimal interpretation analysis in Inomata et al. (2016), the main plume of F1NPS-^{137}Cs exists in the centre in the North Pacific Ocean (longitude range of 165°E-170°W and latitude range of 30-50°N), which corresponds to the subarctic, western, and eastern North Pacific Ocean boxes in this study in 2012. The zonal transport median speed of F1NPS-^{137}Cs was estimated to be approximately 8 cm s^{-1} from March 2011 to March 2012 (Aoyama et al., 2013). The arrival of F1NPS derived radio caesium was detected in June 2013 in the Canadian continental shelf and these continued until February 2014 (Smith, et al., 2015). The ^{137}Cs activity concentrations reached to 2 Bqm^{-3}, which is two times larger than those in the nuclear weapons derived ^{137}Cs.

A slight increase in the 0.5-yr median value of ^{137}Cs also occurred in the Eastern China Sea and Japan Sea after 2013 and reached maximum values in 2015/2016 (Fig. 17b). The ^{137}Cs activity concentrations in the Eastern China Sea and Japan Sea increased following the processes elucidated in our previous studies (Inomata et al., 2018). The increase in ^{137}Cs activity concentrations was first observed in the subsurface layer in 2012/2013 around southern Japan in the western North Pacific Ocean. Based on the potential temperature density (σ_θ), the ^{137}Cs peak existed in the subtropical mode water. In the Eastern China Sea, the increase in the ^{137}Cs activity concentrations also started in subsurface seawater (140 m) in 2013, and ^{137}Cs activity in the surface mixed layer (0-50 m) in the Eastern China Sea reached a maximum in 2014/2015 (Inomata et al., 2018). Increased ^{137}Cs in the Eastern China Sea is caused by the following processes: the ^{137}Cs entrained into the subtropical mode water is transported westwards in the subsurface seawater and upwells along the continental shelf in the Eastern China Sea and the Kuroshio counter current around the meandering Kuroshio (Ito et al., 1994). Furthermore, the ^{134}Cs/^{137}Cs ratios in subtropical mode water were almost the same as those in seawater in the Eastern China Sea and Japan Sea (Aoyama et al., 2017; Inomata et al., 2018). Then, the F1NPS-derived ^{137}Cs flowed into the Japan Sea via the Tsushima Strait by the Tsushima warm current and reached a maximum in 2015/2016. The propagation of F1NPS-derived ^{137}Cs from the Eastern China Sea to the Japan Sea occurred over 1-2 years.
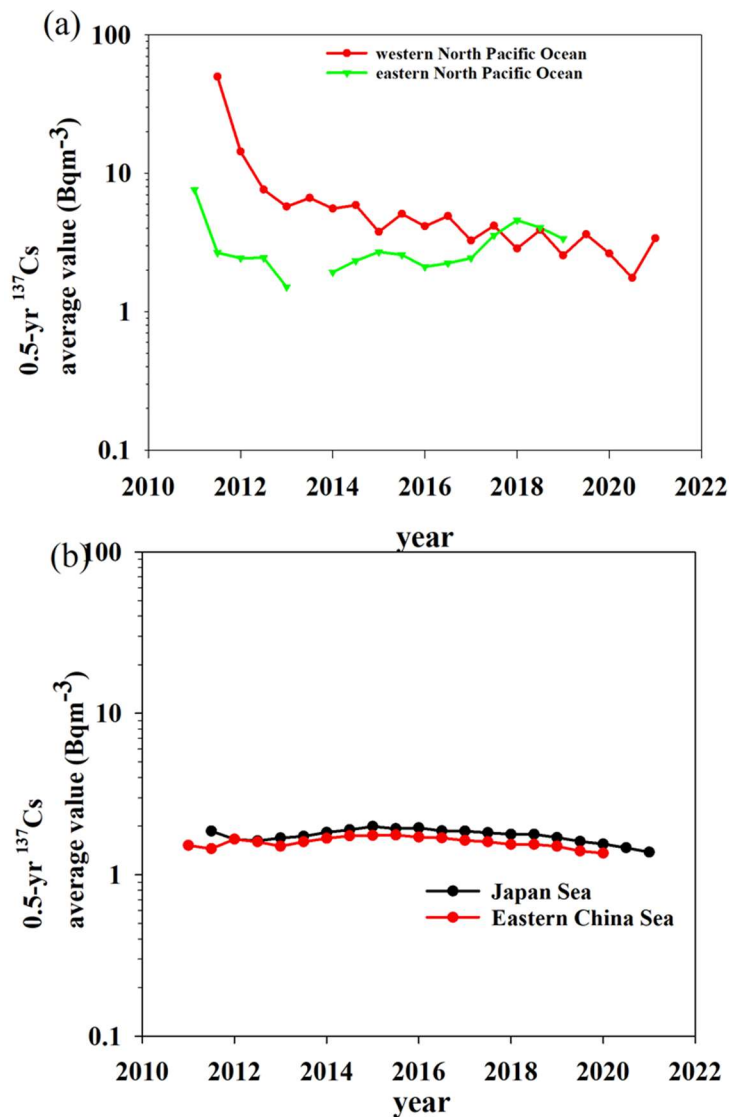
Figure 17: Temporal variations in the 0.5-yr median values of surface ^{137}Cs in the North/equatorial Pacific Ocean and its marginal seas after 2011. (a) Western and eastern North Pacific Ocean, (b) Japan Sea and Eastern China Sea.

4.4 Estimation of the amount of ^{137}Cs outflow to the downstream box and/or below the surface mixed layer

1400   The ^{137}Cs deposited into the ocean surface is transported via advection and diffusion in the surface seawater, then is transported to deep water below the mixed layer depth, where it undergoes radioactive decay ($T_{1/2}$ = 30.17 yr). In 1st January 1970, ^{137}Cs existing in the surface seawater in the global ocean was estimated to be 187 ± 26 PBq. This value corresponds to 32% of the deposited ^{137}Cs until 1970, although the ^{137}Cs released from reprocessing plants is included. The remaining approximately 68% of deposited ^{137}Cs, which is estimated to be 577 ± 60 PBq, would be transported downwards below the

1405   surface mixed layer in the global ocean on a decadal timescale. According to the estimation by using a model simulation (Kamidaira et al., 2015), the amount of F1NPS-^{137}Cs transported below the surface mixed layer within 4 months is almost half.

Fig. 18 shows the horizontal distributions of the net inflow/outflow ^{137}Cs amount in the surface mixed layer based on the ^{137}Cs deposition amount until the 1st of January 1970. Positive values (red) indicate that net inflowed ^{137}Cs is larger, whereas negative values (blue) indicate that net outflowed ^{137}Cs is larger in each Box. The decrease of ^{137}Cs occurred in the North

1410   Pacific Ocean. The largest decrease, which was estimated to be 61.2 PBq, occurred in the subarctic North Pacific Ocean. On the other hand, an increase in the ^{137}Cs amount occurred in the western subtropical South Pacific Ocean (2.8 PBq), eastern South Pacific Ocean (9.6 PBq), middle Southern Ocean (2.6 PBq), Southern Ocean (12.4 PBq), and Antarctic Ocean (1.2-4.0

PBq). This suggests that some of the ^{137}Cs deposited into the Pacific Ocean was transported to the South Pacific Ocean (south of 40°N), followed by movement to the Indian Ocean within 10-20 years. The outflow of ^{137}Cs in the northern North Atlantic Ocean and North Atlantic Ocean was also large (41.4 PBq and 57.1 PBq, respectively). The increase in ^{137}Cs in the Irish Sea (Irish Sea.1; 2.3 PBq), North Sea (0.7 PBq), and northern North Atlantic Ocean (0.5 PBq) was due to the discharged ^{137}Cs from the Sellafield and La Hague plants (Fig. 18).

The temporal variation in the outflow/inflow pattern of the ^{137}Cs amount is shown in Figs. 19-21. Fig. 19 shows the inflowed or outflowed ^{137}Cs amount in each area in the global ocean from 1975 to 2015 at 5-year intervals. The inflowed or outflowed ^{137}Cs amount corresponds to the sum of the ^{137}Cs amount for the previous five years. In 1975, 1980 and 1985, the values in the subarctic, western, and eastern North Pacific Ocean were negative (-0.5−-2.7 PBq; -0.4−-1.8 PBq; and -0.03−-1.2 PBq, respectively), whereas the subtropical North Pacific Ocean and equatorial Pacific Ocean showed positive values (0.1−1.3 PBq; 0.08−1.3 PBq; and 0.07−1.3 PBq, respectively). The inflowed ^{137}Cs also occurred in the subtropical eastern South Pacific Ocean (5.2 and 1.1 PBq) and Southern Ocean (1.7 and 1.7 PBq) in 1975 and 1980 and the eastern South Pacific Ocean (0.8 PBq) in 1980. Distribution of negative and positive values reflect the ^{137}Cs transport or distribution: ^{137}Cs deposited in the surface mixed layer in the western North Pacific Ocean was transported eastwards and accumulated into the eastern subtropical Pacific Ocean. Then, these were transported southwards with subsidence associated with California Current and westwards in the equatorial Pacific Ocean. ^{137}Cs moved southwards due to subduction in the eastern subtropical North Pacific Ocean and upwelled in the western/eastern equatorial Pacific Ocean. The negative values (-0.9−-1.7 PBq for 1975; -0.4−-1.1 PBq for 1980) in the western subtropical South Pacific Ocean, western South Pacific Ocean, and eastern Southern Ocean and positive values (0.3−2.5 PBq for 1975; 0.3−1.7 PBq for 1980) in the Arabian Ocean, Indian Ocean and Southern Ocean would result in the transport of ^{137}Cs from the Pacific Ocean into the Indian Ocean through the Indonesian Archipelago in 1975 and 1980. After 1990, the positive ^{137}Cs values in the eastern/western subtropical North Pacific Ocean and equatorial Pacific Ocean became negative (Fig. 19d). This suggests that the main ^{137}Cs plume derived from the large-scale nuclear weapon tests would pass through until 1990. It is also noted that a small amount of ^{137}Cs inflowed into the South Atlantic Ocean in 1975 (0.1 PBq) and 1980 (0.01 PBq) (Fig. 19a,b). A small ^{137}Cs increase also occurred in the Central Atlantic Ocean after 1995 (Fig. 19c). In 2015, increased ^{137}Cs in the subarctic, western, and eastern North Pacific Ocean (0.02−1.2 PBq) would be caused by the ^{137}Cs released from the F1NPS (Fig. 19i).

In the northern North Atlantic Ocean and its marginal seas (Fig. 20), the increase in the ^{137}Cs amount due to the discharged ^{137}Cs from the reprocessing plants was significant in the northern North Atlantic Ocean, North Sea, and Barents Sea and coast of Norway and transported to the Arctic Ocean (Fig. 20a-d). The contribution of the discharged ^{137}Cs from reprocessing plants decreased after 1985. The contribution from the Chernobyl accident found in the Baltic Sea, Black Sea, and Mediterranean Sea in 1990 (Fig. 20d).

In the Irish Sea and English Chanel, the contributions of ^{137}Cs released from reprocessing plants were large in 1975, and it appears that this ^{137}Cs was transported to the northern North Atlantic Ocean and North Sea until 1980. In 1980, the ^{137}Cs amount around the source region, Irish Sea 1, showed negative values. After 1985, the contribution from the reprocessing plants was negatively associated with the decreased discharged ^{137}Cs amount (Fig. 21).

(a)

1450

(b)

(c)
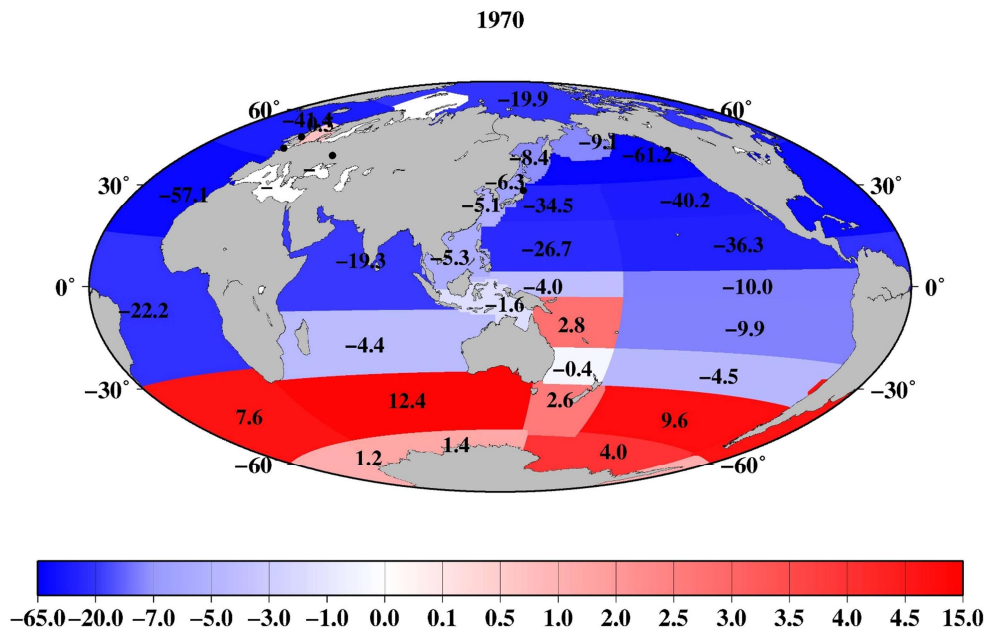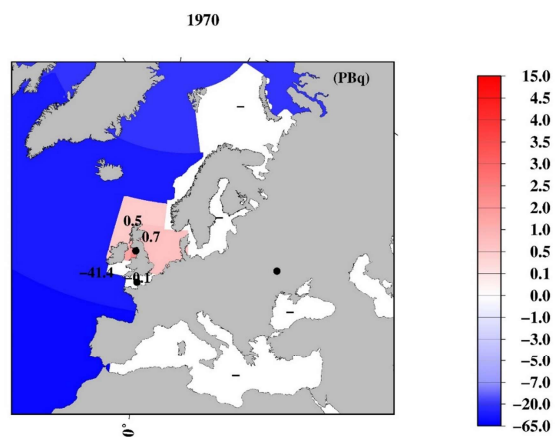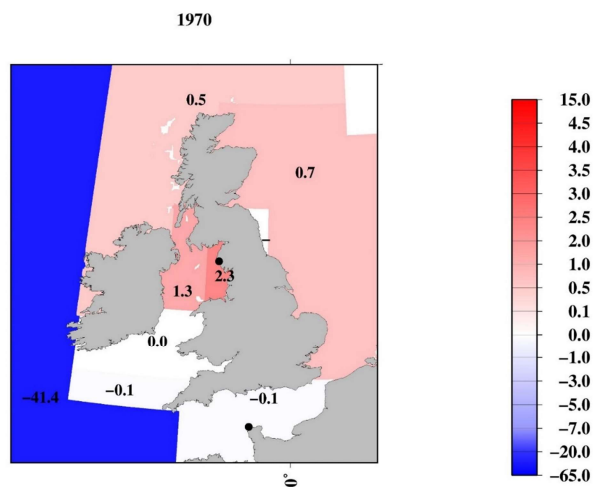
Figure 18: Horizontal distribution of the ^{137}Cs outflow amount in each box against the deposition amount in 1970 based on the 0.5-year ^{137}Cs activity concentration data. The amount of ^{137}Cs outflow includes the downwards transport portion below the surface mixed layer and horizontal transport in the surface mixed layer to the downstream boxes. A positive value (red) indicates the inflow amount, and negative values (blue) indicate the outflow amount. (a) Global ocean, (b) northern North Pacific Ocean and its marginal seas, (c) Irish Sea and English Chanel. The unit is PBq.

1460

(a)

1465

(b)

1470

(c)

(d)

(e)

(f)

1490

1495

1500

(g)

(i)
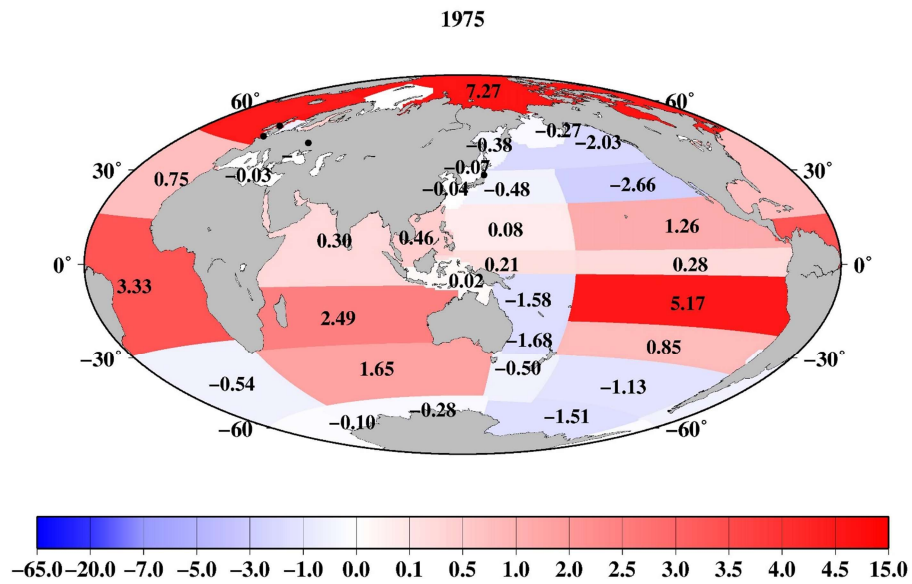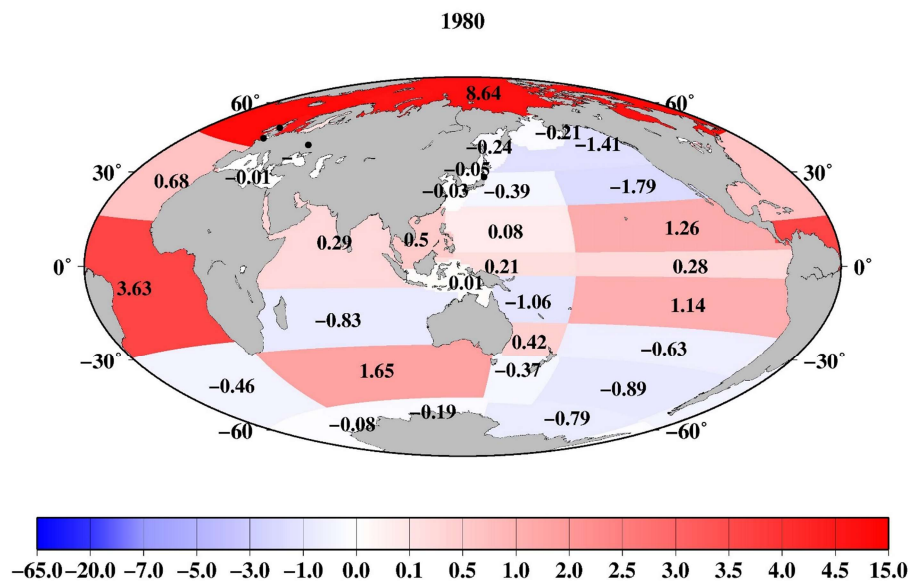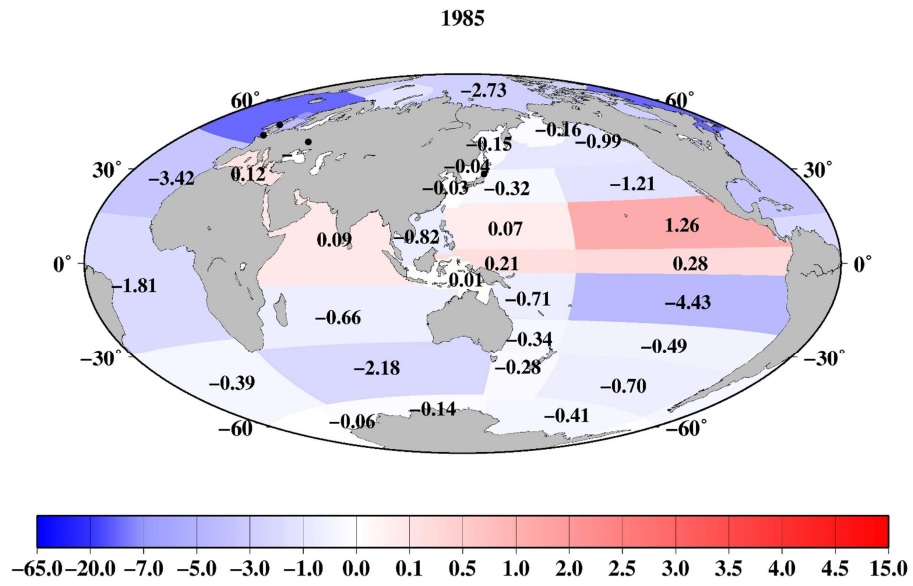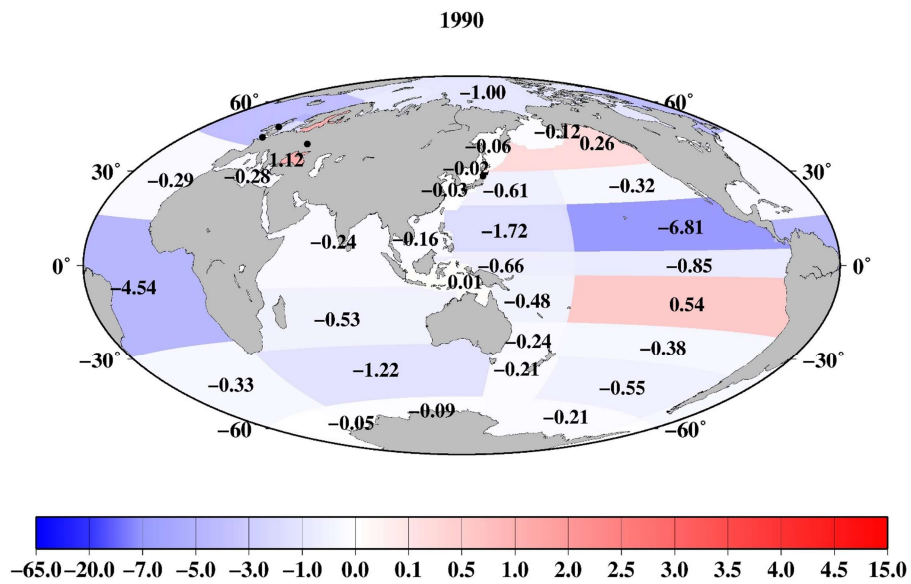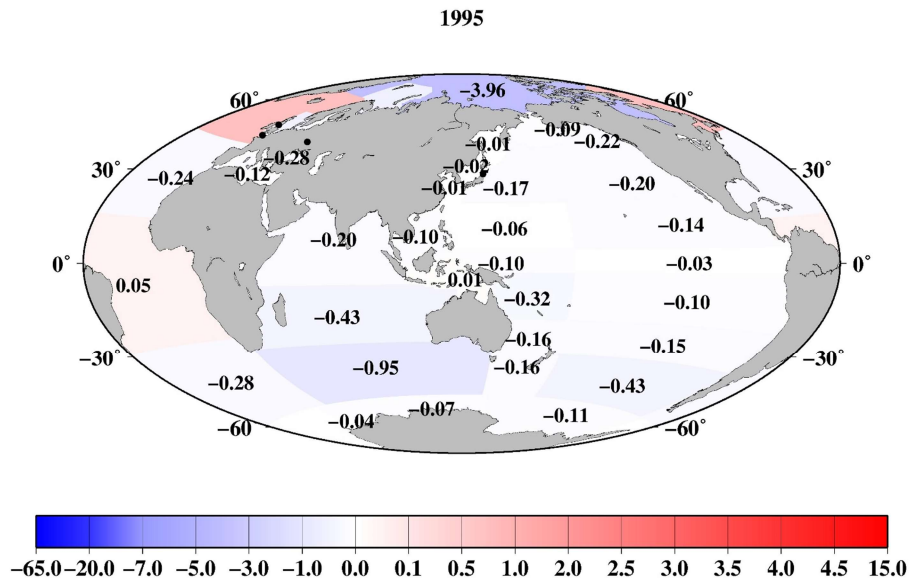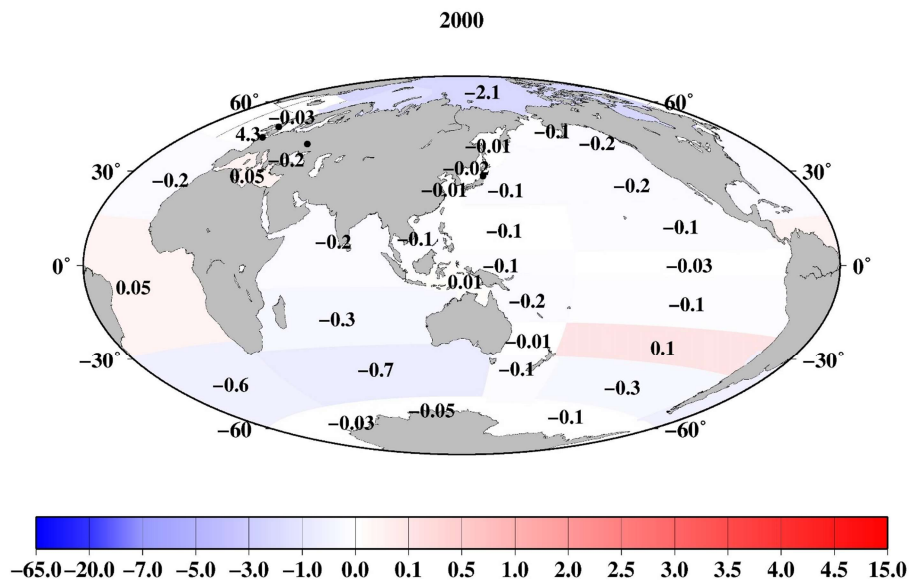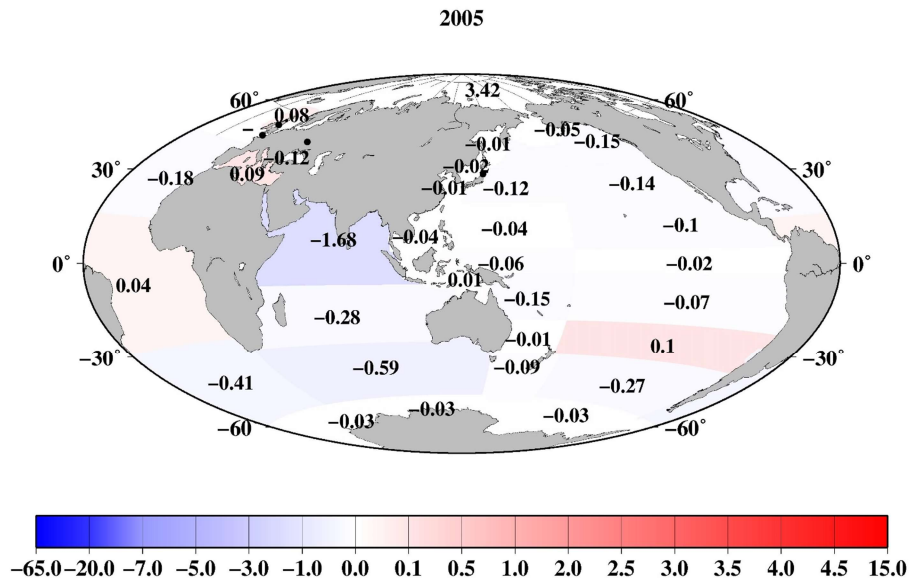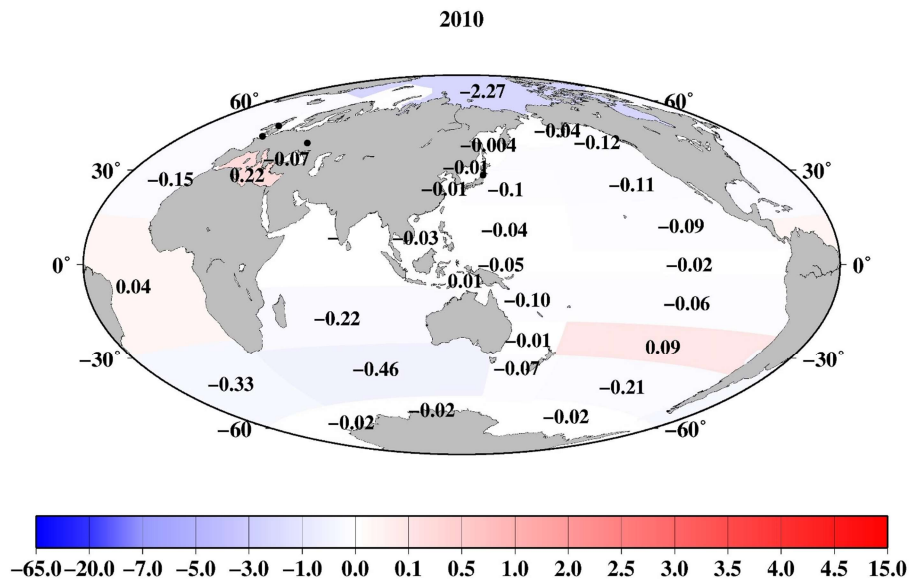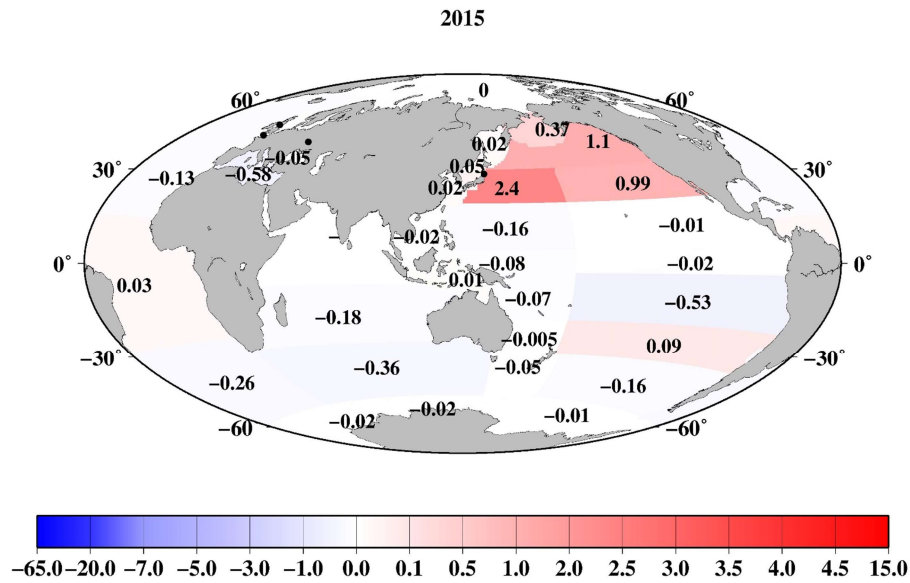
Figure 19: Mass balance of ^{137}Cs in the surface seawater in each box in the global ocean. A positive value (red) indicates a larger inflow from the upstream boxes, and negative value (blue) indicates a larger outflow to the downstream boxes or below the surface mixed layer compared to the previous 5 years. The unit is PBq. (a) 1975, (b) 1980, (c) 1985, (d) 1990, (e) 1995, (f) 2000, (g) 2005, (h) 2010, and (i) 2015.

(a)

1535   (b)

(c)

1540

1545

1550

(d)

 (e)

1560

1565

 (g)

(h)
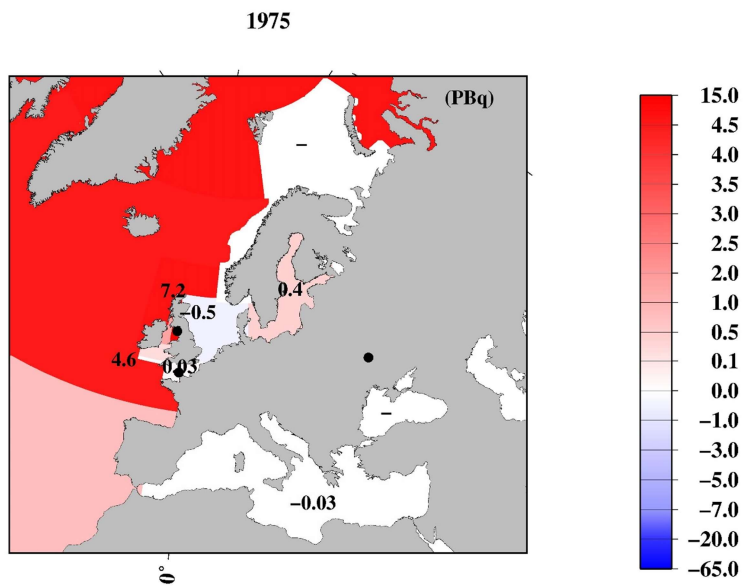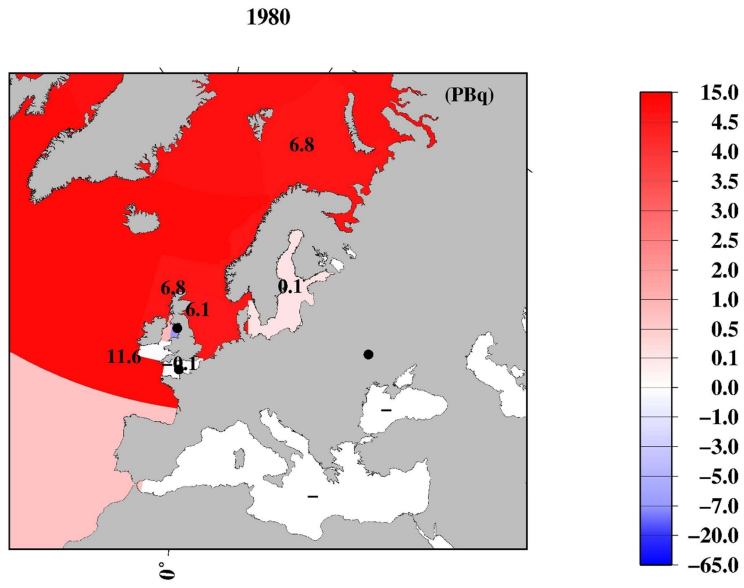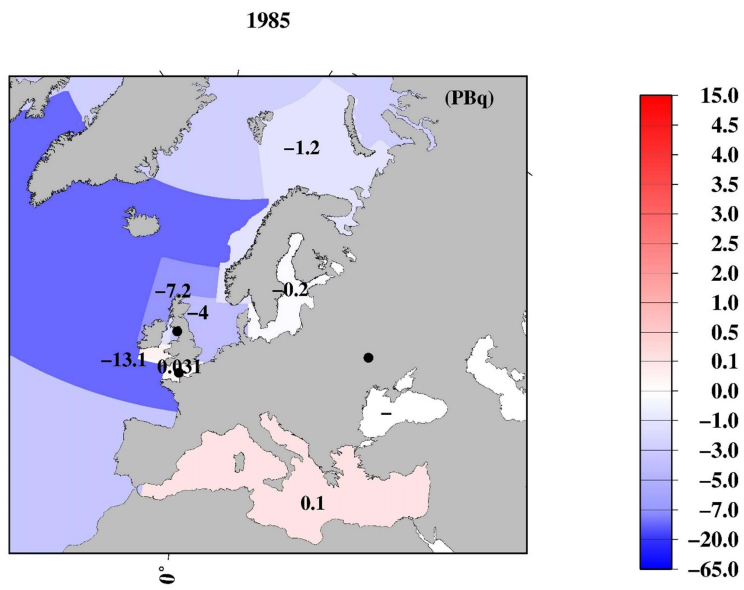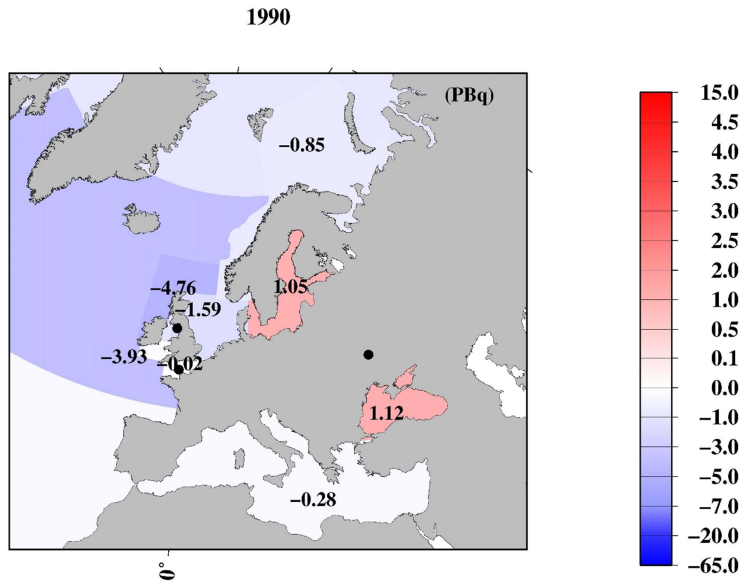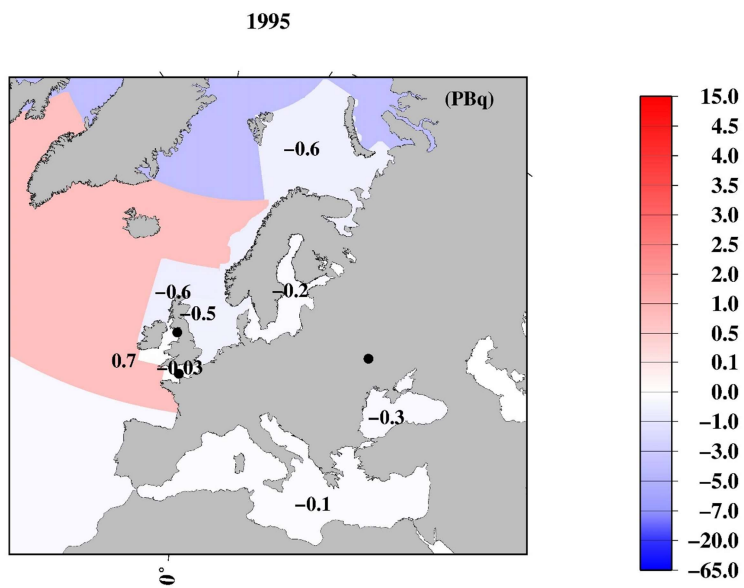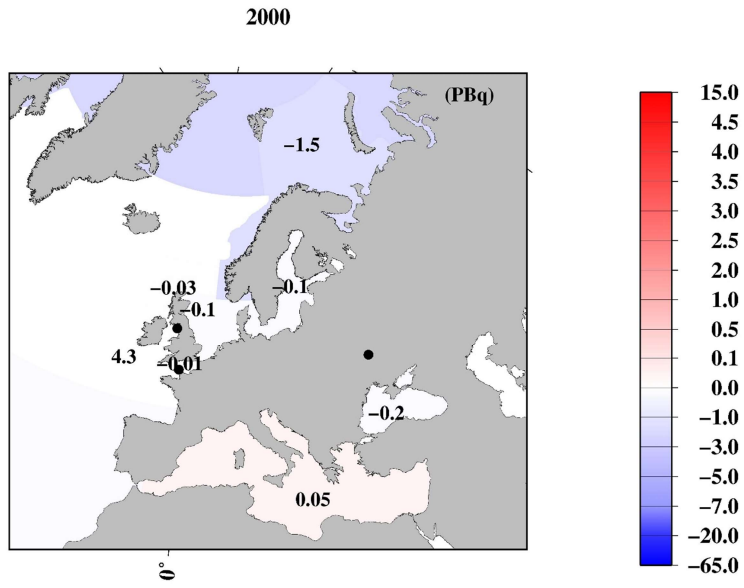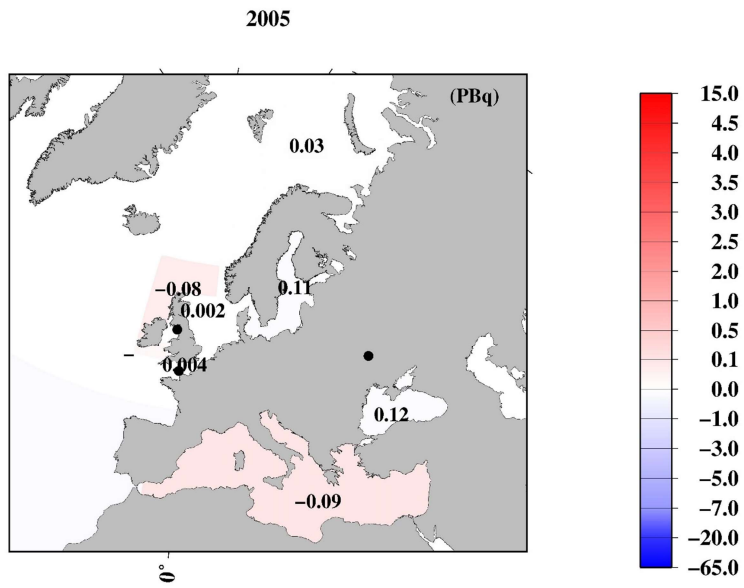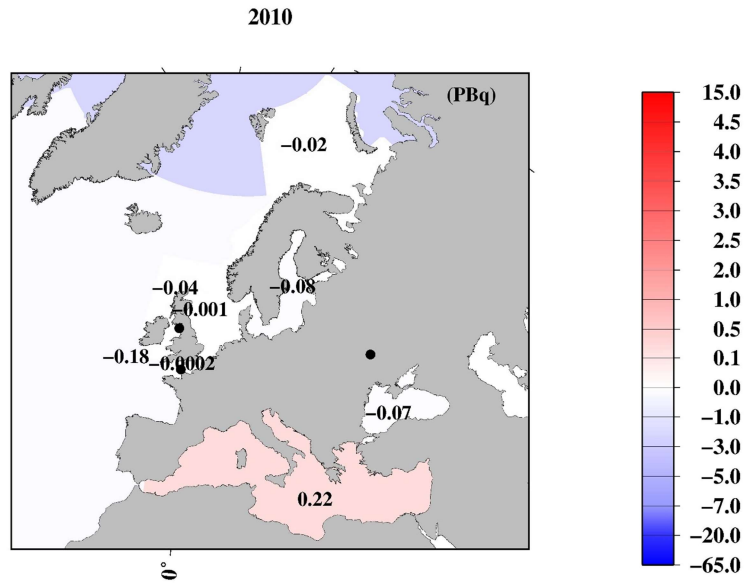
(i)
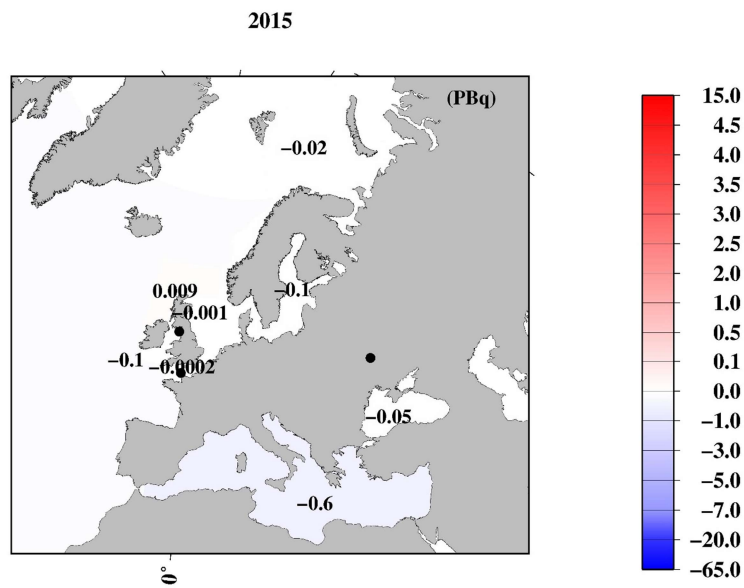
Figure 20: Mass balance of ^{137}Cs in the surface seawater in each box in the northern North Atlantic Ocean and its marginal seas. A positive value (red) means the larger inflow from the upstream boxes, and a negative value (blue) indicates a larger outflow to the downstream boxes or below the surface mixed layer compared to the previous 5years. The unit is PBq. (a) 1975, (b) 1980, (c) 1985, (d) 1990, (e) 1995, (f) 2000, (g) 2005, (h) 2010, and (i) 2015.

(a)

1975

1600

(b)

1980

1605

1610

1615 (c)

1985

(d)

1990

1620

1625

1630

(e)

1995

(f)

2000

1635

1640

1645

(g)

(h)

(i)
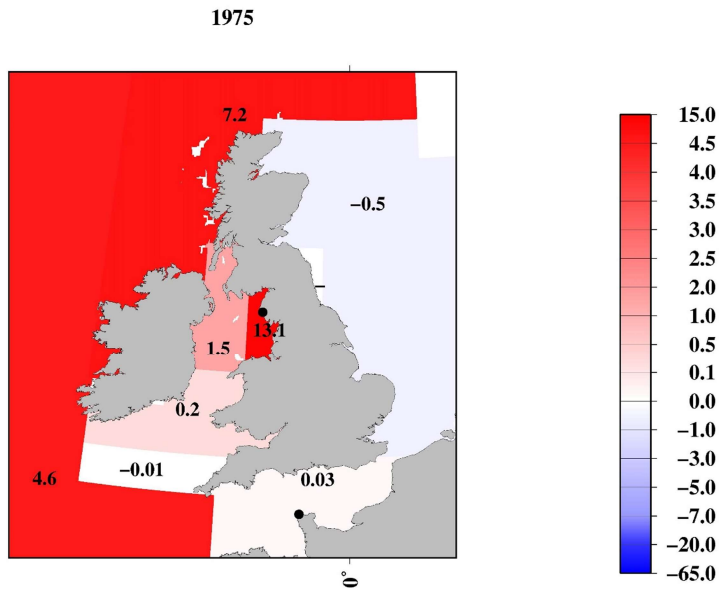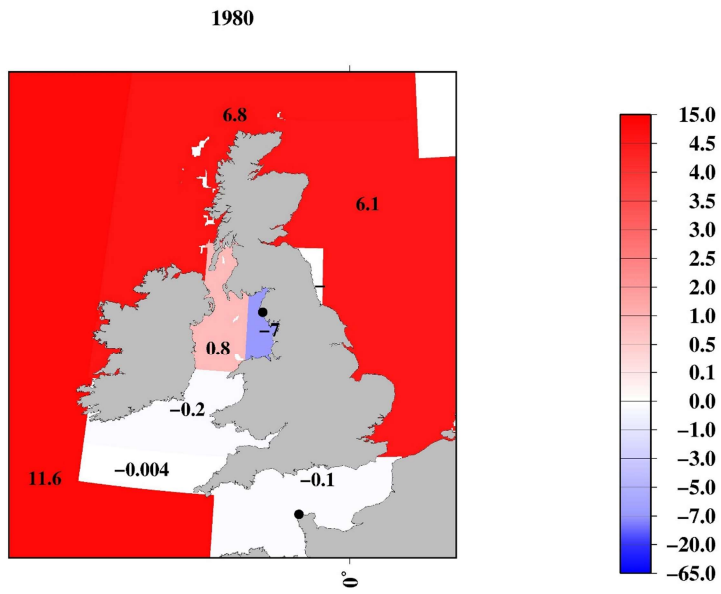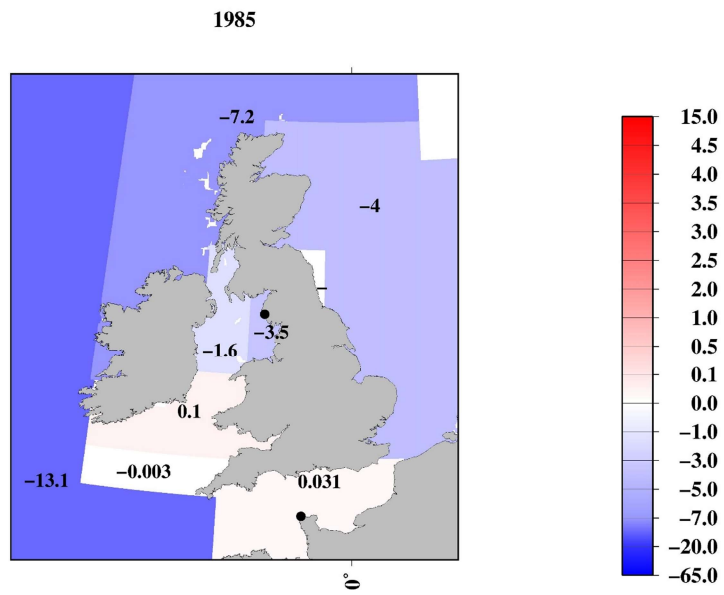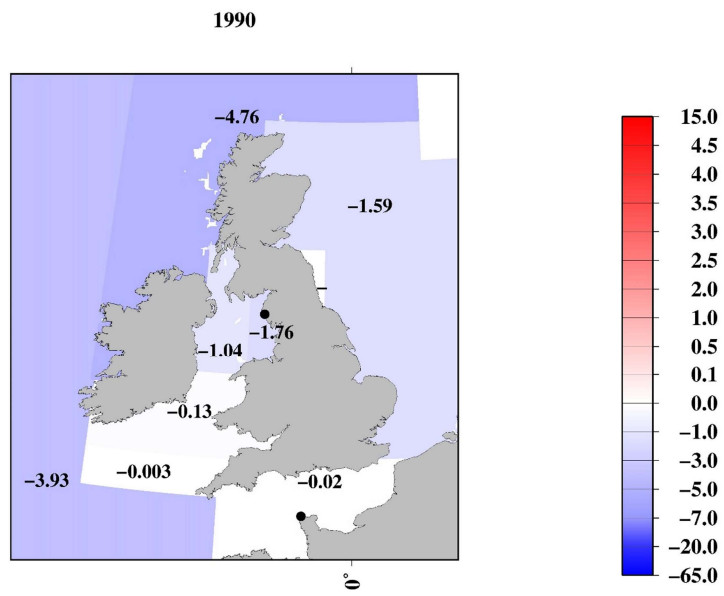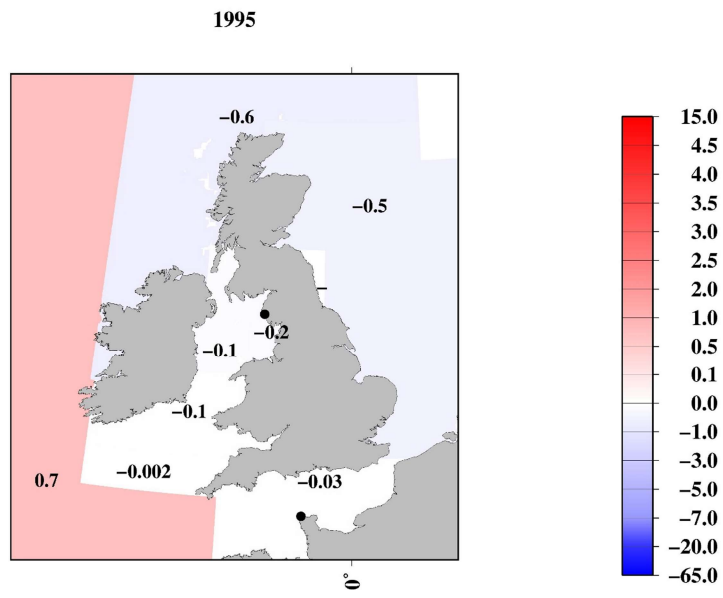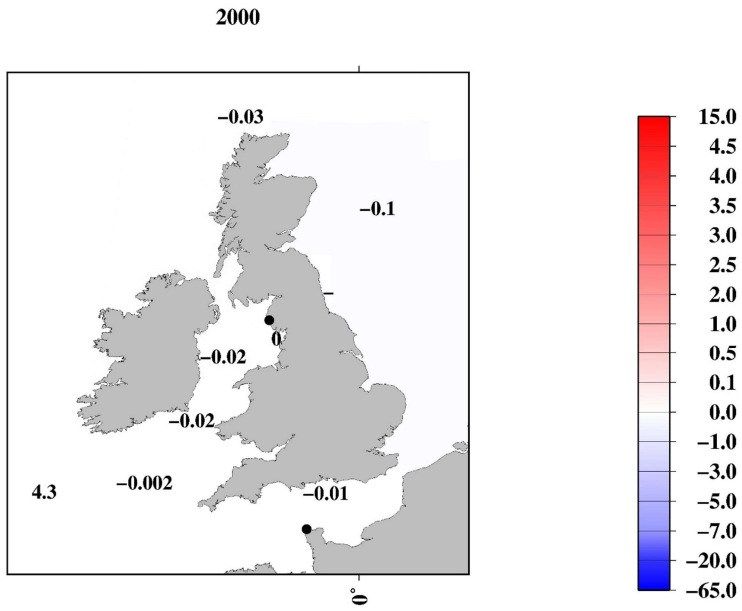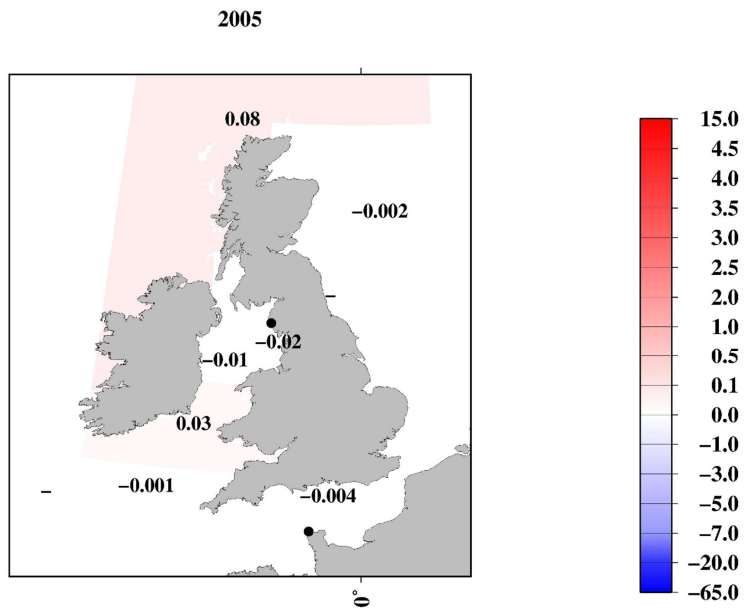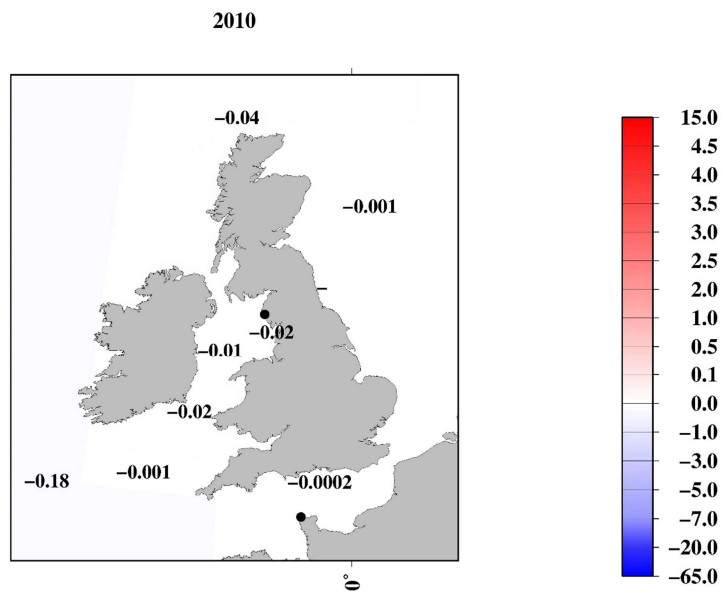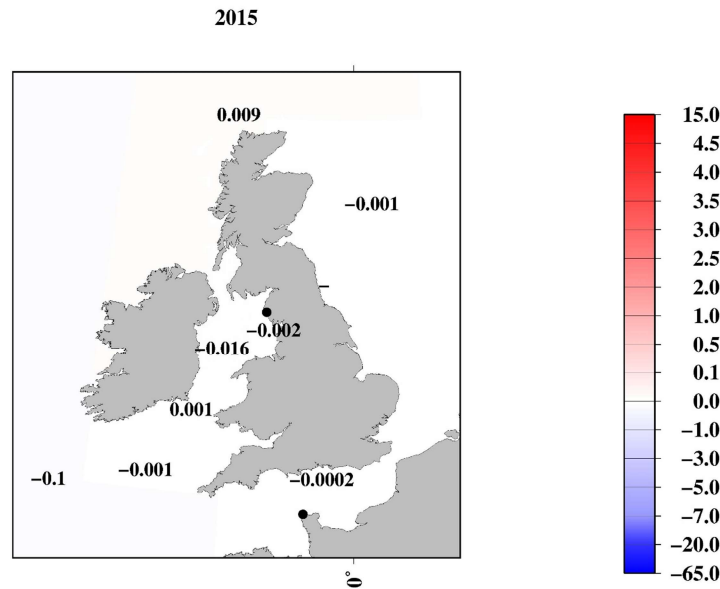
Figure 21: Mass balance of ^{137}Cs in the surface seawater in each box in the Irish Sea and English Chanel. A positive value (red) indicates a larger inflow from the upstream boxes, and a negative value (blue) indicates a larger outflow to the downstream boxes or below the surface mixed layer compared to the previous 5years. The unit is PBq. (a) 1975, (b) 1980, (c) 1985, (d) 1990, (e) 1995, (f) 2000, (g) 2005, (h) 2010, and (i) 2015.

4.5. Time scale of ^{137}Cs basin/global scale transport in the global ocean

Time scale of basin/global scale transport of ^{137}Cs are summarized in Figure 22 based on the spatiotemporal variation in the ^{137}Cs inventory, density, and mass balance analysis. The colour means that the ^{137}Cs deposition amount in each area until 1st January 1970. The ^{137}Cs deposited by the large-scale nuclear weapons tests and F1NPS accident in the western North Pacific Ocean was transported eastwards within 1-2 years by the Kuroshio and its extension. After reaching the western coast of America continent with the Kuroshio Current, and its extension, the F1NPS derived ^{137}Cs were bifurcated to toward northern and southern flowing along the current in the North Pacific Ocean. The ^{137}Cs derived from the F1NPS accident in northern transported seawater was along with the Alaska Current (3-4 years). An increase in ^{137}Cs activity concentrations was observed in the Bering Sea, Okhotsk Sea for 6 years. The ^{137}Cs might be entered in the Arctic Ocean (Kumamoto et al., 2019). On the other hands, the ^{137}Cs derived from the large scale nuclear weapons test were arrived near the coast of California, this ^{137}Cs was transported southwards with subsidence in the equatorial Pacific Ocean and transported westwards in the equatorial Pacific Ocean for 8-10 years. Following then the ^{137}Cs entered into the Indian Ocean from the Pacific Ocean over the 2-3 decadal timescale. Furthermore, ^{137}Cs was transported into the South and Central Atlantic Ocean over a period of 3-4 decadal time scale. The ^{137}Cs deposited into the western North Pacific Ocean by the F1NPS accident were entrained in the subtropical mode water, transported in the subsurface layer, and attained to the East China Sea and Japan Sea with 2-3 years timescale. The ^{137}Cs transported to northern part of the Japan Sea was about 4 years. In the northern North Atlantic Ocean and its marginal seas, a significant amount of ^{137}Cs was discharged from reprocessing plants transported to the North Sea, Barents Sea and coast of Norway, and the Arctic Ocean over approximately 1-2 decadal time scale.
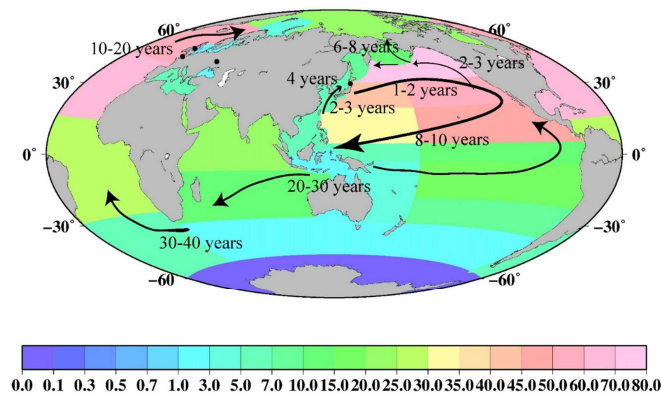
Figure 22: Distribution of ¹³⁷Cs deposition in 1 January 1970 and ¹³⁷Cs transport route in the surface seawater of the global ocean deduced. Circles are location of the nuclear reprocessing plants, Chernobyl, and F1NPS.

5. Conclusions

In this study, we analysed the ^{137}Cs activity concentrations in the surface seawater in the global ocean by using almost all of the available historical data in the global ocean. The surface seawater was divided into 37 boxes, and the temporal variations in the 0.5-yr median ^{137}Cs values in each box were investigated to determine the ^{137}Cs distribution and transport in the global surface seawater.

The ^{137}Cs deposition as of 1st January 1970, with two × two minutes resolution, is estimated to be 874±90 PBq. In 1970, due to the minor contribution of atmospheric deposition, the ^{137}Cs inventory in the surface mixed layer in the global ocean was estimated to be 184±26 PBq. This suggests that 68% of the ^{137}Cs deposited into the surface seawater in the global ocean (577±60 PBq) had already been transported below the surface mixed layer on a decadal timescale. The ^{137}Cs inventory increased slightly and reached a maximum (214±11 PBq) in 1980. The increased ^{137}Cs inventory was due to the discharged ^{137}Cs from the reprocessing plants: Sellafield and La Hague. Then, the ^{137}Cs inventory decreased, and the value in 2010, immediately before the F1NPS accident, was estimated to be 37.2±3.6 PBq. The relative contributions in the South Pacific Ocean, Indian Ocean, and Atlantic Ocean to the ^{137}Cs inventory in the surface mixed layer in the global ocean increased gradually. In 2011, the ^{137}Cs inventory increased to 50.7±7.3 PBq, in which the F1NPS-derived ^{137}Cs accounted for 15.5±3.9 PBq.

The ^{137}Cs derived from the large scale weapons tests and F1NPS accident were released into the almost same region in the western North Pacific Ocean. The ^{137}Cs transported eastward along with Kuroshio and its extension and coast of the America with 1-2 years timescale, and then transported to southward and northward. In the southward transported part, seawater with higher ^{137}Cs activity concentration transported to southward associated with the Pacific subtropical gyre and subducted in the subtropical North Pacific Ocean and equatorial Pacific Ocean. The seawater with high ^{137}Cs activity concentrations entered the Indian Ocean over the 2-3 decades. Then, ^{137}Cs was transported into the South and Central Atlantic Ocean over a period of 3-4 decades. On the other hands, northward transported seawater along with the North America continent with 1-2 years timescale, transported westward to 6-8 years. Part of the seawater would be transported into the Arctic Ocean. The seawater entrained into the subtropical mode water in the North Pacific Ocean were transported westward in the subsurface layer and entered into the Eastern China Sea and the Japan Sea with 2-3 years. Finally, because ^{137}Cs is water soluble, its transport and distribution strongly depend on seawater circulation. The transport of ^{137}Cs-labelled seawater can be examined to interpret the circulation of substances in seawater, as well as the climate change associated with gaseous exchange between the atmosphere and the ocean surface.

Author contribution

YI (corresponding author) conducted data analysis and the preparation of the manuscript. MA developed the database of radioactivity. All authors discuss about the results of the data analysis.

Data availability

Data described in this manuscript can be accessed at repository under data doi.

References

Aoyama (2021) HAM, Histroical Artifial radioacitity database in Marine environment, Global2021. Center for Research in Isotopes and Environmental Dynamics, University of Tsukuba, doi: 10.34355/CRiED.U.Tsukuba.00085.

Inomata and Aoyama (2022a) ^{137}Cs measurement points in the surface seawater in the global ocean based in the HAM database2021. Center for Research in Isotopes and Environmental Dynamics, University of Tsukuba, 2021. doi: 10.34355/ Ki-net.KANAZAWA-U.00149.

Inomata and Aoyama (2022b) Temporal variations of ^{137}Cs activity concentrations and these 0.5-yr median values in the surface seawater in the global ocean. Center for Research in Isotopes and Environmental Dynamics, University of Tsukuba, 2021. doi: 10.34355/ Ki-net.KANAZAWA-U.00150.

Inomata and Aoyama (2022c) Dataset of 0.5-yr median values of ^{137}Cs activity concentrations in the surface seawater in the global ocean during the period from 1957 to 2021. Center for Research in Isotopes and Environmental Dynamics, University of Tsukuba, 2021. doi: 10.34355/ Ki-net.KANAZAWA-U.0015.

Competing interests

The authors declare that they have no conflict of interest.

Disclaimer

Publisher's note: Copernicus Publications remains neutral with regard to jurisdictional claims in published maps and institutional affiliations.

Acknowledgements

The author thanks to Prof. Baily du Bois to provide the ^{137}Cs data measured in the northern North Atlantic Ocean and its marginal sea. This research was financially supported by the Grant-in-Aid for Scientific Research on Innovative Areas, "Interdisciplinary study on environmental transfer of radionuclides from the Fukushima Dai-ichi NPP Accident" (Project No. 25110511) of the Japanese Ministry of Education, Culture, Sports, Science, and Technology (MEXT). This research was also supported by the cooperation program of the Environmental Radioactivity Research Network Centre (F-19-02, F-20-08, F-21-18, F-22-04) and the Institute of Nature and Environmental Technology, Kanazawa University (18009, 19022, 20043).

References

Aarkrog, A.: Radioactivity in polar-regions—Main sources. J. Environ. Radioact. 25, 21–35,1994.

1755   Aarkrog, A., Baxter, M.S., Berttencourt, A.O., Bojanowski, R., A. Bologa, S. Charmasson, I. Cunha, R. Delfanti, E. Duran., E. Holm, R. Jeffree, H.D. Livingston, S. Mahapanyawong, H. Nies, I.Osvath, Li. Pingyu, P.P.Povinec, A.Sanchez, and D.Swift: Comparison of doses from ^{137}Cs and ^{210}Po in marine food: A major international study. J. Environ. Radioact. 34, 69–90, 1997.

Aarkrog, A.: Input of anthropogenic radionuclides into the World Ocean. Deep Sea Res. Part II Top. Stud. Oceanogr., 50,
1760   2597–2606, 2003.

Aoyama, M., Hirose, K., Suzuki, Y., Inoue, H., and Sugimura, Y.: High level radioactive nuclides in Japan in May. Nature. 321, 819–820, 1986.

Aoyama, M., and Hirose, K.: The temporal and spatial variation of ^{137}Cs concentration in the Western North Pacific and its marginal seas during the period from 1979 to 1988. J. Environ. Radioact. 29, 57–74, 1995.

1765   Aoyama, M., Hirose, K., Miyao, T., Igarashi, Y., Povonec, P.P.: ^{137}Cs activity in surface water in the western North Pacific. J. Radioanal. Nucl. Chem. 248, 789–793, 2001a.

Aoyama, M., Hirose, K., Miyao, T., Igarashi, Y., and Povonec, P.P.: Temporal-variation of ^{137}Cs inventory in the western North Pacific. J. Radioanal. Nucl. Chem. 248, 785–787, 2001b.

Aoyama, M., and Hirose, K.: Artificial radionuclides database in the Pacific Ocean: HAM database. Sci. World J. 4, 200–215,
1770   2004.

Aoyama, M., Hirose, K., and Igarashi, Y.: Re-construction and updating our understanding on the global weapons tests ^{137}Cs fallout. J. Environ. Monit. 8, 431–438, 2006.

Aoyama, M., Hirose, K., and Nemoto, K., Takatsuki, Y., and Tsumune, D: Water masses labeled with global fallout ^{137}Cs formed by subduction in the North Pacific. Geophys. Res. Lett. 35, L01604, 2008.

1775   Aoyama, M.: Oceans and seas, in: Atwood, D. (Ed.), Encyclopedia of Inorganic Chemistry. Wiley, pp. 339–346, 2010.

Aoyama, M., Fukasawa, M., Hirose, K, Hamajima, Y., Kawano, T., Povinec, P.P., Sanchez-Cabeza, J.A. : Cross equator transport of ^{137}Cs from North Pacific Ocean to South Pacific Ocean (BEAGLE2003 cruises), Prog. Oceanogr. 89, 7–16, 2011.

Aoyama, M. Uematsu, M., Tsumune, D., and Hamajima, Y.: Surface pathway of radioactive plume of TEPCO Fukushima
1780   NPP1 released ^{134}Cs and ^{137}Cs. Biogeosci. 10, 3067–3078, 2013.

Aoyama, M., Hamajima, Y., Hult, M., Uematsu, M., Oka, E., Tsumune, D., and Kumamoto, Y.: ^{134}Cs and ^{137}Cs in the North Pacific Ocean derived from the March 2011 TEPCO Fukushima Dai-ichi Nuclear Power Plant accident, Japan. Part one: Surface pathway and vertical distributions. J. Oceanogr. 72, 53–65, 2016a.

Aoyama, M., Kajino, M., Tanaka, T.Y., Sekiyama, T.T., Tsumune, D., Tsubono, T., Hamajima, Y., Inomata, Y., and Gamo,
1785   T.: ^{134}Cs and ^{137}Cs in the North Pacific Ocean derived from the March 2011 TEPCO Fukushima Dai-ichi Nuclear Power Plant accident, Japan. Part two: Estimation of ^{134}Cs and ^{137}Cs inventories in the North Pacific Ocean. J. Oceanogr. 72, 67–76, 2016b.

Aoyama, M., Hult, M., Hamajima, Y., Lutter, G., Marissens, G., and Stroh, H.: Tracing radioactivity from Fukushima in the Northern Pacific Ocean. Appl. Radiat. Isot. 109, 435–440, 2016c.

1790   Aoyama, M.: Long-range transport of radiocaesium derived from global fallout and the Fukushima accident in the Pacific Ocean since 1953 through 2017-Part I: Source term and surface transport. J. Radioanal. Nucl. Chem. 318, 1519–1542, 2018a.

Aoyama, M., Hamajima, Y., Inomata, Y., Kumamoto, Y., Oka, E., Tsubono, T., and Tsumune, D.: Radiocaesium derived from the TEPCO Fukushima accident in the North Pacific Ocean: Surface transport processes until 2017. J. Environ.
1795   Radioact. 189, 93–102, 2018b.

Aoyama, M.: HAM, Histroical Artifial radioacity database in Marine environmnet, Global2021. Center for Research in Isotopes and Environmental Dynamics, University of Tsukuba, 2021. doi: 10.34355/CRiED.U.Tsukuba.00085.

Aoyama, M.: Artificial Radionuclides. Encyclopedia of Ocean Science (Third Edition), 136-152, Elsevier, Co. Ltd., 2019. https://doi.org/10.1016/B978-0-12-409548-9.10896-6.

Bezhenar, R., Maderich, V., Schirone, A., Conte, F., and Martazinova, V.: Transport and fate of ^{137}Cs in the Mediterranean and Black Seas system during 1945-2020 period: A modelling study. J. Environ. Radioact. 208–209, 2019.

Baily du Bois, P., Duman, F., Voiseux, C., Morillon, M., Oms, P-E., and Soiler, L.: Dissolved Radiotracers and Numerical Modeling in North European continental dispersion studies (1982-2016): Datsebases, methods and applications. Water. 12, 1667, 2020.

Ballestra, S., Bojanowski, R., Fukai, R., and Vas, D.: Proc. Int. Symposium on the Behavior of Long-lived Radionuclides in the Marine Environment. Luxembourg, EUR-ReasternPOrt 9214, 215–232. 2019.

Bezhenara, R., Madericha, V., Schironeb, A., Conteb, F., Martazinovac, V. Transport and fate of ^{137}Cs in the Mediterranean and Black Seas system during 1945–2020 period: A modelling study. 208-209, 106023, 2019.

Buesseler, K.: Fishing for answers off Fukushima, Science. 338, 480–482, 2012.

Buesseler, K., Dai, M., Aoyama, M., Benitez-Nelson, C., Charmasson, S., Higley, K., Maderich, V., Masqué, P., Oughton, D., and Smith, J.N.: Fukushima Daiichi–derived radionuclides in the ocean: Transport, fate, and impacts. Ann. Rev. Mar. Sci. 9, 173–203, 2017.

Bourlat, Y., Millies-Lacroix, J.-C., Petit, G.L., and Bourguignon, J.: ^{90}Sr, ^{137}Cs and $^{239+240}$Pu in world ocean water samples collected from 1992 to 1994. P. Guegueniat, P. Germain, H. Metivier (Eds.), Radionuclides in the oceans. Input and inventories, Les editions de Physique, Les Ulis. 75–93, 1996.

Bowen, V.T., Noshkin, V.E., Livingston, H.D., and Volchok, H.L.: Fallout radionuclides in the Pacific Ocean: Vertical and horizontal distributions, largely from GEOSECS stations. Earth Planet. Sci. Lett. 49, 411–434, 1980.

Broecker, W.S., Bonebakker, E.R., and Rocco, G.G.: The vertical distribution of cesium137 and strontium90 in the oceans, 2. J. Geophy. Res. 71, 1999–2003, 1966.

Broecker, W.S., and Simpson, H.J.: A summary of Lamont Sr90 and Cs137 measurements on ocean water samples. HASL-197, I-9–I-104, 1968.

Cochran, J.K., Livingston, H.D., Hirschberg, D.J., and Surprenant, L.D.: Natural and anthropogenic radionuclide distributions in the northwest Atlantic Ocean. Earth Planet. Sci. Lett. 84, 135–152, 1987.

CEC. The radiological exposure of the population of the European Community from radioactivity in North European waters, Project Marina. Report EUR 12483 EN, Commission of the European Communities, Brussels, 1990.

Dahlgarrd, H.: On the background level of ^{99}T~, ^{90}Sr and ^{137}Cs in the North Atlantic J. Mar. Sys. 6, 571–578, 1995.

Delfanti, R., Papucci, C., Salvi, S., Lorenzelli R.: IAEA CRP "Worldwide Marine Radioactivity". Research Contract - Agreement No. ITA-26803, ENEA, Italy, 2000.

Delfanti, R., and Pappuci, C.: Mediterranean Sea, in: Atwood, D. (Ed.), Encyclopedia of Inorganic Chemistry. Wiley, pp. 401–414, 2010.

Delfanti, R., Özsoy, E., Kaberi, H., Schirone, A., Salvi, S., Conte, F., Tsabaris, C., and Papucci, C.: Evolution and fluxes of ^{137}Cs in the Black Sea/Turkish Straits System/North Aegean Sea. J. Mar. Systems. 135, 117–123, 2014.

Egorov, V.N., Povinec, P.P., Polikarpov, G.G., Stokozov, N.A., Gulin, S.B., Kulebakina, L.G., and Osvath, I.: ^{90}Sr and ^{137}Cs in the Black Sea after the Chernobyl NPP accident: Inventories, balance and tracer applications. J. Environ. Radioact. 43, 137–155, 1999.

Feng, M., Zhang, N. Liu, Q. and Wijffels, S. The Indonesian throughflow, its variability and centennial change. Geosci. Lett. 5:3, 2018, https://doi.org/10.1186/s40562-018-0102-2.

Fin, R.A., Lukas, R., Bingham, F.M., Warner, M.J., and Gammon, R.H: The western equatorial Pacific: A water mass

crossroads. J. Res. Lett. 99, 25063–25080, 1994.

1840   Folsom, T.R., Mohanrao, G.J., and Winchell, P.: Fallout caesium in surface sea water off the California coast (1959–60) by
            gamma-ray. Nature. 187, 480–482, 1960a.

Folsom, T.R., and Mohanrao, G.J.: Measurement of fallout cesium in the Pacific Ocean and in terrestrial effluents likely to
            alter coastal waters. J. Radiat. Res. 1–2, 150–154, 1960b.

Folsom, T.R., Mohanrao, G.J., Pillai, K.C., and Sreekumaran, C.: Distributions of Cs137 in the Pacific. HASL-197, I-95–I-
1845   203, 1968.

Folsom, T.R., Sreekumaran, C., Hansen, N., Moore, J.M., and Grismore, R.: Some Concentrations of Cs137 at Moderate
            Depths in the Pacific 1965–1968. HASL-217, 1970.

Folsom, T.R., Hansen, N., Tatumi, T., and Hodge, V.F.: Recent improvements in methods for concentrating and analyzing
            radiocesium in sea water. J. Radiat. Res. 16, 19–27, 1975.

1850   Folsom, T.R.: Summary of Cs-137 Concentrations Measured at Scripps Institution in N. Pacific Surface Waters. EML-356,
            1979.

Fowler, S.W., Small, L.F., Rosa, J.L., Lopez, J.J., and Teyssie, J.L.: Interannual variation in transuranic flux at the vertex time-
            series station in the northeast Pacific and its relationship to biological activity, in: Kershaw, P.J. and Woodhead, D.S.,
            (Eds.), Radionuclides in the Study of Marine Processes. Kluwer, Dordrecht. pp. 286–298, 1991.

1855   Gordon, A.: Oceanography of the Indonesian Seas and their throughflow., Oceanography. 18(4), 14–27, 1995.

Gordona, A.L., Sprintall, J. Aken, H.M., Susanto, D., Wijffels, S., Molcard, R., A. Ffield, A., Pranowo, W., Wirasantosa, S:
            The Indonesian throughflow during 2004–2006 as observed by the INSTANT program. Dynamics Atmospheres and
            Oceans 50, 115–128, 2010.

Gray, J., Jones, S.R., and Smith, A.D.: Discharges to the environment from the Sellafield site, 1951e1992. J. Radiolo. Protect.
1860   15, 99-131, 1995.

Guegueniat, P., Kershaw, P., Hermann, J., and du Bois, P.B.: New estimation of La Hague contribution to the artificial
            radioactivity of Norwegian waters (1992–1995) and Barents Sea (1992–1997). Sci. Total Environ. 202, 249–266,
            1997.

Gulin S. B., and Stokozov, N.A.: ^{137}Cs concentrations in Atlantic and western Antarctic surface waters: results of the 7th
1865   Ukrainian Antarctic Expedition, 2002. J. Environ. Radioact. 83, 1–7, 2005.

Gulin, S. B., Mirzoyeva, N.Yu., Egorov, V.N., Polikarpov, G.G., Sidorov, I.G., Proskurnin, V.Y.: Secondary radioactive
            contamination of the Black Sea after Chernobyl accident: recent levels, pathways and trends. J. Environ. Radioact.
            124, 50–56, 2013.

Helsinki Communication: Baltic Marine Environment Protection Commission, Helcom, Radioactivity in the Baltic
1870   Sea 1984-1991. Balt. Sea Environ. Proc. 61, 1995.

Hanawa, K. and Talley, L.D.: Mode Waters, In Ocean Circulation and Climate, Edited by Gerold Siedler, Church, J., and
            Gould, J. pp. 373-386.

Hirose, K., Sugimura, Y., and Aoyama, M.: Plutonium and ^{137}Cs in the western North Pacific Estimation of residence time of
            plutonium in surface waters. Int. J. Rad. Appl. Instr. Part A Appl. Radiat. Isot. 43, 349–359, 1991.

1875   Hirose, K., Amano, H., Baxter, M.S., Chaykovskaya, E., Chumiche, V.B., Hong, G. H., Isogai, K., Kim, C.K., Miyao, T.,
            Morimoto, T., Nikitin, K., Oda, K., Pettersson, H.B.L., Povinec, P.P., Seto, Y., Tkalin, A., Togawa, O, and Veletova,
            M.K.: Anthropogenic radionuclides in seawater in the East Sea/Japan Sea Results of the first-stage Japanese-Korean-
            Russian expedition. J. Environ. Radioact. 43, 1–1, 1999.

Hirose, K., and Aoyama, M.: Present background levels of surface ^{137}Cs and ^{239,240}Pu concentrations in the Pacific. J. Environ.
1880   Radioact. 69, 53–60, 2003a.

Hirose, K, and Aoyama, M.: Analysis of ^{137}Cs and ^{239,240}Pu concentrations in surface waters of the Pacific Ocean. Deep Sea

Res. Part II Top. Stud. Oceanogr. 50, 2675–2700, 2003b.

Hirose, K., Aoyama, M., Katsuragi, Y., and Sugimura, Y.: Annual deposition of Sr-90, Cs-137 and Pu-239, 240 from the 1961-1980 Nuclear Explosions: A simple model. J. Meteoro. Soc. Jan. Ser. II. 65, 259–277, 1987.

1885 IAEA: Worldwide marine radioactivity studies (WOMARS). Radionuclide levels in oceans and seas. Final report of a coordinate research project. IAEA-TECDOC-1429, 2005.

IAEA: The Fukushima Daiichi Accident, Pub1710-TV1-Web.pdf., 2015.

IHA: Limits of Oceans and Seas. Special Edition N°23, 3rd Edition, 1953.

Ikeuchi, Y., Amano, H, and Aoyama, M. et al.: Anthropogenic radionuclides in seawater of the Far Eastern Seas. Sci. Total
1890 Environ., 237/238, 203–212, 1999.

Inomata, Y., Aoyama, M., and Hirose, K.: Analysis of 50-y record of surface ^{137}Cs concentrations in the global ocean using the HAM-global database. J. Environ. Monit. 11, 116–125, 2009.

Inomata, Y.: Global trends in cesium distribution, in: Atwood, D. (Ed.), Encyclopedia of Inorganic Chemistry. Wiley, pp. 453–466, 2010.

1895 Inomata, Y., Aoyama, M., Tsumune, D., Motoi, T., and Nakano, H.: Optimum interpolation analysis of basin-scale ^{137}Cs transport in surface seawater in the North Pacific Ocean. J. Environ. Monit. 14, 3146–3155, 2012.

Inomata, Y., Aoyama, M., Tsubono, T., Tsumune, D., and Hirose, K.: Spatial and temporal distributions of ^{134}Cs and ^{137}Cs derived from the TEPCO Fukushima Daiichi Nuclear Power Plant accident in the North Pacific Ocean by using optimal interpolation analysis. Environ. Sci. Process. Impacts. 18, 126–136, 2016.

1900 Inomata, Y., Aoyama, M., Hamajima, Y., and Yamada, M.: Transport of F1NPS-derived radiocaesium from subtropical mode water in the western North Pacific Ocean to the Sea of Japan. Ocean Sci., 14, 813–826, 2018.

Inomata, Y., Aoyama, M., Hamajima, Y., and Yamada, M.: Analysis of increased radiocaesium activity derived from Fukushima Dai-ichi Nuclear Power Plant accident until 2017. Proceedings of the 5th International Conference on Environmental Radioactivity ENVIRA 2019: Variations of Environmental Radionuclides, 27–30, 2019.

1905 Inomata, Y. and Aoyama, M.: ^{137}Cs measurement points in the surface seawater in the global ocean based in the HAM database2021. Center for Research in Isotopes and Environmental Dynamics, University of Tsukuba, 2021. doi: 10.34355/ Ki-net.KANAZAWA-U.00149, 2022a.

Inomata, Y. and Aoyama, M.: Temporal variations of ^{137}Cs activity concentrations and these 0.5-yr median values in the surface seawater in the global ocean. Center for Research in Isotopes and Environmental Dynamics, University of
1910 Tsukuba, 2021. doi: 10.34355/ Ki-net.KANAZAWA-U.00150, 2022b.

Inomata, Y. and Aoyama, M.: Dataset of 0.5-yr median values of ^{137}Cs activity concentrations in the surface seawater in the global ocean during the period from 1957 to 2021. Center for Research in Isotopes and Environmental Dynamics, University of Tsukuba, 2021. doi: 10.34355/ Ki-net.KANAZAWA-U.00151, 2022c.

Ito, T., Aramaki, T., Kitamura, T., Otosaka, S., Suzuki, T., and Togawa, O., et al.: Anthropogenic radionuclides in the Japan
1915 Sea: their distributions and transport processes. J. Environ. Radioact.68, 249–267, 2003.

Ito, T., Aramaki, T., and Otosaka, S., et al.: Anthropogenic radionuclides in seawater of the Japan Sea. J. Nuclear Sci. Technol. 42, 90–100, 2005.

Ito, T., Kaneko, A, Tsubota, H., and Gohda, H.: The characteristic distribution of silica over the East China Sea shelf slope. J. Oceanograp. 50, 465–477, 1994.

1920 Kaeriyama, H., Ambe, D., Shimizu, Y., Fujimoto, K., Ono, T., and Yonezaki, S., et al.: Direct observation of ^{134}Cs and ^{137}Cs in surface seawater in the western and central North Pacific after the Fukushima Dai-ichi nuclear power plant accident. Biogeosci. 10, 4287–4295, 2013.

Kaeriyama, H., Shimizu, Y., Ambe, D., Masujima, M., Shigenobu, Y., and Fujimoto, K., et al.: Southwest intrusion of 134Cs and ^{137}Cs derived from the Fukushima Dai-ichi nuclear power plant accident in the Western North Pacific. Environ.

1925   Sci. Technol. 48, 3120–3127, 2014.

Kaeriyama, H., Fujimoto, K., Ambe, D., Shigenobu, Y., Ono, T., Tadokoro, K., Okazaki, Y., Kakehi, S., Ito, S., Narimatsu, Y., Nakata, K., Morita, T., and Watanabe, T.: Fukushima-derived radionuclides [134]Cs and ^{137}Cs in zooplankton and seawater samples collected off the Joban-Sanriku coast, in Sendai Bay, and in the Oyashio region. Fisheries Sci. 81, 139–153, 2015.

1930 Kamidaira, Y., Uchiyama, Y., Kawamura, H., Kobayashi, T., and Furuno, A.: Submesoscale mixing on initial dilution of radionuclides released from the Fukushima Daiichi Nuclear Power Plant. J. Geophys. Res. Oceans. 123, 2808–2828. https://doi.org/10.1002/2017JC013359, 2018.

Kameník, J., Dulaiova, H., Buesseler, K.O., Pike, S.M., and Št'astná, K.: Cesium-134 and 137 activities in the central North Pacific Ocean after the Fukushima Dai-ichi nuclear power plant accident. Biogeosci. 10, 4287–4295, 2013.

1935 Kautsky, H.: Investigations on the distribution of Cs and Sr and the water mass transport times in the Northern North Atlantic and the North Sea. Dt. Hydrogr. Z. 40, 50–67, 1987.

Kim, C.K., Byun, J.I., Chae, J.S., Choi, H.Y., Choi, S.W., and Kim, D.J., et al.: Radiological impact in Korea following the Fukushima nuclear accident. J. Environ. Radioact. 111, 70–82, 2012.

Kumamoto, Y., Aoyama, M., Hamajima, Y., Aono, T., Kouketsu, S., and Murata, A., et al.: Southward spreading of the

1940   Fukushima-derived radiocesium across the Kuroshio Extension in the North Pacific. Sci Rep. 4, 4276, 2014.

Kumamoto, Y., Aoyama, M., Hamajima, Y., Murata, and A., Kawano, T.: Impact of Fukushima-derived radiocesium in the western North Pacific Ocean about ten months after the Fukushima Dai-ichi nuclear power plant accident. J. Environ. Radioact. 140, 114–122, 2015.

Kumamoto, Y., Aoyama, M., Hamajima, Y., Nishino, S., Murata, A., and Kikuchi, T.: Meridional distribution of Fukushima-

1945   derived radiocesium in surface seawater along a trans-Pacific line from the Arctic to Antarctic Oceans in summer 2012. J. Radioanal. Nucl. Chem. 307, 1703–1710, 2016.

Kumamoto, Y., Aoyama, M., Hamajima, Y., Nagai, H., Yamagata, T., Kawai, Y., Yamaguchi, A., Imai, K., Murata, A.: Fukushima-derived radiocesium in the western North Pacific in 2014. J. Radioanal. Nucl. Chem. 311, 1209–1217, 2017.

1950 Kumamoto, Y., Aoyama, M., Hamajima, Y., Oka, E., and Murata, A.: Time evolution of Fukushima-derived radiocesium in the western subtropical gyre of the North Pacific Ocean by 2017. J. Radioanal. Nucl. Chem. 318, 2181–2187. https://doi.org/10.1007/s10967-018-6133-5, 2018.

Kumamoto, Y., Yamada, M., Aoyama, M., Hamajima, Y., Kaeriyama, H., Nagai, H., Yamagata, T., Murata, A., and Masumoto, Y.: Radiocesium in North Pacific coastal and offshore areas of Japan within several months after the Fukushima

1955   accident. J. Environ. Radioact., 198, 79–88, 2019.

Livingston H.D., Bowe'n, V.T., Casso, S.A., Volchok, H.L., Noshkin, V.E., Wong, K. M., and Beasley, T.M.: Fallout Nuclides in Atlantic and Pacific Water Columns: GEOSECS Data. Technical Report., WHOI-85-19, 1985.

Livingston, H.D., and Povinec, P.P.: Anthropogenic marine radioactivity. Ocean Coast. Manag. 43, 689–712, 2000.

Matishov, G.G., Matishov, D.G., and Namjatov, A.A.: Artificial radionuclides in sediments of the Don River Estuary

1960   and Azov Sea. J. Environ. Radioact. 59, 309–327, 2002.

Maderich, V., Kim, K.O., Bezhenar, R., Jung, K.T., Martazinova, V., and B. Igor: Transport and Fate of [137]Cs Released From Multiple Sources in the North Atlantic and Arctic Oceans. Front. Mar. Sci., 8, 806450.

Mignot, J., de Boyer Montégut, C., Lazar, A., and Cravatte, S.: Control of salinity on the mixed layer depth in the world ocean: 2. Tropical areas. J. Geophys. Res. 112, 2007.

1965 Miroshnichenko, O.N., and Paraskiv, A.A.: [137]Cs concentration in surface waters of Far Eastern seas: Results of expeditionary research in 2018. Mar. Biolog. J. 5, 55–63, 2020.

Miyake, Y., Saruhashi, K., and Katsuragi, Y.: Strontium 90 in western North Pacific surface waters. Pap. Meteorol. Geophys.

XI, 188–191, 1960.

Miyake, Y., Saruhashi, K., Katsuragi, Y., and Kanazawa, T.; Cesium 137 and Strontium 90 in sea water. J. Radiat. Res. 2–1, 25–28, 1961.

Miyake, Y.: Penetration of ^{90}Sr and ^{137}Cs in deep layers of the Pacific and vertical diffusion rate of deep water. J. Radiat. Res. 3–3, 141–147, 1962.

Miyake, Y. : Artificial radioactivity in the Pacific Ocean, in: Radioactive Tracers in Oceanography. I.U.G.G.Monograph. International Union of Geodesy and Geophysics. pp. 21–30, 1963.

Miyake, Y., and Sugimura, Y.: Plutonium content in the western North Pacific waters. Pap. Meteorol. Geophys. 19, 481–485, 1968.

Miyake, Y., and Sugimura, Y.: The Plutonium Content of Pacific Ocean Waters. IAEA-SM-199/22. pp. 91–105, 1978.

Miyake, Y., Saruhashi, K., Sugimura, Y., Kanazawa, T., and Hirose, K.: Contents of ^{137}Cs, plutonium and americium isotopes in the Southern Ocean waters. Pap. Meteorol. Geophys. 39, 95–113, 1988.

Miyao, T., Hirose, K., Aoyama, M., and Igarashi, Y.: Temporal Variation of ^{137}Cs and ^{239,240}Pu in the Sea of Japan. J. Environ. Radioact. 40, 239–250, 1998.

Montégut, C.: Mixed layer depth over the global ocean: An examination of profile data and a profile-based climatology. J. Geophys. Res. 109, C12003, doi:10.1029/2004JC002378, 2004.

Molero, J., Sanchez-Cabeza, J.A., Merino, J., Mitchell, P.I., and Vidal-Quadrasa, A.: Impact of ^{134}Cs and ^{137}Cs from the Chernobyl reactor accident on the Spanish Mediterranean marine environment, J. Environ. Radioact. 43, 357–370, 1999.

Nakano, H., Motoi, T., Hirose, K., and Aoyama, M.: Analysis of ^{137}Cs concentration in the Pacific using a Lagrangian approach J. Geophys, Res., 115, C06015, doi:10.1029/2009JC005640, 2010.

Nagaya, Y., Shiozaki, and M., Seto, Y.: Radioactive contamination of the Indo-Antarctic Ocean water in each earlier period in 1961 and 1962. J. Radiat. Res. 5–3–4, 206–214, 1964a.

Nagaya, Y., Shiozaki, M., and Seto, Y.: Radiological survey of sea water of adjacent Sea of Japan in 1963. 78, 63–67, 1964b.

Nagaya, Y., Shiozaki, M., and Seto, Y.: Some fallout radionuclides in deep waters around Japan. J. Radiat. Res. 6–1, 23–31, 1965.

Nagaya, Y., Nakamura, K.: A study on the vertical transport of ^{90}Sr and ^{137}Cs in the surface waters of the seas around Japan. J. Radiat. Res. 11–1, 32–43, 1970.

Nagaya, Y., and Nakamura, K.: ^{90}Sr and ^{137}Cs contents in the surface waters of the adjacent seas of Japan and the North Pacific during 1969 to 1973. J. Oceanogr. Soc. Jpn. 32, 228–234, 1976.

Nagaya, Y., and Nakamura, K.: Artificial radionuclides in the western Northwest Pacific (I): ^{90}Sr and ^{137}Cs in the deep waters. J. Oceanogr. Soc. Jpn. 37, 135–144, 1981.

Nagaya, Y., and Nakamura, K.: ^{239,240}Pu, ^{137}Cs and ^{90}Sr in the central North Pacific. J. Oceanogr. Soc. Jpn. 40, 410–424, 1984.

Nagaya, Y., and Nakamura, K.: Artificial radionuclides in the western Northwest Pacific (II): ^{137}Cs and ^{239,240}Pu inventories in water and sediment columns observed from 1980 to 1986. J. Oceanogr. Soc. Jpn. 43, 345–355, 1987.

Nagaya, Y., and Nakamura, K. Distributions and mass-balance of 239,240Pu and 137Cs in the northern North Pacific, in: Teramoto, T. (Ed.), Deep Ocean Circulation, Physical and Chemical Aspects. Elsevier Oceanography Series, Elsevier, Amsterdam, 157-167, 1993.

Nakanishi, T., Satoh, M., Takai, M., Ishikawa, A., Murata, M., Dairyoh, M., and Higuchi, S.: Successive determinations of ^{210}PB, ^{210}PO, ^{226}RA, ^{228}RA and selected actinides in seawater and sea sediment. J. Radioanal. Nucl. Chem. 138, 321–230, 1990.

Nakanishi, T., Shiba, Y., Muramatsu, M., and Haque, M.A.: Estimation of mineral aerosol fluxes to the Pacific by using environmental plutonium as a tracer, in: Sakai, H., Nozaki, Y. (Eds.), Biogeochemial Processes and Ocean Flux in

the Western Pacific. Terra Science Publishing Company, Tokyo, pp. 15–30, 1995.

NOAA National Geophysical Data Center: 2-minute Gridded Global Relief Data (ETOPO2) v2. doi:10.7289/V5J1012Q, 2006.

Nucler Energy Agency; Chernobyl: Assessment of radiological and Health Impacts. Chapter II. The release, dispersion, deposition and behaviour of radionuclides. 2002 Update of CHernobul: Ten Years On., 2002.

Nies, H.: The distribution of the Chernobyl fallout over the Baltic sea and its change during 1987 and 1988 in seawater. Baltic Sea Environment Proceedings, No. 31, pp. 31–41, 1989.

Noshkin, V.E., Eagle, R.J., and Wong, K.M.: Plutonium levels in Kwajalein Lagoon. Nature. 262, 745–748, 1976.

Noshkin, V.E., Wong, K.M., Jokela, T.A., Eagle, R.J., and Brunk, J.L.: Radionuclides in the Marine Environment Near the Farallon Island. UCRL-52381. pp. 16, 1978.

Noshkin, V.E., Wong, K.M., and Eagle, R.J.: Plutonium concentrations in fish and seawater from Kwajalein Atoll. Health Phys. 37, 549–556, 1979.

Noshkin, V.E., Brunk, J.L., Jokela, T.A., and Wong, K.M.: ^{238}Pu concentrations in the marine environment at San Clemente Island. Health Phys. 40, 643–659, 1981.

Noshkin, V.E.: Concentrations of Radionuclides in Some Seawater and Sediment Samples from the Equatorial Pacific with Emphasis on Samples from the Western Pacific Ocean. Preliminary report prepared for the 1st Coordinated Research Project on Worldwide Marine Radioactivity Studies, IAEA, Monaco, 1999.

Oki, T., and Kanae, S.: Estimation of areas within a cartesian grid box considering the ellipticity of the earth, J. Japan Soc. Hydrol. Water Resour. 10, 371–374, 1997.

OSPAR: Annual report and assessment of discharges of liquid discharges from nuclear installations, 2021.

Open University: Ocean Circulation, second edition 2001. Reprinted 2004.

Pillay, K.C., Smith, R.C., Folsom, and T.R.: Plutonium in the marine environment. Nature. 203, 568–571, 1964.

Povinec, P.P., Bailly du Bois, P., Kershaw, P.J., Nies, H., Scotto, P.: Temporal and spatial trends in the distribution of ^{137}Cs in surface waters of Northern European Seas—a record of 40 years of investigations. Deep Sea Res. Part II Top. Stud. Oceanogr. 50, 2785–2801, 2003.

Povinec, P.P., Aoyama, M., Fukasawa, M., Hirose, K., Komura, K., Sanchez-Cabeza, J.A., Gastaud, J., Ješkovský, M., Levy, I., and Sýkora, I.: ^{137}Cs water profiles in the South Indian Ocean–An evidence for accumulation of pollutants in the subtropical gyre. Prog. Oceanogr. 89, 17–30, 2011.

Prandle, D., A modelling study of the mixing of ^{137}Cs in the seas of the European continental shelf. Journal Philosophical Transactions of the Royal Society. A310, 407-430.

Prandle, D., Beechey, J., 1991. Marine dispersion of caesium 137 released from Sellafield and Chernobyl. Geophys. Res. Lett., 18, 9, 1723-1726.

Sanchez-Cabeza, J.A., Levy, I., Gastaud, J., Eriksson, M., Osvath, I., Aoyama, M., Povinec, P.,P., Komura, K.: Transport of North Pacific ^{137}Cs labeled waters to the south-eastern Atlantic Ocean. Prog. Oceanogr. 89, 31–37, 2011.

Shirasawa, T.H., Schuert, E.A.: Fallout Radioactivity in the North Pacific Ocean: Data Compilation of Sr-90 and Cs-137 Concentrations in Seawater. HASL-197 I-66–I-94, 1968.

Smith, J.N., Ellis, K.M., Kilius, L.R.: ^{129}I and ^{137}Cs tracer measurements in the Arctic Ocean. Deep Sea Res. 45, 959–984, 1998.

Smith, J.N., Rossi, V., Buesseler, K.O., Cullen, J.T., Cornett, J., Nelson, R., Macdonald, A.M., Robert, M., and Kellogg, M.: Recent transport jistory of Fukushima Radioactivity in the Northeast Pacific Ocean. Environ. Sci. Technol. 51, 10494–10502, 2017.

Steinhauser, G., Brandl, A., and Johnson, T.E. : Comparison of the Chernobyl and Fukushima nuclear accidents: A review of

the environmental impacts. Sci. Total Environ. 470–471, 800–817, 2014.

Stramma, L., and England, M.: On the water masses and mean circulation of the South Atlantic Ocean. J. Geophys. Res. 104, 20863–20883, 1999.

2055   Suga, M., Ando, A., Ubukawa, T., and Ueda, M. : Calculation of "Sea and Land Areas and Their Ratio of Each Latitude Band" by Global Map Version. Kokudochiriin Jihou. 124, 95–98, 2013 [In Japanese].

Tsubono, T., Misumi, K., Tsumune, D., Bryan, F.O., Hirose, K., and Aoyama, M. : Evaluation of radioactive cesium impact from atmospheric deposition and direct release fluxes into the North Pacific from the Fukushima Daiichi nuclear power plant. Deep Sea Res. Part I Oceanogr. Res. Papers, 115, 10–21, 2016.

2060   Tsumune, D., Aoyama, M., Hirose, K.: Numerical simulation of 137Cs and 239,240Pu concentrations by an ocean general circulation model. Journal of Environmental Radioactivity 69, 61–84, 2003.

Tsumune, D., Aoyama, M., Hirose, K., Bryan, F.O., Lindsay, K., and Danabasoglu, G.: Transport of ^{137}Cs to the Southern Hemisphere in an ocean general circulation model. Prog. Oceanogr. 89, 38–48, 2011.

Tsumune, D., Tsubono, T., Aoyama, M., and Hirose, K.: Distribution of oceanic ^{137}Cs from the Fukushima Dai-ichi Nuclear

2065   Power Plant simulated numerically by a regional ocean model, J Environ Radioact, 111, 100-108, 10.1016/j.jenvrad.2011.10.007, 2012.

Tsumune, D., Tsubono, T., Aoyama, M., Uematsu, M., Misumi, K., Maeda, Y., Yoshida, Y., and Hayami, H.: One-year, regional-scale simulation of ^{137}Cs radioactivity in the ocean following the Fukushima Dai-ichi Nuclear Power Plant accident, Biogeosciences, 10, 5601-5617, 10.5194/bg-10-5601-2013, 2013.

2070   UNSCEAR : Sources, Effects and Risks of Ionizing Radiation, Vol. I. Sources, Report to the general assembly with scientific annexes, 2000.

UNSCEAR : Sources, Effects and Risks of Ionizing Radiation, Vol. I. Scientific Annex A., Report to the general assembly with scientific annexes, 2013.

Wessel, P., Smith, W. H. F., Scharroo, R., Luis, J., and Wobbe, F.: Generic Mapping Tools: Improved Version Released, EOS

2075   Trans. AGU, 94, 409-410, 2013.

Yamada, M., Wang, Z.L., and Zheng, J.: The extremely high ^{137}Cs inventory in the Sulu Sea: A possible mechanism. J. Environ. Radioact., 90, 163–171, 2006.

Yamada, M., and Wang, Z.L.: ^{137}Cs in the western South Pacific Ocean. Sci. Total Environ. 382, 342–350, 2007.

Wong, K.M., Jokela, T.A., Eagle, R.J., Brunk, J.L., and Noshkin, V.E.: Radionuclide concentrations, fluxes, and

2080   residence times at Santa Monica and San Pedro Basins. Prog. Oceanogr. 30, 353–391, 1992.

Zaborska, A., Winogradow, A., and Pempkowiak, J.: Caesium-137 distribution, inventories and accumulation history in the Baltic Sea sediments. J Environ. Radioact. 127, 11–25, 2014.